F.A. Dikland

Semi-Automatic Generation of Preoperative Surgical Plans for Complex Femoral Deformity Correction

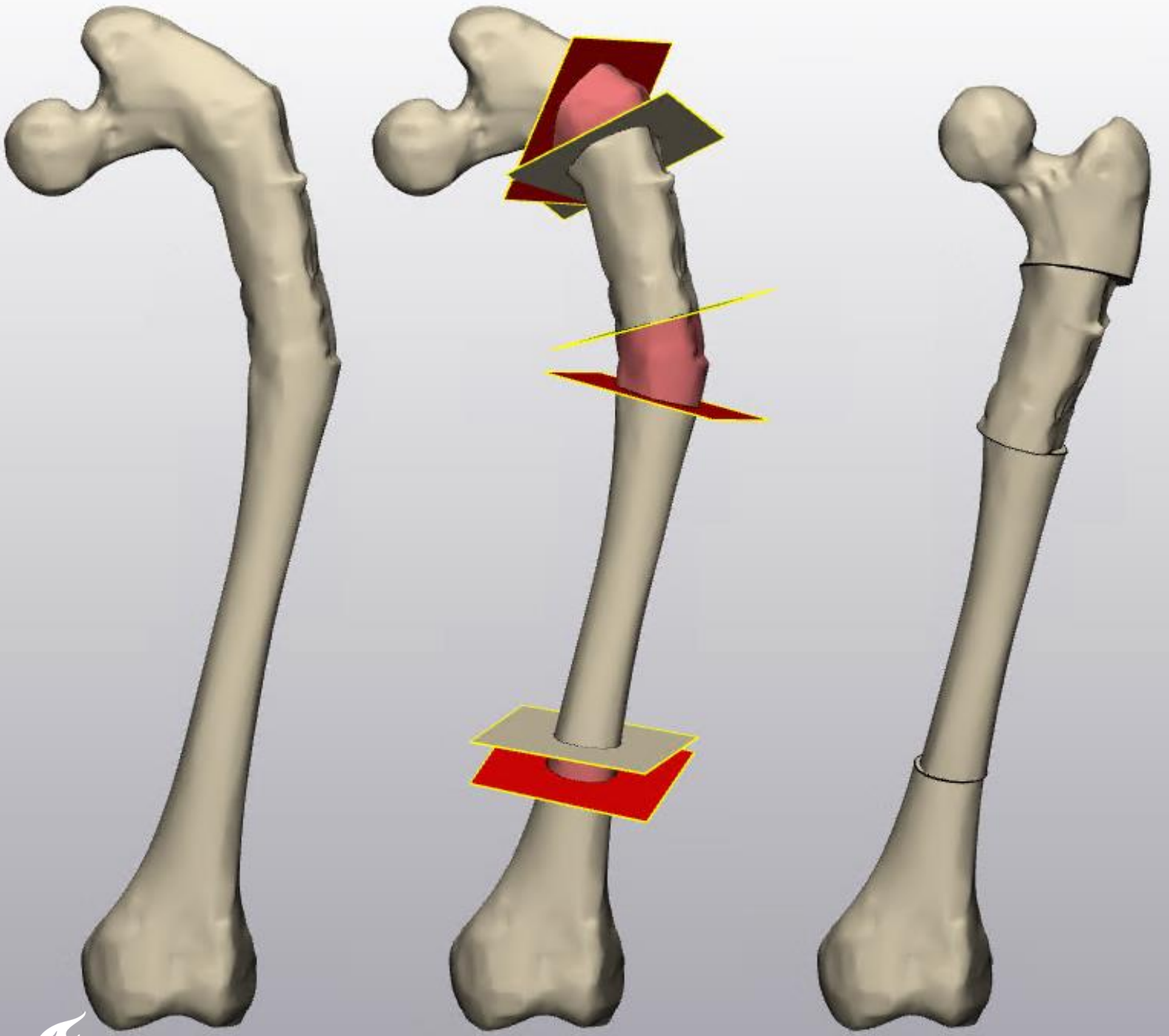

TU Delft
LUMC Leids Universitair Medisch Centrum

Semi-Automatic Generation of Preoperative Surgical Plans for Complex Femoral Deformity Correction

By

F.A. Dikland

in partial fulfilment of the requirements for the degree of

Master of Science
in Technical Medicine

at the Delft University of Technology,
to be defended publicly on Wednesday December 20, 2023 at 13:00.

Supervisors:	Dr. ir. B.L. Kaptein	
	Dr. J.G. Gerbers	
Thesis committee:	Dr. ir. B.L. Kaptein,	Leiden University Medical Centre
	Dr. J.G. Gerbers,	Leiden University Medical Centre
	Dr. J.J. Tolk,	Erasmus Medical Centre

TU Delft

Preface

Femoral closed wedge osteotomies are the preferred surgery for the treatment of complex bony deformity with functional impairment. The technological advancements of the past decades have transformed the line of thinking about preoperative planning of these osteotomies. In early days of preoperative planning, the osteotomies were drawn in on physical radiographs. Nowadays, the osteotomies are drawn in on three dimensional bone model data using computer-aided design software. However this process is still manual, which makes it time consuming and subjective. In this work a method for semi-automatic generation of preoperative plans is presented. The technical aspect of automation, without disregarding the intra-operative feasibility and the goal of achieving improved patient function outcome, calls for a multidisciplinary approach.

This work consists of three separate parts that can be read as individual pieces. First a paper is presented that gives an overview of the clinical relevance and performs a subjective and objective validation of the proposed algorithm. For this, preoperative plans are created for 20 deformed femora. In a retrospective study at the Leiden University Medical Centre, CT and MRI data from subjects with non-traumatic femoral deformity were collected. The semi-automatically generated preoperative plans are presented to two independent assessors for subjective validation. Four of twenty cases are randomly selected and were compared to their manual counterpart, for objective validation.

The second part consists of a technical document. In this document an in-depth description of the proposed solution is given. All steps of the translation from clinical problem to technical solution are outlined, including the development of the algorithm, the design of the cost function and the optimization strategy.

The third part is a step by step guide with visuals on the best practices of the proposed semi-automatic planning tool.

F.A. Dikland
Delft, December 2023

Acknowledgements

Many thanks to Bart Kaptein for his technical insights on the subject, and Jasper Gerbers for his kind introduction to the clinical practice of the orthopedic department as well as his ingenuity in clinical problem solving. Special thanks to both for their close involvement in the project and overall approachability.
Thanks should also go to Pieter Bas de Witte and Demiën Broekhuis for their time in the validation of the final solution and sharing their experience with intra-operative obstacles of femoral correction osteotomies.
Special thanks to my friends and fellow students for listening and empathizing with me during the full length of this research. Lastly, I am thankful for all doctors in training for giving me the opportunity to develop myself as a clinical technical expert in the outpatient clinical and operation room.

Contents

Abstract

Disease of bone or trauma can result in significant bony deformation. Functional impairment as a result of such deformity is an indication for surgical correction. Indicated surgery is often closed wedge osteotomy and internal fixation. Manual design of a preoperative plan using computer-aided design software is the current golden standard for complex correction surgery planning. However, these manually designed plannings are time consuming and subjective. The goal of this study was to develop an algorithm capable of generating good quality preoperative plans for correction surgery, in less time than an expert in preoperative planning.

A software solution integrated in Blender (Blender Foundation, The Netherlands), has been developed to generate semi-automatic preoperative plans. The software optimizes one to three closed wedge osteotomies, by minimizing the dissimilarity from a deformity shape after osteotomy, to a target shape. The deformity shape is the centreline of the deformed femur. The target shape in this study is the centreline of an intramedullary nail.

A cost function was created that makes use of the Hausdorff distance and the root mean squared error to quantify the dissimilarity between the deformity shape after osteotomy and the target shape. Clinical constraints to the model are femoral length and collum anteversion angle. Using a multi-objective genetic algorithm the cost function is minimized within the bounds of the set clinical constraints.

To validate the method of semi-automatic generation, 20 bone models of deformed femora have been created from retrospectively collected CT data. The proposed solution was used to generate preoperative plans, which were scored by two independent assessors. After the creation of an initial preoperative plan and a maximum of two revisions of the plan, 18 of 20 semi-automatically generated preoperative plans were eligible for surgery. Four cases of femoral deformity were randomly selected from the dataset and counterparts to the existing automatic preoperative plans were created manually. 30% to 575% more time was needed to design a preoperative plan manually compared to the semi-automatic generation. In all preoperative plans in the automatic group, the collum anteversion angle of the postoperative configuration was within the normal range of 8-15 degrees. In the manual group, one of four postoperative configurations had a collum anteversion angle within this normal.

The proposed method for semi-automatic preoperative plan generation is a novel, versatile approach with the ability to optimize multiple osteotomies to mimic a given target shape. The automatic planning tool is a promising aide to both technicians and clinicians for a fast preoperative planning withing the boundaries of clinical anatomical normal ranges.

1 Validation paper

Semi-Automatic Generation of Preoperative Surgical Plans for Complex Femoral Deformity Correction

F.A. Dikland[a], J.G. Gerbers[a], B.L. Kaptein[a]

[a]*Department of orthopaedics, Leiden University Medical Center, Leiden, The Netherlands*

Abstract

Functional impairment as a result of bony deformity is an indication for surgical correction. Such bony deformities are most prevalent in the lower extremity due to the influence of weightbearing and leg musculature. Indicated surgery is often closed wedge osteotomy and internal fixation. Current technology enables the preoperative planning and intra-operative execution of these osteotomies with high accuracy. In this study a novel software solution is presented that generates preoperative plans for femoral osteotomy corrections, using Blender and its in-build Python scripting module. The model optimizes the femoral shaft shape within the boundaries of clinical constraints. 20 cases of femoral deformity were processed by the model retrospectively. Eighteen of twenty preoperative plans were accepted by two independent clinical experts, in a maximum of three iterations. This shows the ability of the model to generate preoperative plans of sufficient quality that are tailored to the wishes of the clinical expert. Four cases were randomly picked to perform manual preoperative planning. The manual plans were compared with their automatic counterparts. These showed comparable results with a systematically higher femoral neck shaft angle and articulo-trochanteric distance in the automatic group compared to their manual counterparts. The collum anteversion angle was within the normal range for all four cases in the automatic group and only in one case for the manual group. The manual planning process was slower in every case, ranging from 31% slower to 575% slower. It can be concluded that the model produces satisfactory preoperative plans in a short time. Furthermore, it allows fast exploration of different surgical options within a constraint based design. In summary, the automatic planning tool is a promising aide to both technicians and clinicians for fast preoperative planning within the boundaries of clinical anatomical normal ranges.

Keywords: femoral osteotomy, preoperative planning, automation, computer-aided design, morphometric characteristics

1. Introduction

Diseases of bone or trauma can result in significant bony deformation. Non-traumatic deformities can be of congenital, developmental, neuromuscular or dysplastic nature. Examples of causes for deformity are fibrous dysplasia, rickets and osteogenesis imperfecta [1, 2, 3]. These deformities can limit range of motion or create biomechanical imbalances [4, 5]. Deformities of non-traumatic origin have a higher prevalence in the lower extremity, where weightbearing and leg musculature deform weak or brittle bone. The proximal femur is an anatomically intricate area; it has a set of complex morphometric features, such as femoral coxa angulation and femoral collum version. Furthermore, it has many soft tissue attachments and its motion is restricted by the femoroacetabular relationship. There can be a great impact on femoral geometry in developmental stage of the femur [6, 7]. Correctional osteotomy is often advised in case of functional impairment as result of a deformity. Computer-aided design (CAD) is used to effectively quantify the deformity in three dimensions and to design a surgical plan to restore anatomy by means of osteotomy. As these surgeries often require multiplanar corrections these are highly demanding.
Patient specific cutting guides can be used to execute the plan intra-operatively with high accuracy [8]. Gigi et al. show that a good preoperative plan, followed by surgical execution using intra-operative cutting guides, lead to a significantly improved surgical workflow. This reflects in significantly shorter surgery time and lower hemoglobin drop intra-operatively [9].
The design of a preoperative plan is often time-consuming. The goal of this study is to develop a software solution capable of lowering time needed for the design of high quality preoperative plans. In this study, a model is created to semi-automatically generate a preoperative surgical plan using a quantifiable measure of femoral shaft anatomy, bounded by morphometric clinical constraints. The time to design a preoperative plan manually and automatically are compared and the quality of the automatically generated plans are validated by expert assessment.

2. Method

An experimental in silico study was designed and performed at the Leiden University Medical Center (LUMC). Patients with non-traumatic femoral deformity with a CT scan were included. A semi-automatic tool for preoperative surgical plan suggestion was created using Blender 3.1 (Blender Foundation, The Netherlands) and its open-source python scripting modules.
A discrete sampling of the femoral centreline is used to represent the femoral shaft anatomy. The model makes use of a semi-automatic software that finds bony landmarks representing the

simplified version of a femoral model. All landmarks that are automatically calculated, can be manually adapted before application in optimization. The identical method of finding the centreline of the femoral shaft is used to find the centreline of an intramedullary nail.
The goal of the algorithm is to automatically generate one or multiple closed or hybrid osteotomy wedges in order to correct the deformed femur shape. The development of the model can be divided in three subcategories: 1) defining a simplified representation of the femur and osteotomy planes, 2) defining clinical optimization boundaries, 3) defining a cost function and optimization algorithm.
The development of the algorithm is focused on achieving improved postoperative functional outcome. Important factors for achieving this, are the collum anteversion angle (CAA) and femoral bone length as well as reconstructing the shape of a non-pathological bone. Visual explanation of these morhpometrics are also appended in Appendix A.
Preoperative plans generated using CT data are subjectively validated by 2 independent experts and objectively validated based on post-operative morphometric characteristics and the time needed for preoperative plan design. As a secondary goal, to investigate the versatility of the model, a single case was performed on MRI data, and for a single case the shaft centreline of the healthy side was used as target shape.

2.1. Model architecture

2.1.1. clinical optimization boundaries

Crucial for the generation of preoperative plans are the post-operative correction of the shaft anatomy as well as the correction of morphometric characteristics correlated with patient functional post-surgical outcome. These morphometric characteristics are calculated from bony landmarks identified on the femur model. The most important femur characteristics in clinical decision making are the femoral length pre and post-surgery, the CAA, the FNSA and the mechanical axis.
To calculate these indicators of femoral anatomy several anatomical landmarks are required. For the FNSA, these are the vector describing the midline of the collum and the vector representing the shaft direction. For the CAA the latter two landmarks are used, as well as the posterior condylar axis. The femoral bone length is defined as the shortest distance between the knee joint and the centre of the femoral head plus the radius of the femoral head. The knee joint is defined as the location in between the most distal medial and lateral condyle points. The postoperative mechanical axis deviation in comparison to the preoperative anatomy can be estimated using the epicondylar axis and the centre of the femoral head. The femoral landmarks and the parameters calculated from these landmarks are summarized in Table 1, and visualized in Appendix A. Anatomical landmarks are semi-automatically found on the femur model. For this, four regions have to be manually annotated by placing a box around the medial and lateral condyle and placing a sphere around the caput femoris and trochanter major.

2.1.2. Femur and Osteotomy Wedge

In order to generate a preoperative plan automatically, the deformed femur as well as the osteotomy plane need to be defined. For simplification of the algorithm, the shape of the femur shaft is reduced to the centreline. The centreline is found by generating spherical objects from distal to proximal, that intersect with the femur model. The centre of gravity of intersecting coordinates are considered to be a good representation of a single point on the centreline. This centreline is then resampled to 160 three-dimensional (3D) coordinates using a linear interpolation with equal distance.
An osteotomy is defined as the bone enclosed by two planes. A plane in 3D space is defined by the location of the plane as an **<x, y, z>** coordinate and the orientation of the plane as the **<x, y, z>** unit vector of the plane normal. Thus both planes have six degrees of freedom, three translational degrees and three rotational degrees. This combines to a total of 12 degrees of freedom for a single closed wedge osteotomy.

2.2. Model validation

CT data was used to generate 3D models of deformed femurs, using segmentation and model enhancement tools integrated in Mimics 25.0 (Materialise, Belgium) and 3Matic 17.0 (Materialise, Belgium). From these bone models, preoperative plans are generated semi-automatically. The validation of the model consists of three separate parts. Two independent clinicians with experience of performing femoral osteotomies are involved in a user test. In this test the clinician uses the tool with help of the developer to generate a preoperative plan. The clinician is asked to fill in a survey which scores the tool in four categories: 1) adaptability of the model output, 2) clinical adoptability, 3) clinical decision making, 4) output quality.
In the second test the preoperative plans generated by a technician, using the tool, are presented to the same reviewers and scored with a grade ranging from 1 to 5. Preoperative plans scoring a 3 or lower are revisited and scored anew until all preoperative plans score a 4 or higher.
In a third test preoperative plans are generated for 4 randomly chosen deformed bones from the database, both manually and automatically. The manual plans are made by expert planners using 3Matic. The automatic plans are generated by the first author. During the generation of these preoperative plans, the time from first inspection of the model, to exporting of the preoperative plan is recorded. Several morphometric parameters that represent the post-operative outcome are evaluated using measuring tools in 3Matic for both the manual and automatically generated counterparts. The evaluated morphometric measures are the femoral neck shaft angle (FNSA), defined as the angle between the femoral shaft and the femoral collum, CAA, the articulo-trochanteric distance (ATD), defined as the distance between the tip of the greater trochanter and the most proximal femoral caput point, the femoral length, the number of osteotomies and the mean height of the osteotomy wedge. These parameters are visualized and summarized in Appendix A.

Clinical Measure	Anatomical Landmarks	Vectors and Coordinates	Equations
femoral neck shaft angle	caput centre collum centre femoral centreline	collum midline shaft midline	$FNSA = \arccos \vec{V}_{collum} \cdot \vec{V}_{shaft}$
collum anteversion angle	caput centre collum centre lateral posterior condylar coordinate medial posterior condylar coordinate	collum midline shaft midline posterior condylar axis	$x =< 1, 0, 0 >, y =< 0, 1, 0 >$ $\vec{V}_{Xp} = \vec{V}_x - \vec{V}_x \cdot \vec{V}_{shaft} * \vec{V}_{shaft}$ $\vec{V}_{Yp} = \vec{V}_{Xp} \times \vec{V}_{shaft}$ $\vec{V}'_{collum} =< \vec{V}_{collum} \cdot \vec{V}_{Xp}, \vec{V}_{collum} \cdot \vec{V}_{Yp} >$ $\vec{V}'_{condyles} =< \vec{V}_{condyles} \cdot \vec{V}_{Xp}, \vec{V}_{condyles} \cdot \vec{V}_{Yp} >$ $CAA = \arccos \vec{V}'_{collum} \cdot \vec{V}'_{condyles}$
femoral length	caput centre medial distal condylar coordinate lateral distal condylar coordinate	caput centre coordinate knee joint	$\vec{V}_{length} = \overrightarrow{CO}_{caput} - \overrightarrow{CO}_{knee}$ $FemoralLength = \lvert\vec{V}_{length}\rvert + r_{caput}$
mechanical axis	medial epicondyle lateral epicondyle caput centre medial distal condylar coordinate lateral distal condylar coordinate	epicondylar axis knee caput axis knee joint	$MechanicalAxis = \arccos \vec{V}_{KneeCaput} \cdot \vec{V}_{epicondyle}$

Table 1: A summary of morhpometric parameters that correlate with post-operative functional outcome

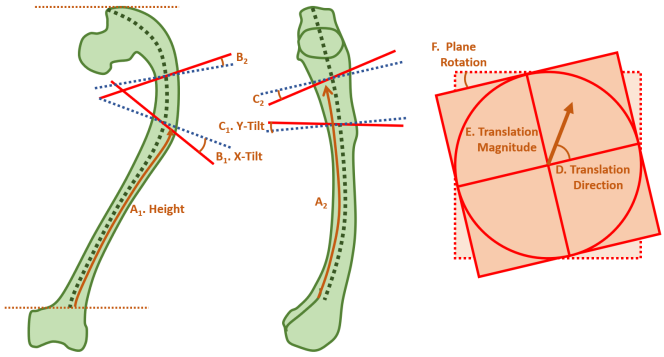

Figure 1: Parameters A-C are specified for both planes. Parameters D-F are only specified for the proximal plane of an osteotomy.

By setting the location of the osteotomy plane to always correspond with a coordinate on the centreline of the femur, the three translational degrees of freedom per plane can be reduced to a single parameter. This parameter is a single value ranging from zero to one that corresponds with the relative location on the femur centreline, where zero is the most distal point and one is the most proximal. Note that the rotation around the x-axis influences the plane orientation in the y and z direction, and a rotation around the y-axis influences the orientation of the plane in the x and z direction. From this statement it can be concluded that all possible plane orientations can be achieved from a combination of x-axis and y-axis rotation alone. A single rotation parameter is introduced in order to allow for the proximal bony segments to rotate around the normal axis of the proximal osteotomy plane. To enable the translation of two bony segments relative to each other after osteotomy, two more parameters are needed to describe the translation in polar coordinates. One parameter describes the direction of translation perpendicular to the normal vector of the osteotomy plane in radians. The second parameter describes the magnitude of translation in mm of distance to the centre of the osteotomy plane. The parameters that describe the osteotomy wedge are visualized in Figure 1. This approach uses nine parameters to describe all possible unique osteotomies in twelve degrees of freedom in the global coordinate system .

2.2.1. Cost function and optimization

For optimization of the preoperative plan, the femoral shape after osteotomy needs to be quantified and combined with anatomical constraints in a global cost function. The femoral shape error is defined as the dissimilarity of the femoral centreline after osteotomy and the centreline of a given intramedullary nail. The postoperative configuration is compared to an intramedullary nail, as these are designed to resemble normal shaft anatomy. The dissimilarity of the shapes is calculated by multiplying the mean shortest distance between the shapes and the Hausdorff distance between the two shapes. This quantification of the dissimilarity is used as the cost function in the optimization of the preoperative plan. Both metrics are calculated as relation of the post-operative femur to intramedullary nail and intramedullary nail to post-operative femur, Equation 1, 2, 3.

$$d_H = d_{YX} + d_{XY} = \max_{y \epsilon Y} \min_{x \epsilon X} d(x,y) + \max_{x \epsilon X} \min_{y \epsilon Y} d(x,y) \quad (1)$$

$$d_{Mean} = \frac{\sum_{i=1}^{n} \min_{x \epsilon X} d(x,y)}{n} + \frac{\sum_{i=1}^{n} \min_{y \epsilon Y} d(x,y)}{n} \quad (2)$$

$$f_{CostShaft} = d_H * d_{Mean} \quad (3)$$

Where d(x,y) are the distances from all points on shape x to all points on shape y, $min_{x \epsilon X}$ are the smallest values of d(x,y) for all points on shape x, $min_{y \epsilon Y}$ are the smallest values of d(x,y) for all points on shape y. Shape x and y are the discrete representations of the centrelines of the femoral shaft and the intramedullary nail respectively.
The anatomical parameters mentioned previously are regarded constraints to the optimization problem. The optimization of the problem is twofold, in which for the first part constraints are considered additional objectives to the problem. In the second part the clinical anatomical indicators are handled as hard constraints.
The cost function is minimized using a genetic algorithm. In order to find the global optimal solution the clinical constraints should be handled in such a way that the constraints do not cause the optimization to quickly converge to a local optimum. Handling the constraints as additional objectives in a multi-objective optimization approach effectively accounts for this problem. Multi-objective optimization approaches aim to find a good approximation of the Pareto-front. Samples on the estimated Pareto-front however, hold solutions with constraint violations. Therefore, after achieving the Pareto-optimal solution the constraints are considered as a hard constraint to the cost function eliminating any solution that violates the constraints. This optimization is performed using the SMS-EMOA algorithm from the PyMOO Python module [10]. The hyper volume measure is used to find a good spread of samples on the Pareto front. A new generation of samples is generated by performing recombination. The fittest offspring is selected based on non-dominated sorting [11].

3. Results

14 patients, with a CT scan of the femur, were included for a total of 20 femora. One patient had a deformity secondary to hypophosphatasia, which caused local proximal varus deformity. 13 patients had polyostotic fibrous dysplasia. 14 femora where left sided and 6 femora right sided. 6 femora were smaller than 350 mm, and the mean leg length discrepancy was 20 mm (SD = 14.4 mm). 4 femora had a shepherds crook , and 2 femora had bowing without a clear centre of rotation of angulation. A single patient was diagnosed with Jaffe–Campanacci syndrome and received a diagnostic MRI. This patient was included in the secondary, versatility study.

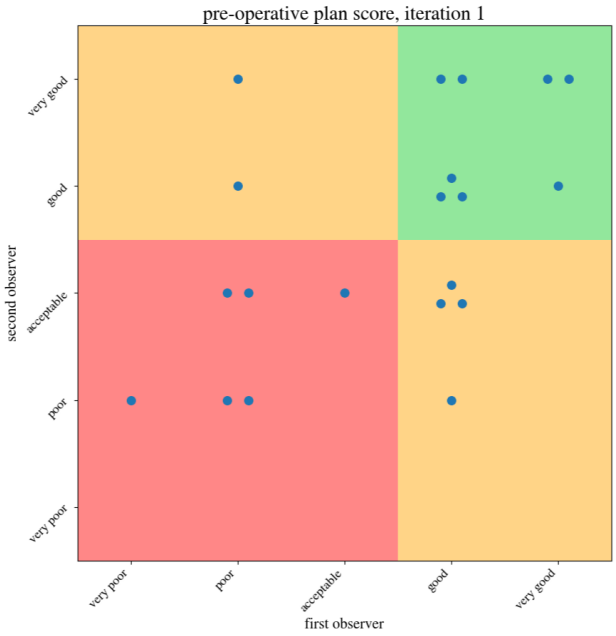

Figure 2: The individual assessment of the preoperative plans by two clinical experts. Each blue dot represents a single case. Points in the green zone are rated to be of good quality by both assessors. Points in the red zone are rejected by both assessors. Points in the yellow zone are rejected by one and accepted by the other assessor.

Overarching Question theme	Mean score
Adaptability of the model output	3.8
Clinical adoptability	4.0
Clinical decision making	4.5
Output quality	4.2

Table 2: The mean questionnaire scores from the user tests of the module

Cause of rejection	Number of cases
Extra osteotomy needed	13
Entrance location γ-nail	5
Bone healing	4
γ-nail fit	3

Table 3: The cause of rejection of preoperative plans and their prevalence divided in 4 categories

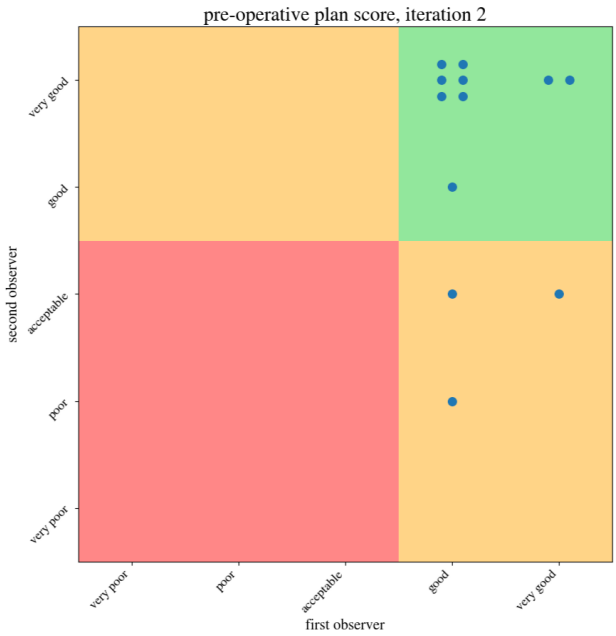

Figure 3: The individual assessment of the preoperative plans by two clinical experts. Each blue dot represents a single case. Points in the green zone are rated to be of good quality by both assessors. Points in the red zone are rejected by both assessors. Points in the yellow zone are rejected by one and accepted by the other assessor.

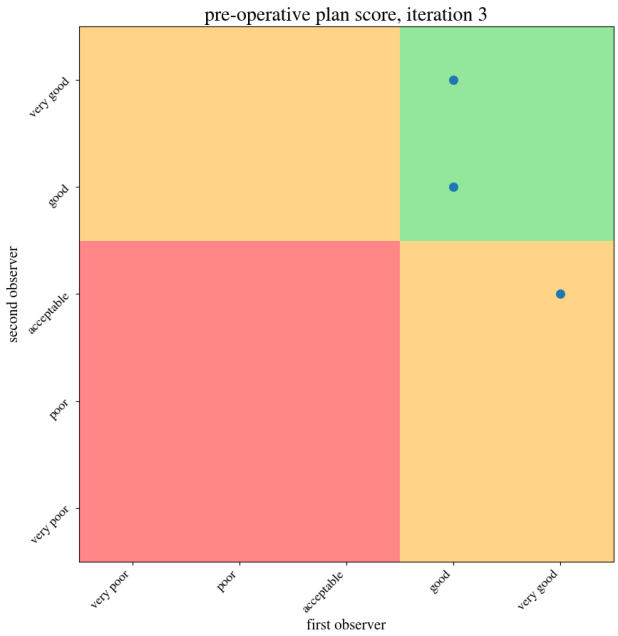

Figure 4: The individual assessment of the preoperative plans by two clinical experts. Each blue dot represents a single case. Points in the green zone are rated to be of good quality by both assessors. Points in the red zone are rejected by both assessors. Points in the yellow zone are rejected by one and accepted by the other assessor.

	Automatic/Manual /Difference	Planning Time [mm:ss]	FNSA [deg]	CAA [deg]	ATD [mm]	Femoral Length [mm]	Mean Wedge Height [mm]	Number of Osteotomies
Case 1	Automatic	08:09	125	12.1	1.8	338	4.9	single
	Manual	55:00	114	18.6	-3.7	336	3.1	single
	Difference	46:51	11	6.5	5.5	2	1.8	
Case 2	Automatic	08:08	121	8.6	13.5	390	5.1	single
	Manual	15:00	111	0.6	7.8	379	11.0	single
	Difference	06:52	10	8.0	5.7	11	5.9	
Case 3	Automatic	18:07	145	13.0	24.5	393	20.1	single
	Manual	65:00	133	5.9	16.1	396	11.3	double
	Difference	46:53	12	7.1	9.4	3	8.8	
Case 4	Automatic	09:09	133	13.2	25.7	457	6.3	single
	Manual	12:00	125	8.9	19.9	448	8.8	single
	Difference	02:51	8	4.3	5.8	9	2.5	
Mean	Automatic	10:53 (08:08 - 18:07)	131 (121 - 145)	11.7 (8.6 - 13.2)	16.4 (1.8 - 25.7)	395 (338 - 457)	9.1 (4.9 - 20.1)	
	Manual	36:45 (12:00 - 65:00)	121 (111 - 133)	8.5 (0.6 - 18.6)	10 (-3.7 - 19.9)	390 (336 - 448)	8.6 (3.1 - 11.3)	
	Difference	25:52 (2:51 - 46:53)	10 (8 - 12)	6.5 (4.3 - 8.0)	6.4 (5.5 - 8.4)	6 (2 - 11)	4.8 (1.8 - 8.8)	

Table 4: This table lists the time needed to produce the preoperative plans and summarizes the morphometric characteristics of the post-operative plan, as measured on the STL models using 3Matic. FNSA = femoral neck shaft angle, CAA = collum anteversion angle, ATD = articulo-trochanteric distance.

3.1. User test

The results showed that the mean score of two independent examiners within each category was 3.8 or higher. All mean results are found in Table 2. The complete filled in questionnaires are found in Appendix B. Interestingly, both clinicians strongly agreed with the statement: "The tool enables the creation of a preoperative plan with minimal technical expertise".

3.2. Subjective plan assessment

In first proposal, eight out of twenty preoperative plans were accepted by both examiners independently. Six out of twenty preoperative plans were rejected by one and accepted by the other. Six out of twenty preoperative plans were rejected by both examiners. One rejected preoperative plan was considered to have no surgery indication and was defined as lost to follow-up. This can be observed in Figure 2. The positive inter-observer agreement on accepting the plan is 0.57. The negative inter-observer agreement on rejecting the plan is 0.50. The total inter-observer agreement is 0.70.
The second iteration resulted in nine out of twelve preoperative plans being passed and three out of twelve preoperative plans being rejected by one and passed by the second, for a total acceptance of 16/20, Figure 3. The remaining three plans were evaluated a third time after recalculation of the preoperative plans, for a total acceptance of 18/20, Figure 4. A single preoperative plan was not accepted in three iterations because of an oblique cut with bad expected bone healing tendency.
Plans were rejected a total time of 25 times. Causes of rejection can be organized in 4 categories: 1) An extra osteotomy is needed for better anatomical results, 2) The entrance location of the gamma nail is not optimal, 3) The osteotomy location or obliqueness of the cut might result in delayed bone union, 4) The gamma nail does not fit the post-operative result. The reasons for rejection and their prevalence are summarized in Table 3.
Of the final 20 presented preoperative plans eight were accepted as a single wedge osteoteomy, seven cases were accepted as double wedge osteotomies and five cases were accepted as a single wedge osteotomy by one assessor and as a double wedge osteotomy by the second assessor.

3.3. Manual vs Automatic

The time needed for planning and the values of post-operative morphometric parameters are summarized in Table 4. The time needed to perform a manual planning is very widespread, ranging from 12 to 65 minutes. The time needed to perform the automatic planning ranges from 8 to 18 minutes. For all individual cases the automatic planning is performed faster than the manual planning. The time needed for creating a manual preoperative plan was designer specific. Where one assessor took 55 and 65 minutes respectively, the second assessor needed 15 and 12 minutes respectively to finish the preoperative plan. The designer of preoperative plan 1 and 3 took 357% times longer to complete its plans. The designer of plan 2 and 4 achieved to complete the preoperative plans in 57% more time than its automatic counterparts.
Concerning the clinical parameters, the FNSA and ATD are consistently larger in the automatic post-operative anatomy in comparison with the manual post-operative anatomy. The mean difference in anteversion angle between the two groups is 6.5 degrees. In the automatic optimization all CAAs are within the range of the anatomical normal. In the manual group for a single case the CAA is within the normal anatomical range. In a single case the manual preoperative pl an decides on a double osteotomy, where the automatic preoperative plan consists of a single osteotomy. The manual and automatic counterpart of the post-operative results of all four cases are visualized in Appendix C.

3.4. Model versatility

The MRI data of a single deformed femur was annotated and an STL created. This low resolution data was used to create a preoperative plan. The model provided a preoperative plan for the STL created with MRI data similarly to STL data created from CT scans. Bony landmarks such as the epicondyles, posterior condyles and trochanteric entry are more challenging to identify on these low resolution models. The results of the MRI model can be seen in Appendix D.
For a single femoral case of which the healthy side was present in the CT data an STL model was created and the centreline of this model was used to optimize the postoperative shape of the deformed femur. This gave comparable results to the use of an intramedullary nail as target shape. The visualization of the results are appended in Appendix E.

4. Discussion

The planning and surgery of multiplanar corrections of femoral bone deformity are highly complex. Preoperative planning software and interoperative surgery guidance are tools that the surgeon can use to achieve desired functional results. This study shows that the proposed algorithm can achieve the semi-automatic preoperative planning for a range of femoral deformities, including shepherds crook deformity and femoral bowing. It can also optimize morphometric characteristic correlated to patient function. Shape optimization bounded by clinical constraints, is a powerful method to semi-automatically generate preoperative plans that improve patient functional outcome.
By validation of two independent experts 90% of the preoperative plans was eligible for surgery. The preoperative planning of a single case was not established to be satisfactory. The created plan included an oblique cut that was considered undesirable for bone healing. The generated plan was however the only closed wedge solution to achieve gamma nail fit and conform to the clinical constraints. The oblique cut was introduced by the tool to achieve a normal CAA within the maximum rotation bounds. Manual planning would introduce a rotation of 36 degrees. Maximum rotation in the automated preoperative plan was set to 30 degrees. This bound is set to reduce rotation induced stress on nerves and vasculature. If

required bounds can be adjusted in this model.

Manual planning towards specific goals such as femoral length and collum anteversion is difficult as the measurements of these parameters can only be performed on the manually planned result. This results in an iterative process of design and check, which makes this process tedious and time-consuming. Furthermore the parameters are not independent. For example the influence of version osteotomy on valgization and valgus and varus osteotomy on version makes the planning of collum version a tedious process [12, 13, 14, 15].

Very limited research on the automatic computation of femoral osteotomy preoperative planning has been performed. Two papers developing and expanding on a software that automatically generates a planning for single and double osteotomy were released by the Helmholtz-Institute for Biomedical Engineering [16, 17]. The planning tool differs strongly from the one proposed in this study. Whereas the optimization of the proposed tool focuses on the shaft anatomy and the osteosynthesis after osteotomy, this is disregarded by the Schkommodau et al. who created a model in which the femur deformity is simplified to four measures: 1) length, 2) angulation, 3) anteversion, and 4) translation. The optimization of the osteotomy planes in their proposed model is based on normalizing these four values.

Carrillo et al. created a software for automated preoperative planning of forearm osteotomies [18]. Their study includes the optimization of a postoperative radius anatomy by minimizing the dissimilarity to a target shape and evaluating the fit of the osteosynthesis material. As the fit of the osteosynthesis says little about the radius anatomy, multiple functions are needed to quantify this, opposed to the single function of γ-nail fit. The antebrachii model optimizes the postoperative situation and calculates the osteotomy needed to achieve that result. The femur model from this study optimizes the osteotomy planes and the postoperative result is calculated from those planes. The method by Carillo et al. of finding the postoperative situation first is a feasible method for single osteotomies, but becomes increasingly challenging for multiple osteotomies. For single osteotomy the proximal and distal segment can be easily registered to the relative parts of their target shape to find the postoperative configuration. This is facilitated by the confinement of the proximal and distal segment at the humeroradial joint and the radiocarpal joint respectively. In multiple osteotomy there is no joint confinement for intermediate bony segments, which makes the registration of the post-operative configuration very challenging.

The shape optimization approach used in this study, is to minimize the dissimilarity of the femur STL model centreline and the centreline of a given gamma nail STL model. The intramedullary nail is selected as target shape, as deformity is often bilateral in systemic disease, and thus the healthy side cannot be mimicked. Besides this, intramedullary nailing is the preferred method of osteosynthesis after complex correction surgery [19, 20]. This method of deformity shape and target shape is highly versatile. A tool created in this study enables the planner to extract the centreline from any given oblong object STL model. The ability to use any deformity shape and target shape facilitates the use of healthy side optimization or similar centreline models to optimize the osteotomy of other bones.

A drawback of the model is that it currently cannot perform open wedge osteotomies or single cut osteotomies. The current model is designed to optimize shape using hybrid and closed wedge osteotomies. The hybrid wedges are mainly closed, meaning that the osteotomy always has 50% surface contact or more. In purely rotational deformity or a combined angulated and rotated deformity caused by malunion after fracture, the most common correctional osteotomy is the single and double oblique cut osteotomy. These osteotomies have the advantage of preserving vascularization and bony volume with large bone surface contact. The planning of the oblique rotational osteotomy is challenging [21]. Note that by parametrization an oblique rotational osteotomy is identical to a rotational closed wedge osteotomy with an infinitely thin wedge. With minor changes to the model it is able to generate pre-operative plans for oblique cut rotational osteotomies, with only four parameters per cut: 1) x tilt, 2) y tilt, 3) relative bone location, 4) rotation. An open wedge osteotomy is mathematically identical to a closed wedge osteotomy in which a single cut is performed at the distal plane and the distal plane is transformed to align with the proximal plane.

The model can fully autonomously generate a preoperative plan with up to 3 osteotomies. The tool does become significantly slower if a solution with 3 osteotomies is calculated. To speed up this process and make the final solution more robust, the planner can manually indicate a region that must be included in an osteotomy wedge. This however reduces some of the creative freedom of the model.

The user test and qualitative testing show that this tool has the potential to support the clinician with the lack of CAD experience with planning an osteotomy. Besides this, it is a powerful tool that aides an experienced technician in generating a preoperative plan within predefined clinical bounds. However, it should be noted that it is challenging to prove the superiority of surgery with preoperative planning, over freehand surgery. Whereas the improvement of cut accuracy is demonstrated, there is only limited evidence that the use of preoperative planning in complex femoral deformity improves the functional outcome of the patient [9, 22]. The tool described in this article automatically calculates the FNSA, femoral length, mechanical axis deviation and CAA, to provide the surgeon with a functional outcome prediction. No significant deviation of these morphometric parameters in the automatic and manual group can be determined as of the low power of the case demonstration.

For validation the measurement of the angles is performed for automatic and manual cases in identical ways. The measurement of the CAA in 3Matic is performed by measuring the angle between two planes perpendicular to the axial bone view. In this view the most posterior part of the greater trochanter is in line with the posterior condyles. This method of calculating the CAA is not a standardized procedure. More commonly the CAA is extracted as the angle between the posterior condyles and the collum in the axial slices of a CT scan with

a specifically designed collum version protocol. Measuring the anteversion angle in 3Matic using this method, has a significantly improved inter and intra-observer correlation, compared to the axial slice method. Cai et al. still observed a maximum one-sided deviation to the true anteversion angle of 1.39 degrees [23].
The generation of three dimensional data from two orthogonal radiographs is a promising method to reduce radiation dose in a mostly young population. Alternatively there is a feasibility for using MRI scans. For anatomically normal patients the generation of three dimensional bone models is feasible, using generic bone models [24]. For pathological anatomy this is more challenging. However as only single coordinates are needed for the computations of this model manual or automatic extraction of the bony landmarks from orthogonal radiographs might be a feasible solution to reduce radiation dose [25]. However, as there is no 3D model of the femur available, the design of cutting guides is not possible and execution of the preoperative plan must be executed using navigation.
Future research should be focussed on optimization of the algorithms architecture improving the speed of the algorithm and its convergence to a global optimal solution. Besides this, the addition of more morphometric constraints such as mechanical knee axis, FNSA, ATD and femoral offset can aide in achieving a preoperative plan that restores functional aspects of the femoral anatomy. This is valuable to maximize the likelihood of patient function improvement. Furthermore, the algorithm can be adapted to allow the generation of open wedge osteotomy and single cut rotational osteotomy. The algorithms method of minimizing dissimilarity of the postoperative shape and a given target shape, enables the exploration of the use of the proposed algorithm in other deformed bones.

5. Conclusion

In this study a novel method for semi-automatic preoperative planning optimization is presented. The optimization is driven by minimizing the dissimilarity of the postoperative femoral shape and a given target shape, within the bounds of clinical constraints.
The results of the user tests show that the method of planning within the constraints of clinical parameters and the instant feedback of morphometric parameters in the post-operative anatomy, support the clinician in decision making while planning a surgery. The quality of the output is good and the assessors see a future for implementation of the model.
During validation of the quality of the preoperative plans, the low positive and negative inter-observer agreement, of respectively 0.57 and 0.50, show that scoring a preoperative plan is a subjective measure. Eighteen of twenty cases were accepted in a maximum of three iterations. From this, it can be concluded that the model can generate preoperative plans of sufficient quality that are tailored to the wishes of the clinical expert. One can conclude that the model enables a technician with minimal clinical expertise to create feasible preoperative plans. For all cases less time was needed to generate a preoperative plan semi-automatically in comparison with their manual counterparts. Besides this, the questionnaire reveals that the tool enables clinicians to create a preoperative plan with minimal expertise.
Using the semi-automatic osteotomy planning tool, much less time is needed to create a preoperative plan. The plans created using the software had an FNSA closer to the anatomical position with a larger ATD. A larger ATD results in the lengthening and thus the biomechanical efficiency improvement of the gluteus musculature. The mean CAA difference of 6.5 degrees is very large considering that the normal ranges from 8-15 degrees. In 3 out of 4 cases of the manual group, the CAA was not within this range. In the automatic group all 4 cases had a post-operative CAA within the normal anatomical range. This large discrepancy compared to the automatic planning shows the difficulty of planning the anteversion angle manually.
In summary, the automatic planning tool is a promising aide to both technicians and clinicians for fast preoperative planning within the boundaries of anatomical normal ranges. The addition of mechanical knee axis, ATD, FNSA and femoral offset as morphometric constraints might improve the generated planning, to optimize the likelihood of patient functional improvement. The implementation of single cut rotational osteotomies and open wedge osteotomies as well as the introduction of other bones are promising future steps to diversify the use of the planning tool.

References

[1] Jun Wan, Can Zhang, Yu-Peng Liu, and Hong-Bo He. Surgical treatment for shepherd's crook deformity in fibrous dysplasia: THERE IS NO BEST, ONLY BETTER. *International Orthopaedics*, 43(3):719–726, March 2019.

[2] Hae-Ryong Song, V. V. J. Soma Raju, Satish Kumar, Seok-Hyun Lee, Seung-Woo Suh, Jung-Ryul Kim, and Jun-Seok Hong. Deformity correction by external fixation and/or intramedullary nailing in hypophosphatemic rickets. *Acta Orthopaedica*, 77(2):307–314, April 2006.

[3] P. C. Brunelli and P. Frediani. Surgical treatment of the deformities of the long bones in severe osteogenesis imperfecta. *Annals of the New York Academy of Sciences*, 543:170–179, 1988.

[4] Turgut Akgül, Cengiz Şen, Halil İbrahim Balci, and Gökhan Polat. Double intertrochanteric osteotomy for trochanteric overgrowth and a short femoral neck in adolescents. *Journal of Orthopaedic Surgery (Hong Kong)*, 24(3):387–391, December 2016.

[5] Ilhan A. Bayhan, Oussama Abousamra, Kenneth J. Rogers, Michael B. Bober, Freeman Miller, and William G. Mackenzie. Valgus Hip Osteotomy in Children With Spondyloepiphyseal Dysplasia Congenita: Midterm Results. *Journal of Pediatric Orthopedics*, 39(6):282–288, July 2019.

[6] Maartje E. Meier, Natasha M. Appelman-Dijkstra, Michael T. Collins, Raya E. S. Geels, Robert P. Stanton, Pieter Bas de Witte, Alison M. Boyce, and Michiel A. J. van de Sande. Coxa Vara Deformity in Fibrous Dysplasia/McCune-Albright Syndrome: Prevalence, Natural History and Risk Factors: A Two-Center Study. *Journal of Bone and Mineral Research: The Official Journal of the American Society for Bone and Mineral Research*, 38(7):968–975, July 2023.

[7] S. M. Sangavi, G. Szöke, D. W. Murray, and M. K. Benson. Femoral remodelling after subtrochanteric osteotomy for developmental dysplasia of the hip. *The Journal of Bone and Joint Surgery. British Volume*, 78(6):917–923, November 1996.

[8] Shinsuke Omori, Tsuyoshi Murase, Toshiyuki Kataoka, Yohei Kawanishi, Keiichiro Oura, Junichi Miyake, Hiroyuki Tanaka, and Hideki

Yoshikawa. Three-dimensional corrective osteotomy using a patient-specific osteotomy guide and bone plate based on a computer simulation system: accuracy analysis in a cadaver study. *The international journal of medical robotics + computer assisted surgery: MRCAS*, 10(2):196–202, June 2014.

[9] Roy Gigi, Yair Gortzak, Juan Barriga Moreno, Eran Golden, Ronnie Gabay, Netta Rumack, Moshe Yaniv, Solomon Dadia, and Eitan Segev. 3D-printed Cutting Guides for Lower Limb Deformity Correction in the Young Population. *Journal of Pediatric Orthopedics*, 42(5):e427–e434, June 2022.

[10] J. Blank and K. Deb. pymoo: Multi-objective optimization in python. *IEEE Access*, 8:89497–89509, 2020.

[11] Nicola Beume, Boris Naujoks, and Michael Emmerich. SMS-EMOA: Multiobjective selection based on dominated hypervolume. *European Journal of Operational Research*, 181(3):1653–1669, September 2007.

[12] Lukas Jud, Lazaros Vlachopoulos, Thomas V. Häller, Sandro F. Fucentese, Stefan Rahm, and Patrick O. Zingg. The impact of mal-angulated femoral rotational osteotomies on mechanical leg axis: a computer simulation model. *BMC musculoskeletal disorders*, 21(1):50, January 2020.

[13] Raymond W. Liu, Paul Toogood, Daniel E. Hart, Dwight T. Davy, and Daniel R. Cooperman. The effect of varus and valgus osteotomies on femoral version. *Journal of Pediatric Orthopedics*, 29(7):666–675, 2009.

[14] B. P. Sangeorzan, R. P. Judd, and B. J. Sangeorzan. Mathematical analysis of single-cut osteotomy for complex long bone deformity. *Journal of Biomechanics*, 22(11-12):1271–1278, 1989.

[15] Sung Soo Kim. Three-dimensional Effect of the Single Plane Proximal Femur Osteotomy. *Hip & Pelvis*, 27(1):23–29, March 2015.

[16] Erik Schkommodau, Alexander Frenkel, Peter Belei, Bettina Recknagel, Dieter-C. Wirtz, and Klaus Radermacher. Computer-assisted optimization of correction osteotomies on lower extremities. *Computer Aided Surgery: Official Journal of the International Society for Computer Aided Surgery*, 10(5-6):345–350, 2005.

[17] P. Belei, E. Schkommodau, A. Frenkel, T. Mumme, and K. Radermacher. Computer-assisted single- or double-cut oblique osteotomies for the correction of lower limb deformities. *Proceedings of the Institution of Mechanical Engineers. Part H, Journal of Engineering in Medicine*, 221(7):787–800, October 2007.

[18] Fabio Carrillo, Simon Roner, Marco von Atzigen, Andreas Schweizer, Ladislav Nagy, Lazaros Vlachopoulos, Jess G. Snedeker, and Philipp Fürnstahl. An automatic genetic algorithm framework for the optimization of three-dimensional surgical plans of forearm corrective osteotomies. *Medical Image Analysis*, 60:101598, February 2020.

[19] Xiaoqi Zhang, Xifu Shang, Yaofei Wang, Rui He, and Guoguang Shi. Intramedullary nailing for fibrous dysplasia of lower limbs. *Oncology Letters*, 4(3):524–528, September 2012.

[20] Ernesto Ippolito, Pasquale Farsetti, Roberto Caterini, Enrico Micciulli, Giulio Gorgolini, and Laura Ruzzini. Intramedullary Nailing for Lower Limb Polyostotic Fibrous Dysplasia in Children: A Long-term Follow-up Study. *Journal of Pediatric Orthopedics*, 42(5):e492–e500, June 2022.

[21] Johannes G. G. Dobbe, Simon D. Strackee, and Geert J. Streekstra. Minimizing the Translation Error in the Application of an Oblique Single-Cut Rotation Osteotomy: Where to Cut? *IEEE transactions on bio-medical engineering*, 65(4):821–827, April 2018.

[22] Yotam Portnoy, Jonathan Koren, Amal Khoury, Shai Factor, Solomon Dadia, Yuval Ran, and Amit Benady. Three-dimensional technologies in presurgical planning of bone surgeries: current evidence and future perspectives. *International Journal of Surgery (London, England)*, 109(1):3–10, January 2023.

[23] Zhencun Cai, Chengzhe Piao, Tianyu Zhang, Lianyong Li, and Liangbi Xiang. Accuracy of CT for measuring femoral neck anteversion in children with developmental dislocation of the hip verified using 3D printing technology. *Journal of Orthopaedic Surgery and Research*, 16(1):256, April 2021.

[24] P. Gamage, S. Q. Xie, P. Delmas, and W. L. Xu. Diagnostic radiograph based 3D bone reconstruction framework: application to the femur. *Computerized Medical Imaging and Graphics: The Official Journal of the Computerized Medical Imaging Society*, 35(6):427–437, September 2011.

[25] B. Guenoun, F. Zadegan, F. Aim, D. Hannouche, and R. Nizard. Reliability of a new method for lower-extremity measurements based on stereoradiographic three-dimensional reconstruction. *Orthopaedics & traumatology, surgery & research: OTSR*, 98(5):506–513, September 2012.

Appendix A. Clinical parameters

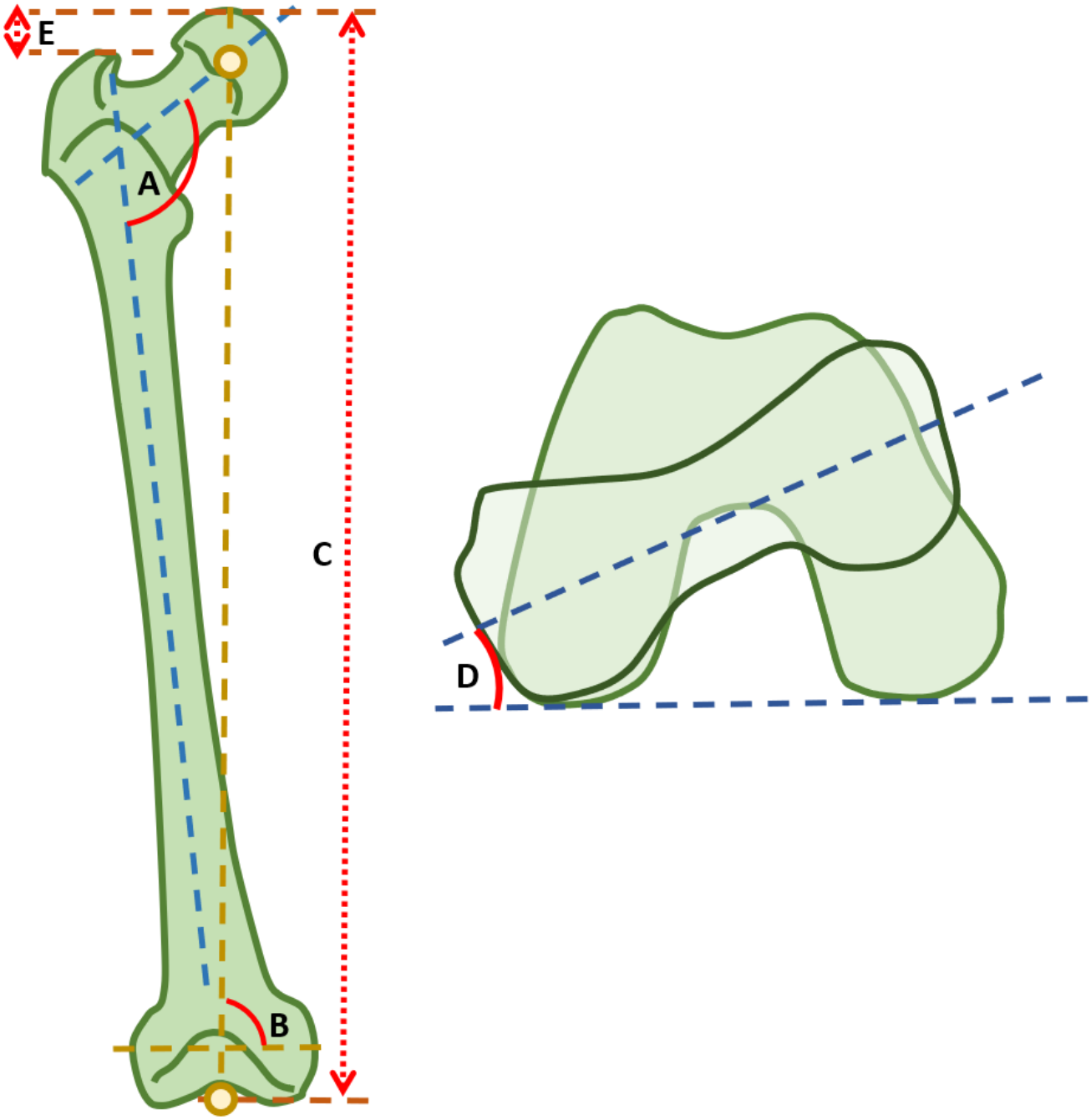

Figure A.5: An overview of functional clinical parameters of the femur. A) FNSA, the angle between femoral collum and femoral shaft, B) Femoral part of mechanical axis, the angle between the epicondylar axis and the line through the centre of the knee joint and the caput centre, C) Femoral length, the distance between the knee joint and the centre of the caput plus the caput radius, D) CAA, the angle between the posterior condylar axis and the femoral collum in the axial view, E) ATD, the distance between the greater trochanter tip and the top of the caput femoris. FNSA = femoral neck shaft angle, CAA = collum anteversion angle, ATD = articulo-trochanteric distance.

Appendix B. Workflow questionnaire

Question	Category	Score 1	Score 2
The tool enables the creation of a pre-operative plan with minimal technical expertise	2	5	5
By altering parameters one can easily manipulate the model outcome	1	3	4
The clinical femur specific parameters generated by the model help with the assessment of the pre-operative plan	3	4	5
The pre-operative plan generated using the model are viable	4	4	5
The plans generated by the model are predictable	1	4	5
The use of the model is intuitive	2	4	3
The visualizations of the model output are insightful	3	5	4
Unfeasible results can be ruled out easily by defining input parameters	1	3	4
It is clear which steps should be performed in order to acquire feasible results	2	4	3
Based on the model output a good decision can be made on whether a plan is clinically acceptable	3	4	5
I would use or recommend the model in a future clinical situation	4	3	5

Table B.5: The full questionnaire and the response of two clinical experts. Category 1) Adaptability of the model, 2) Clinical adoptability, 3) Clinical decision making and visualization, 4) Output quality

Appendix C. Manual vs automatic results

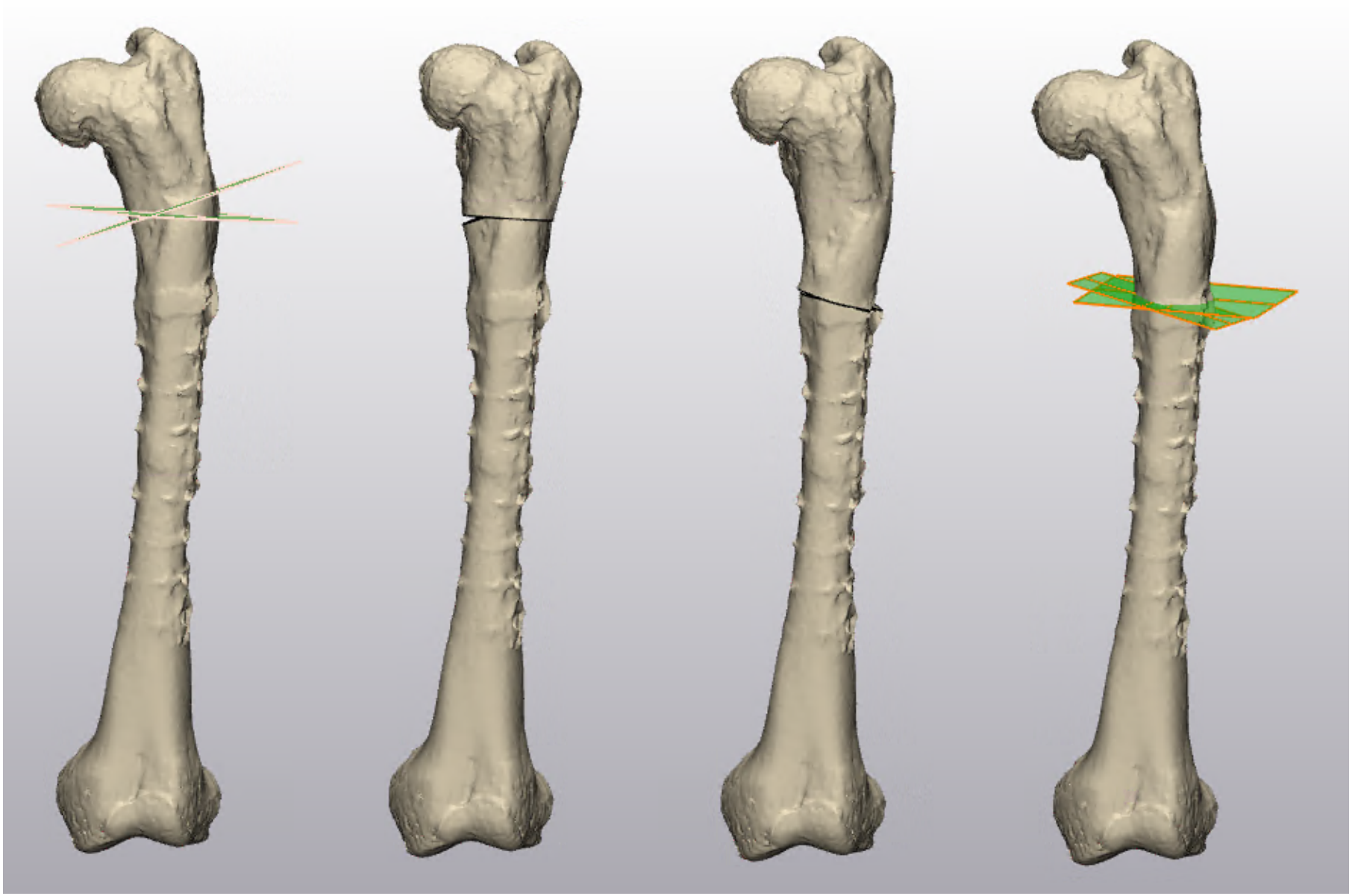

Figure C.6: From left to right the automatic pre-operative plan, the automatic post-operative outcome, the manual post-operative outcome and the manual pre-operative plan, of case 1 in antero-posterior view

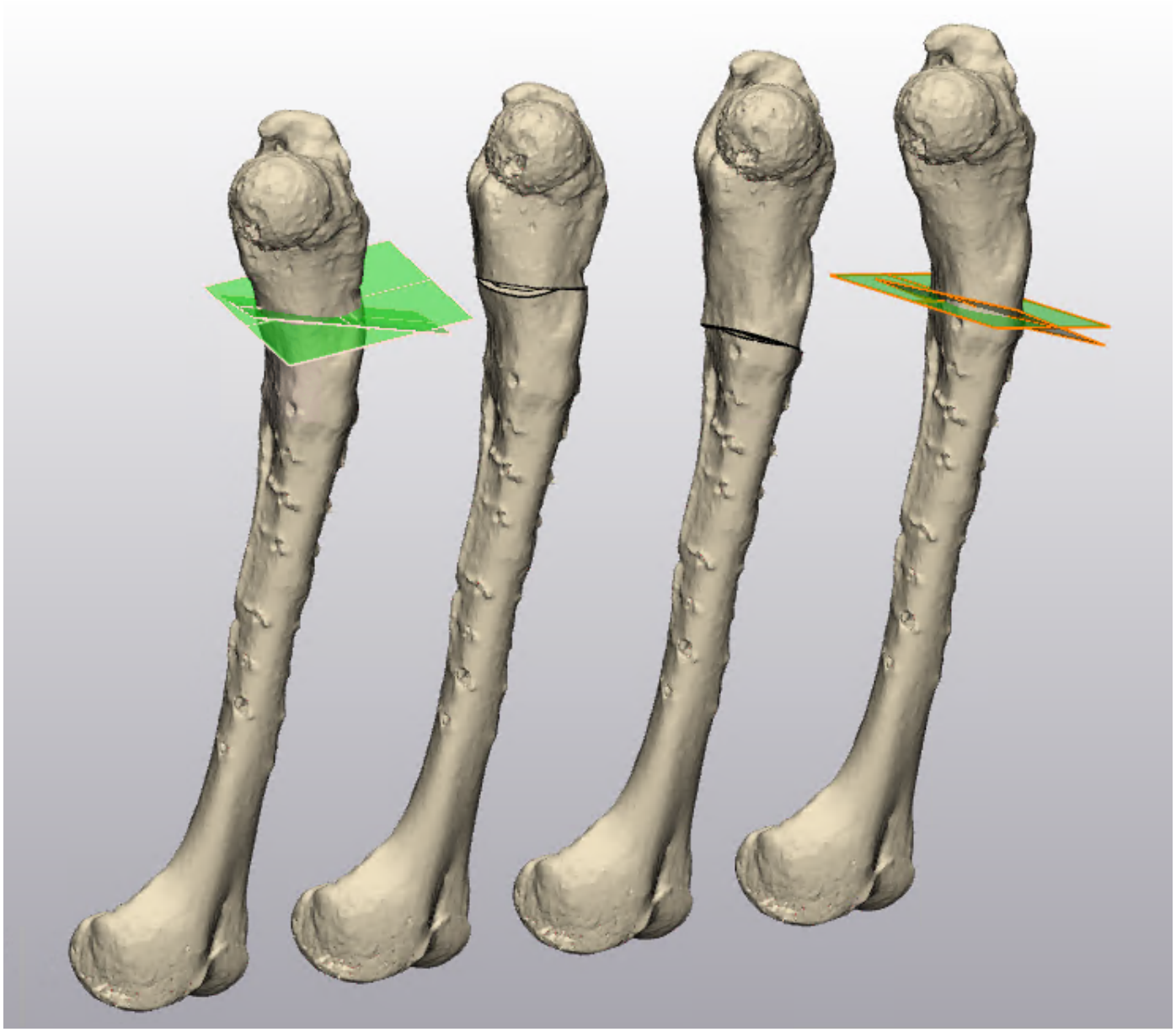

Figure C.7: From left to right the automatic pre-operative plan, the automatic post-operative outcome, the manual post-operative outcome and the manual pre-operative plan, of case 1 in medio-lateral view

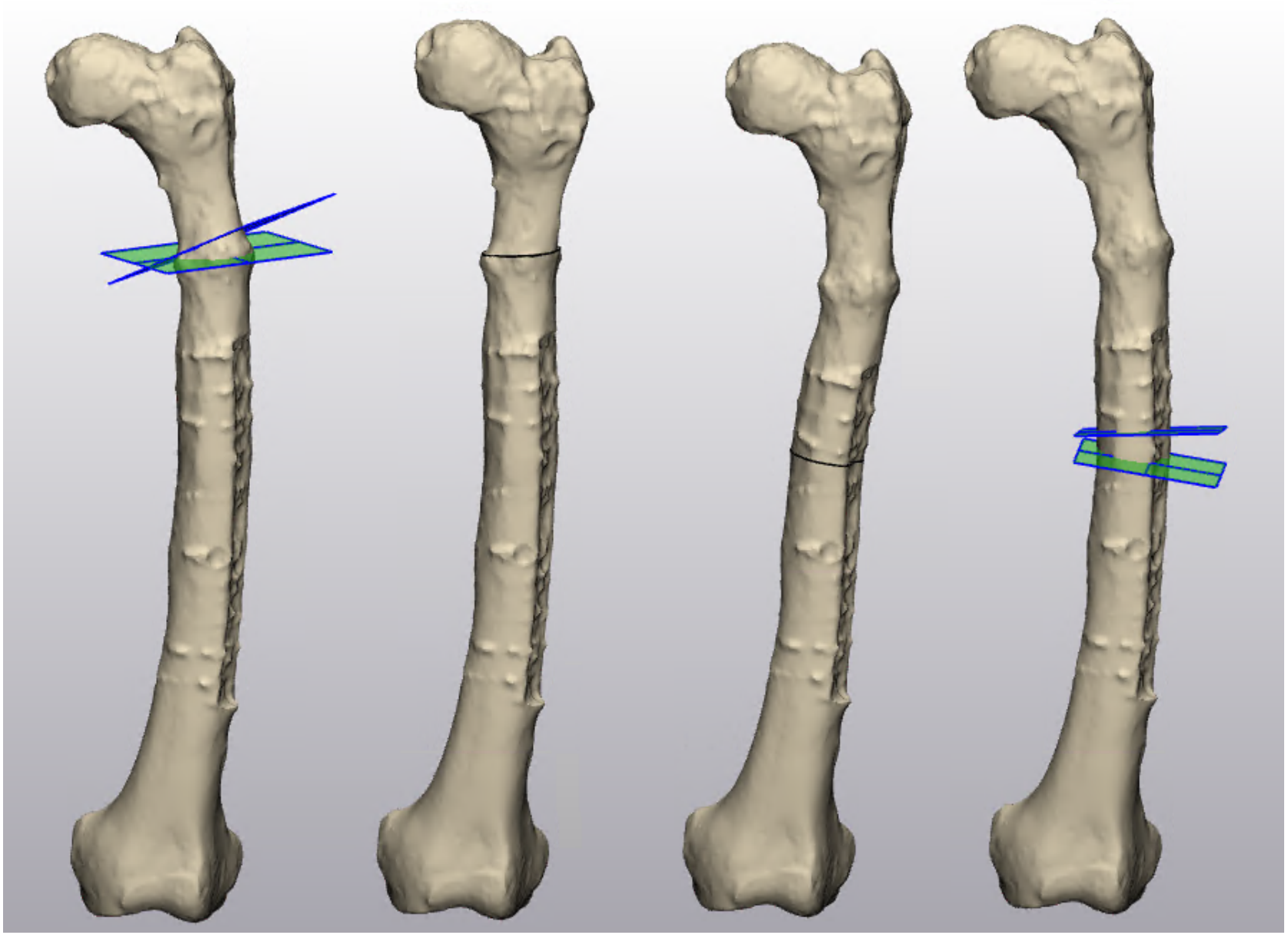

Figure C.8: From left to right the automatic pre-operative plan, the automatic post-operative outcome, the manual post-operative outcome and the manual pre-operative plan, of case 2 in antero-posterior view

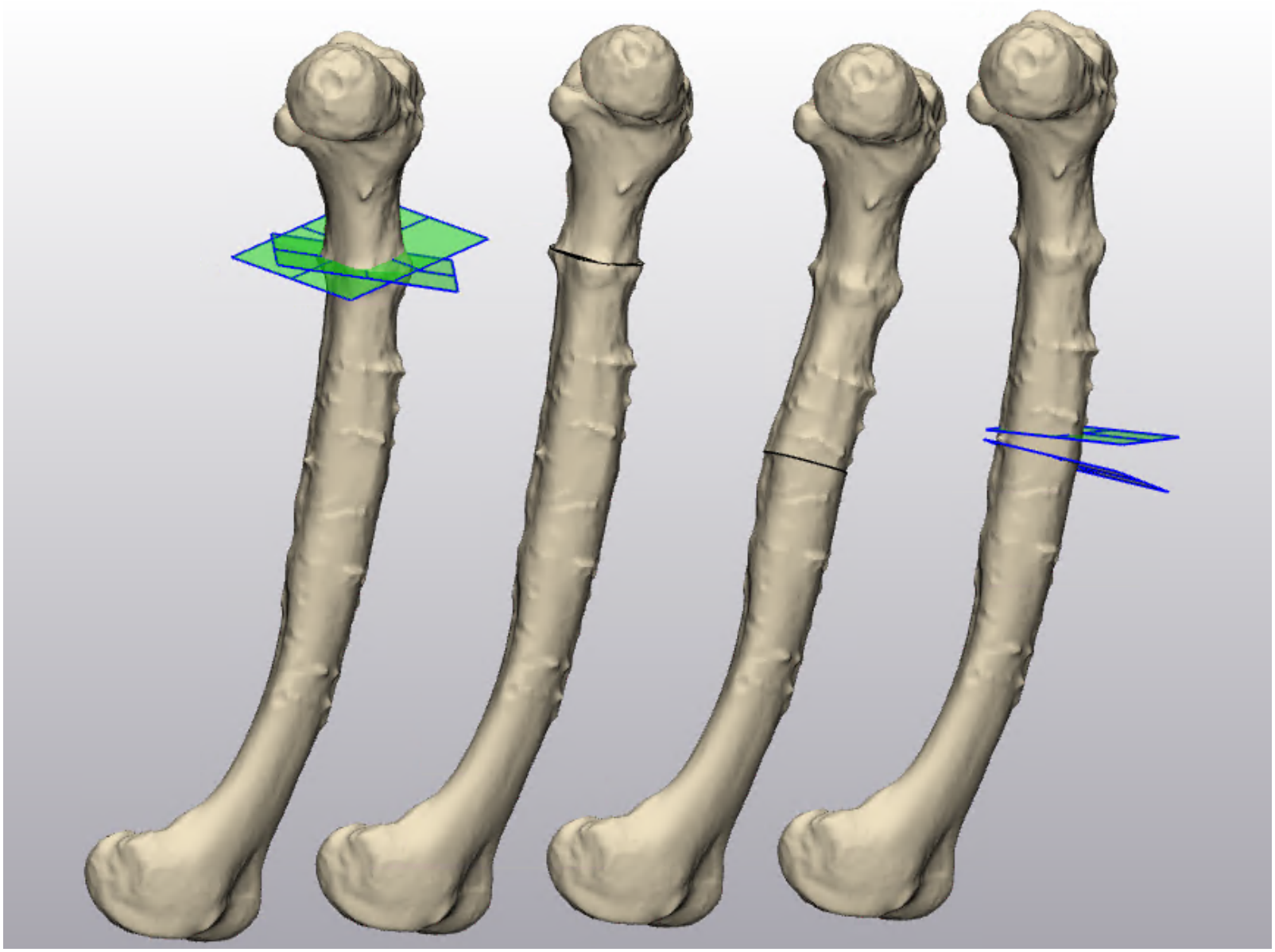

Figure C.9: From left to right the automatic pre-operative plan, the automatic post-operative outcome, the manual post-operative outcome and the manual pre-operative plan, of case 2 in medio-lateral view

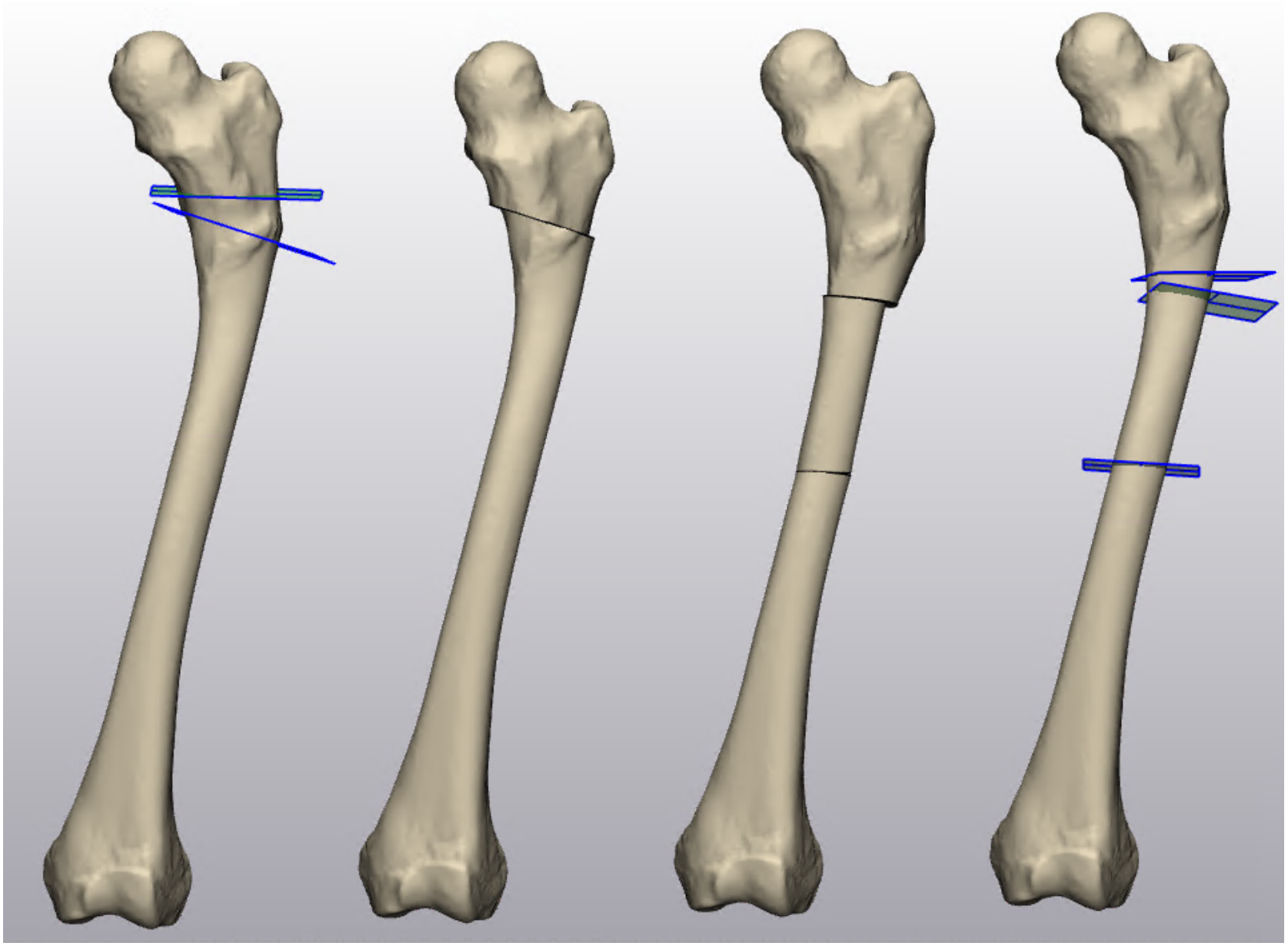

Figure C.10: From left to right the automatic pre-operative plan, the automatic post-operative outcome, the manual post-operative outcome and the manual pre-operative plan, of case 3 in antero-posterior view

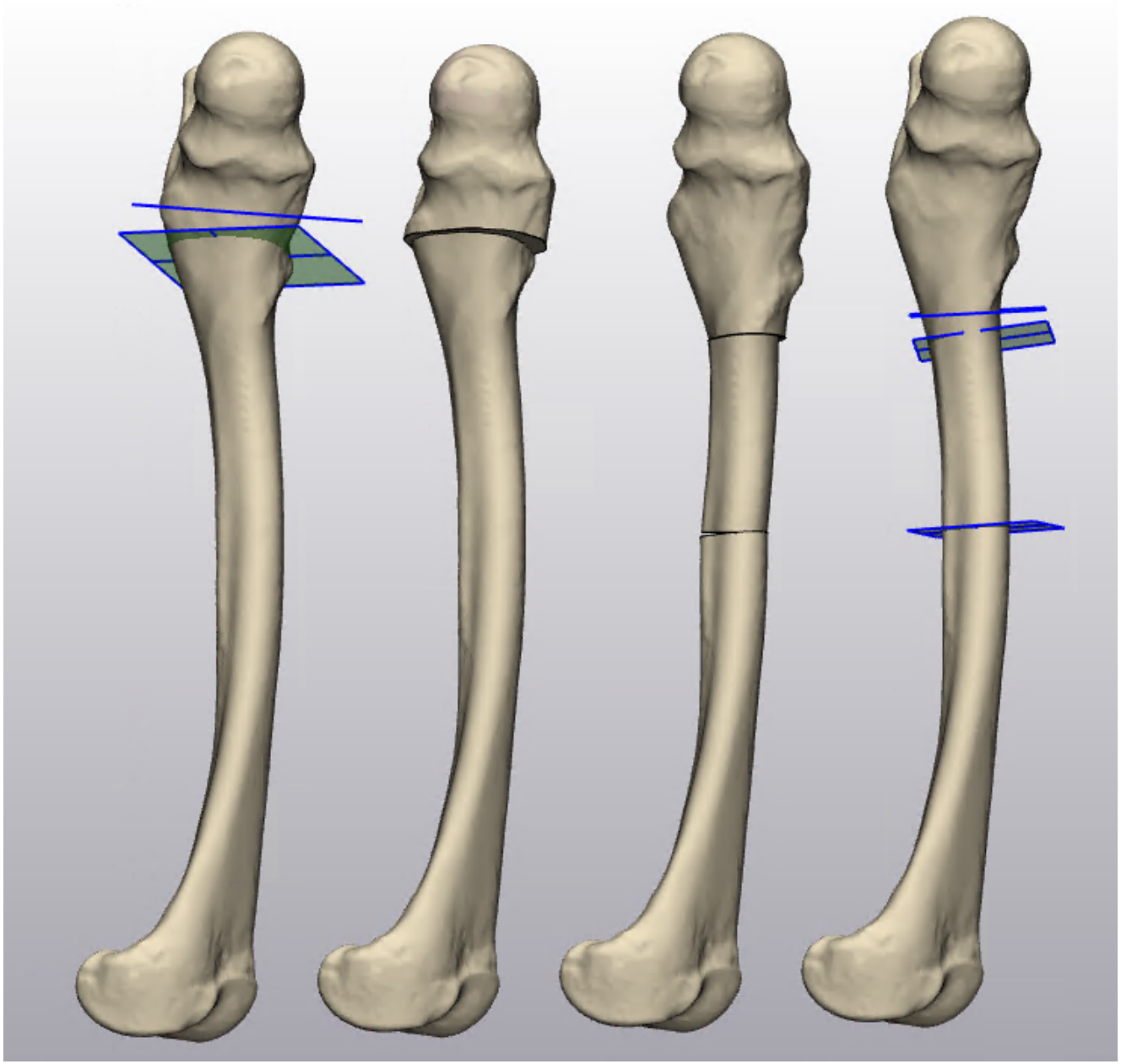

Figure C.11: From left to right the automatic pre-operative plan, the automatic post-operative outcome, the manual post-operative outcome and the manual pre-operative plan, of case 3 in medio-lateral view

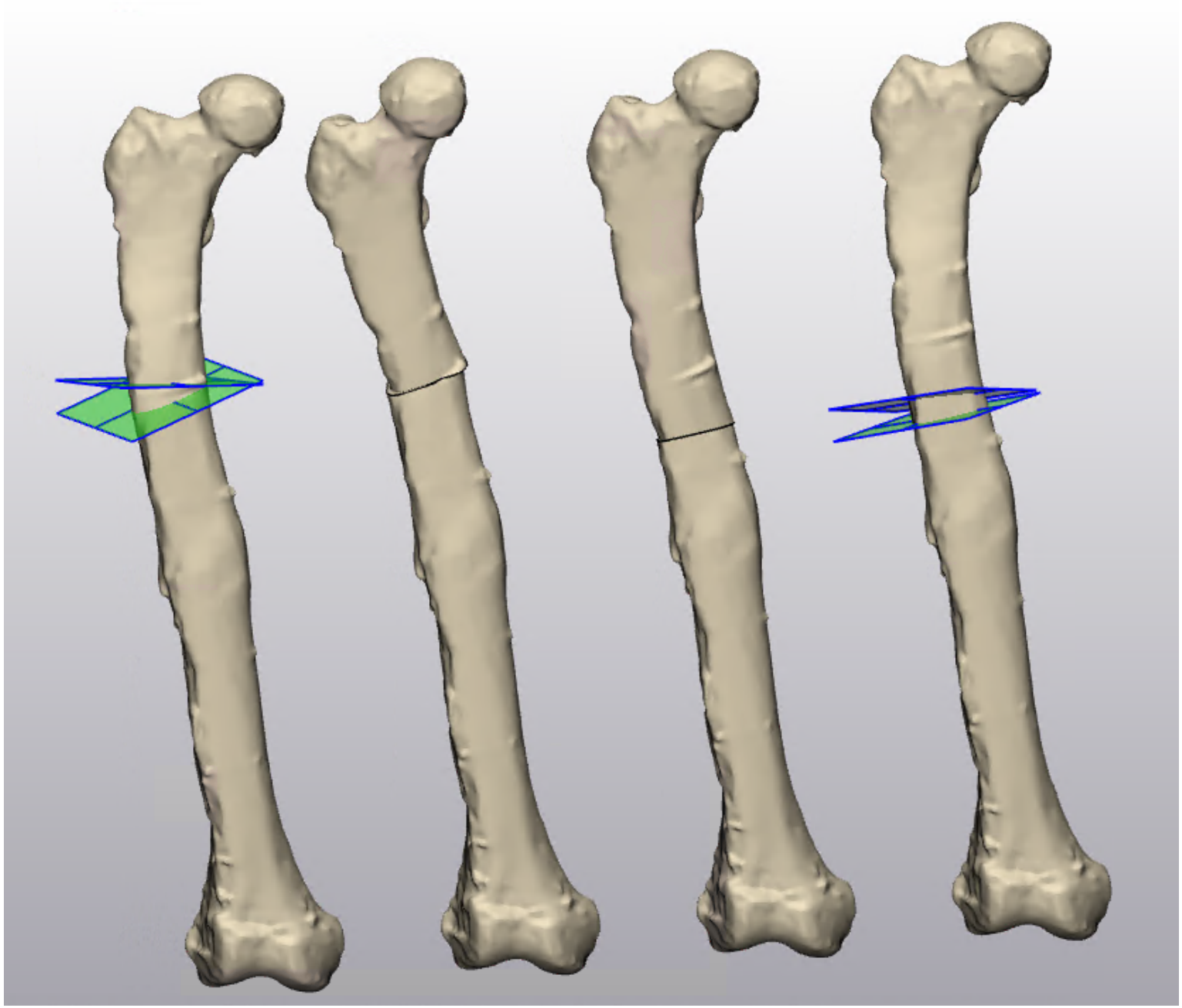

Figure C.12: From left to right the automatic pre-operative plan, the automatic post-operative outcome, the manual post-operative outcome and the manual pre-operative plan, of case 4 in antero-posterior view

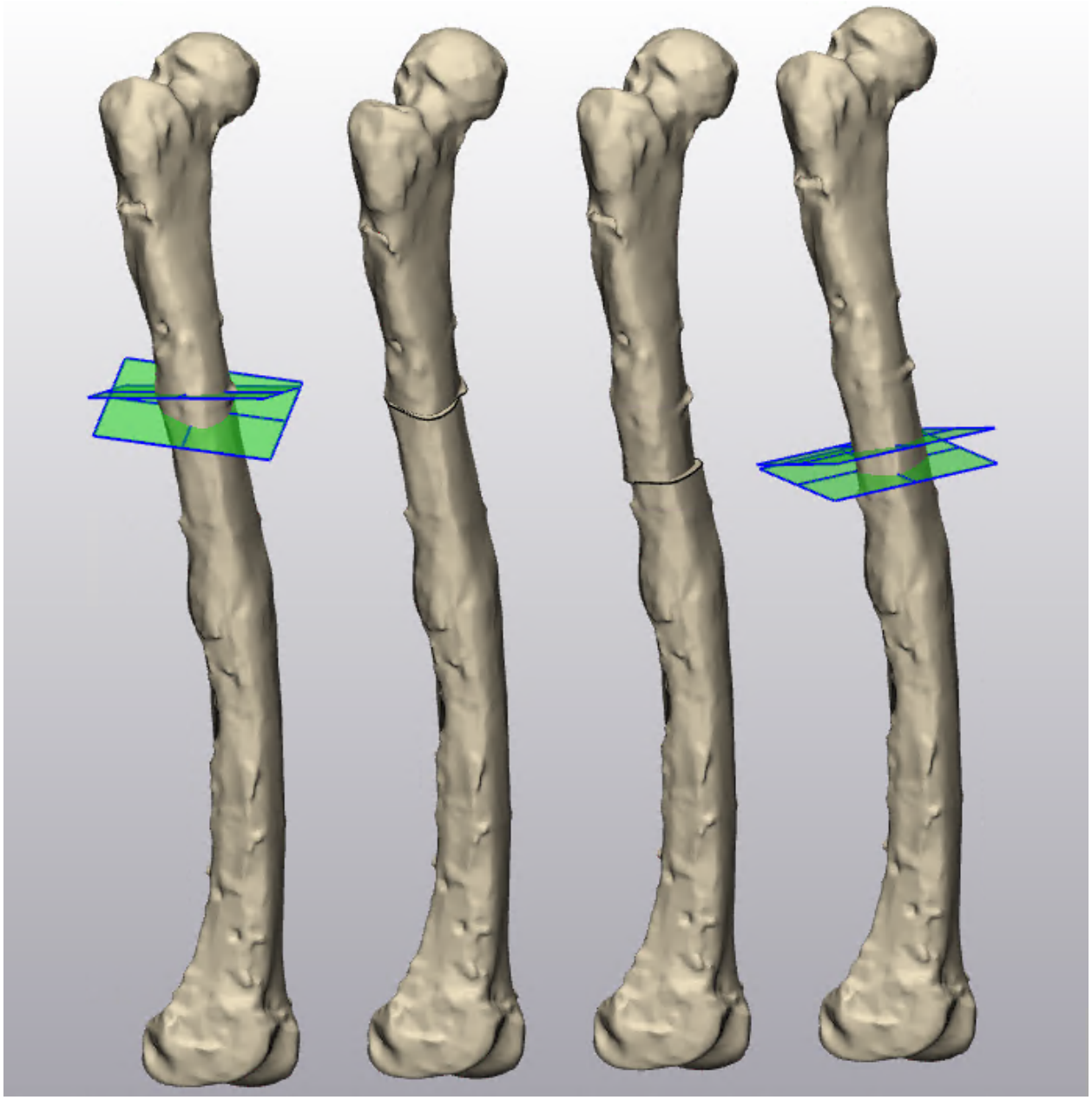

Figure C.13: From left to right the automatic pre-operative plan, the automatic post-operative outcome, the manual post-operative outcome and the manual pre-operative plan, of case 4 in medio-lateral view

Appendix D. MRI case outcome

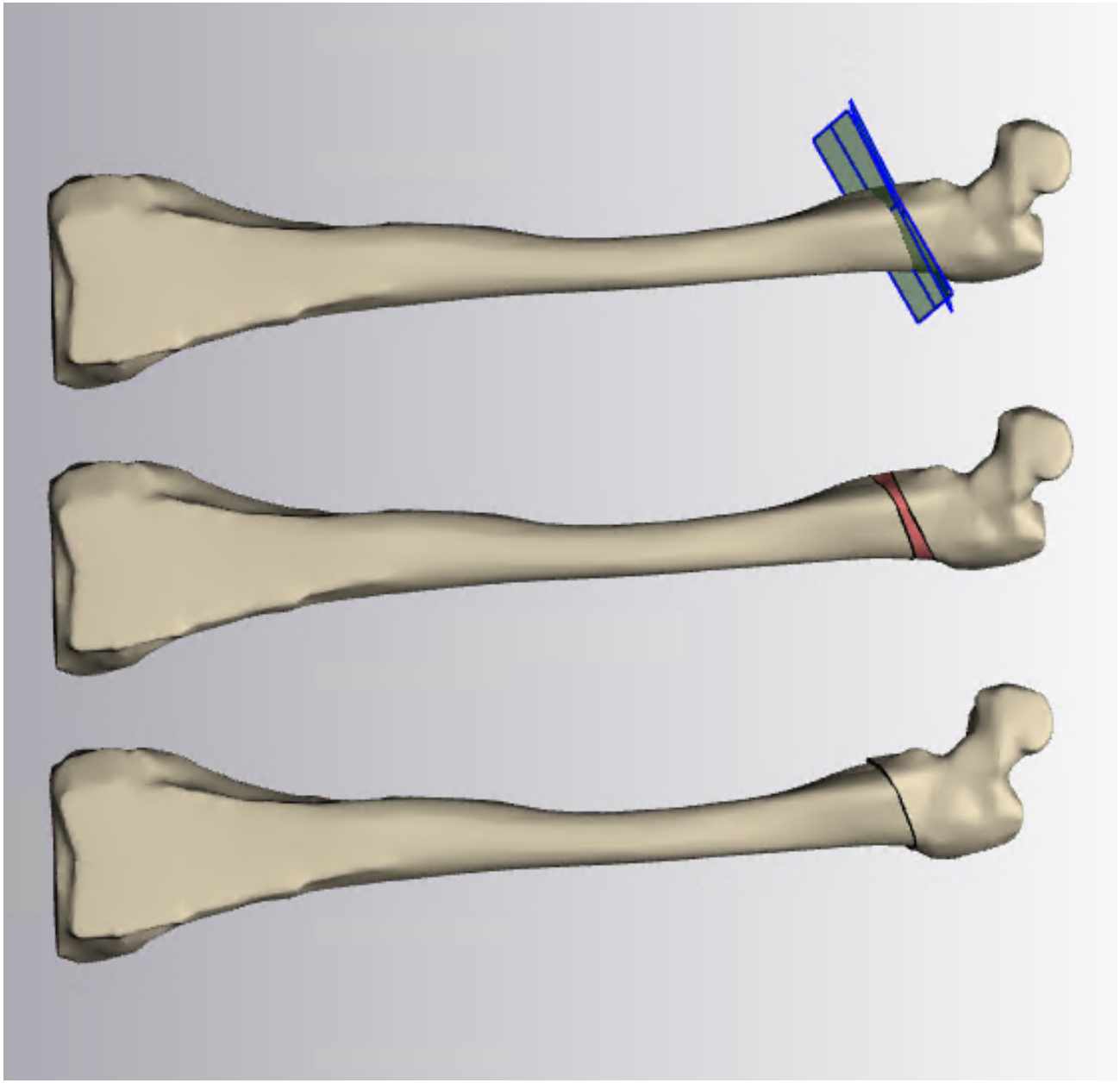

Figure D.14: From left to right the automatic pre-operative plan, the automatic intra-operative situation and the post-operative outcome of the automatic plan in antero-posterior view

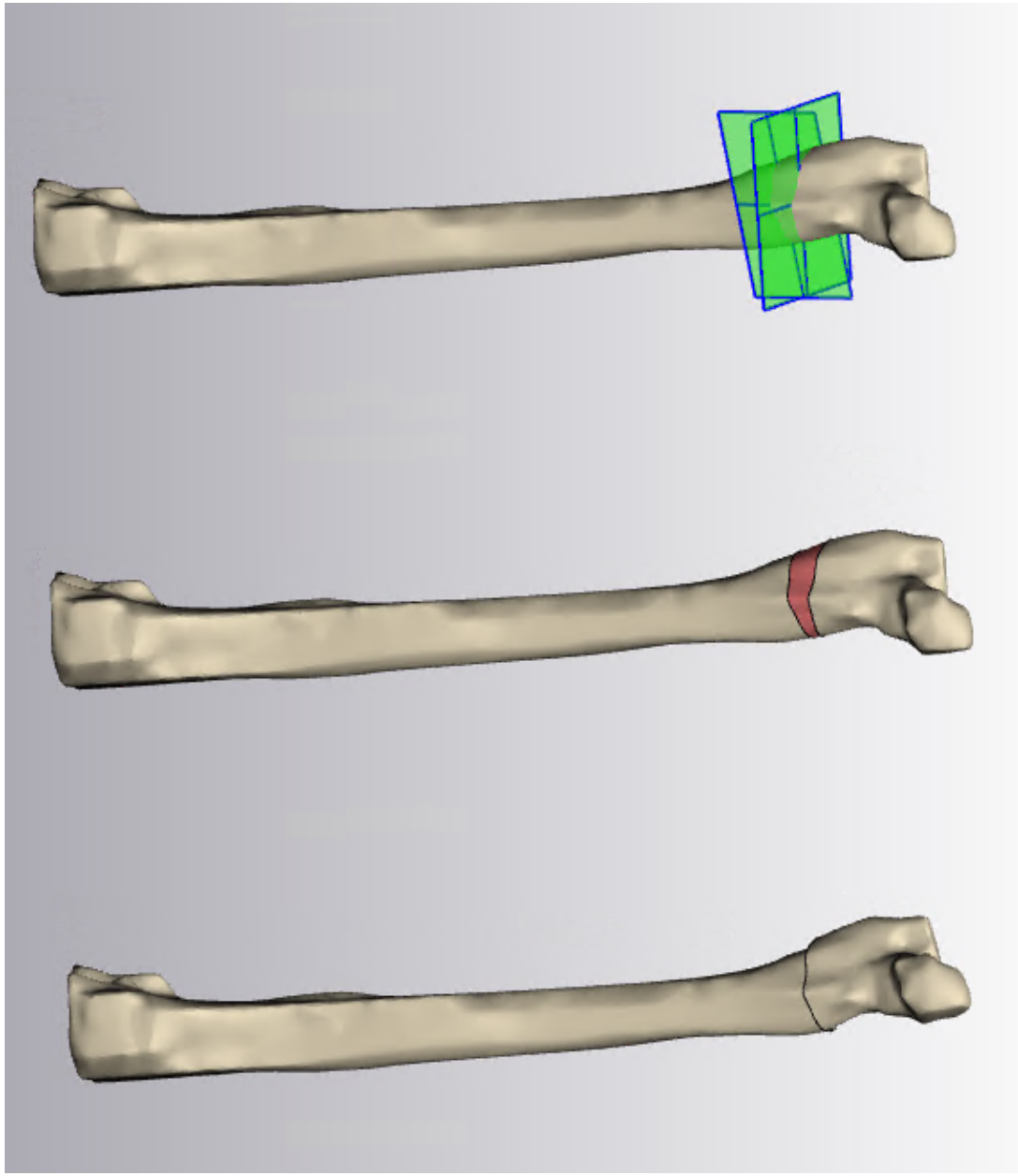

Figure D.15: From left to right the automatic pre-operative plan, the automatic intra-operative situation and the post-operative outcome of the automatic plan in medio-lateral view

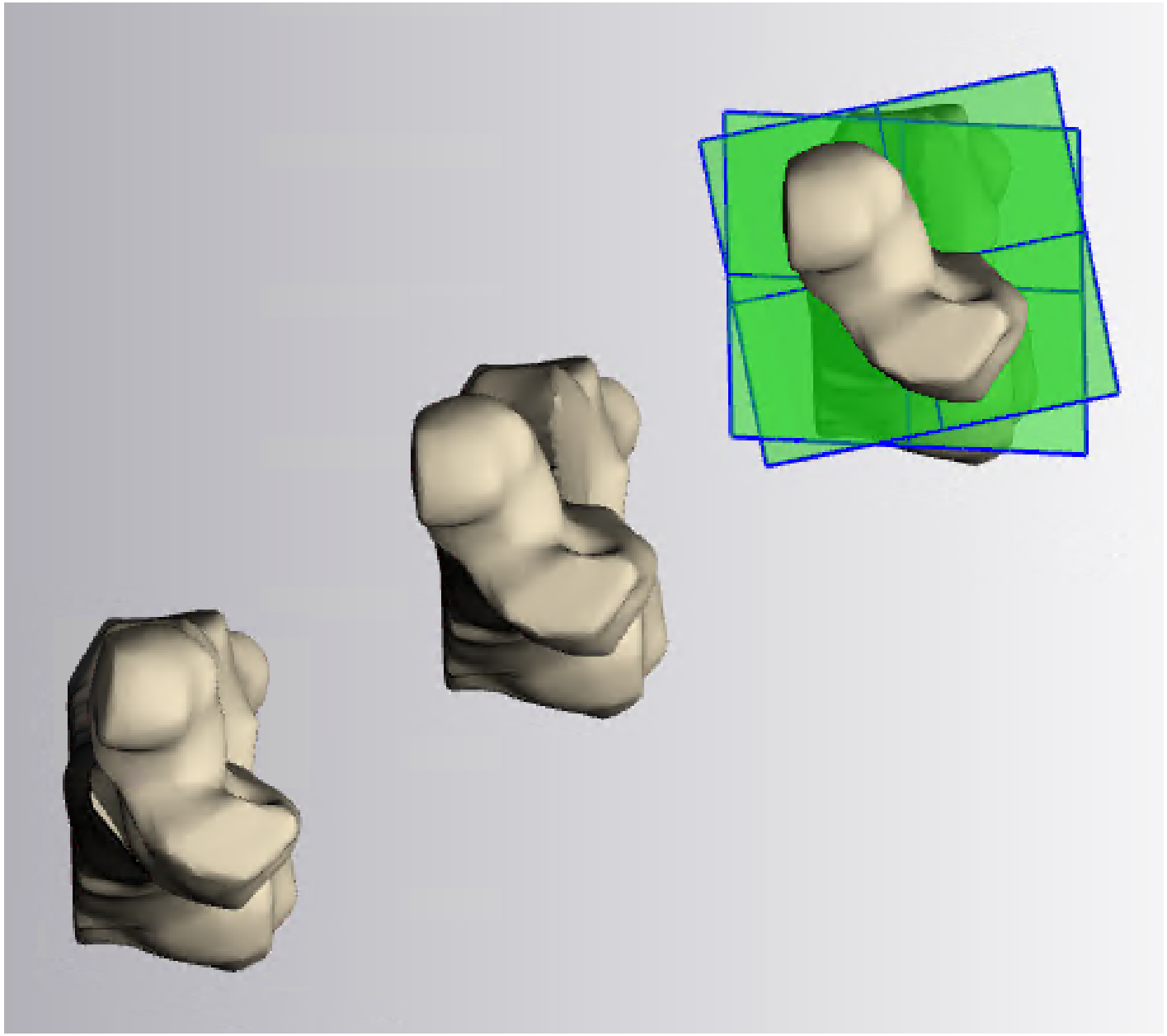

Figure D.16: From left to right the automatic pre-operative plan, the automatic intra-operative situation and the post-operative outcome of the automatic plan in cranio-caudal view

Appendix E. Healthy side target shape

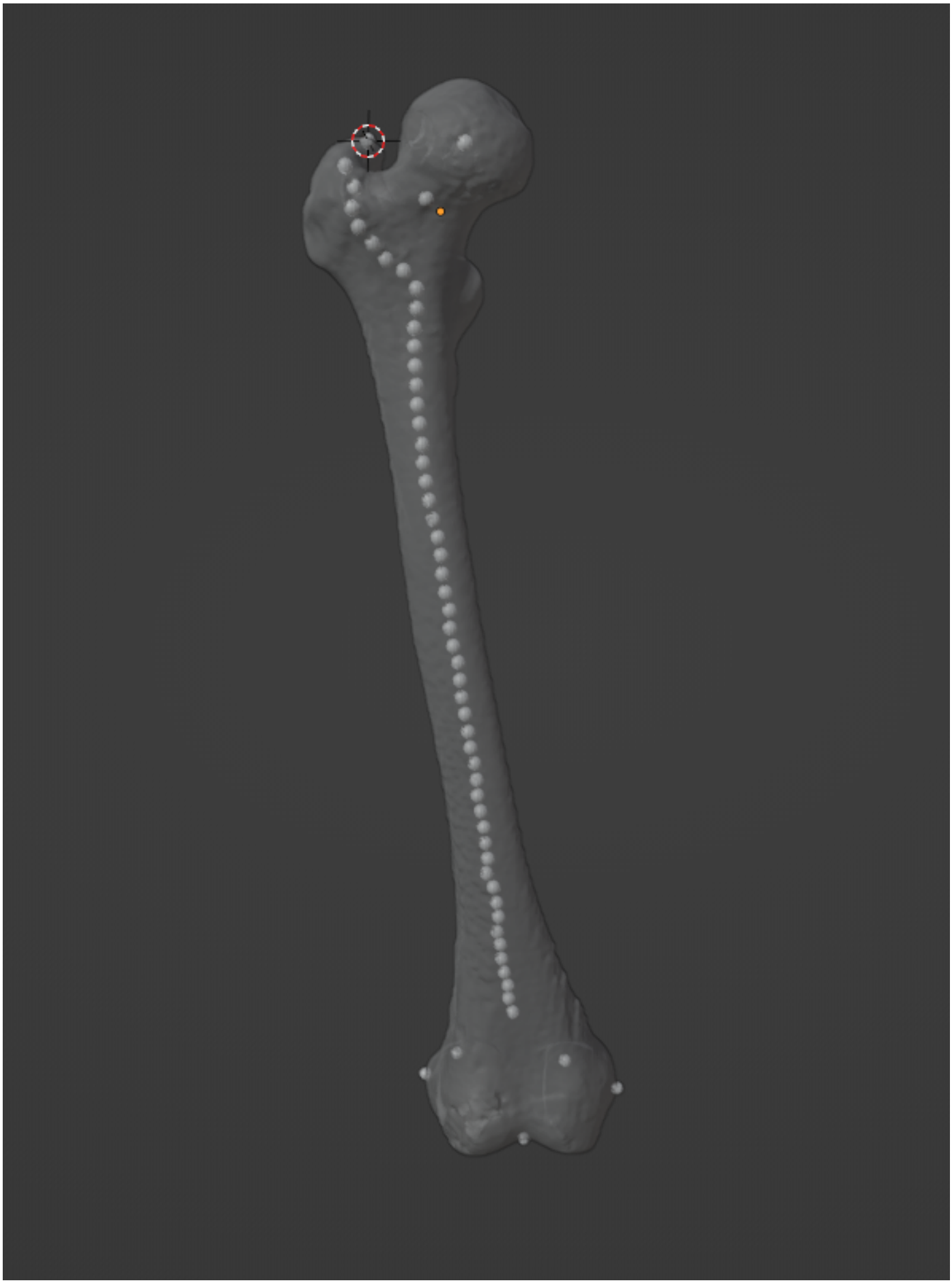

Figure E.17: The transparant STL model of the healthy side. The extracted centreline is visualized using spheres

Figure E.18: The centreline of the healthy femur is mirrored and used as target shape. The preoperative plan is visualized using planes

Figure E.19: The post-operative result is visualized with transparent bony pieces. The mirrored centreline of the healthy side is visualized in the post-operative result

2 Technical document

In this document the several technical aspects of the proposed software solution are mentioned in more detail in order to provide clarity on development choices made based on clinical and technical aspects.
Current techniques for preoperative planning of femoral osteotomy, both manual and automatic, are focussed on finding the centre of rotation of angulation (CORA) and the angle at the CORA at which to correct (1). In some clinical cases however there is no clear CORA present, such as in femoral bowing. In the CORA and angulation approach the assumption is made that there is a single angulation with an angle in x and y direction. In this approach the target shape of the femur is a straight line and the rotational deformity is not taken into account. These assumptions are oversimplifications of the problem. Therefore, a new approach is considered in which a deformity shape and a target shape are defined. The deformity shape is defined as the preoperative centreline. The target shape is the centreline of a given intramedullary nail. By modelling a wedge osteotomy the deformity shape is changed to represent the postoperative situation of the centreline.
The shaft anatomy post osteotomy is quantified as the fit of an intramedullary nail in the post operative configuration, making the intramedullary nail the target shape to mimic. This idea originates from the fact that intramedullary nails are designed to fit the bone of an anatomically normal femur. Fitting the shape of the femur post osteotomy to a target shape makes it a versatile optimization, as changing to a different target shape will lead to a different generated preoperative plan.
Multiple issues arise when finding the optimal osteotomy location based on nail fit. Most important questions are: 1) How to define mathematical definitions for performing an osteotomy, 2) How to register nail and femur in three dimensional space to calculate shape dissimilarity, 3) What mathematical measure to use to define shape dissimilarity, 4) How to find femoral landmarks needed to calculate the latter two, 5) How to optimize the function parameters to minimize the shape dissimilarity between the post-operative bone and the target shape.

Table of Contents

2.1 Femoral landmarks

In order to achieve the generation of preoperative plans that optimize an anatomical postoperative shaft position and morphometric characteristics. The calculation of these measures have to be performed during optimization. Morphometric measures as well as anatomical shaft configuration are calculated from several bony landmarks. The process to determine these bony landmarks is as follows. Based on the annotation of a few bony femoral regions the landmarks are automatically estimated. The estimation is visualized by dots that appear on the femoral STL model. These dots can then be manually adjusted in order to achieve the best possible characterization of the specific femur model. These landmarks are than saved to an excel file from which they are read and used for the optimization of the surgical plan. Landmarks used for determining target shape dissimilarity are the centreline, the collum axis of the femur and the entrance location of the gamma nail in the femur. To calculate anteversion, femoral length and mechanical axis additional required bony landmarks are the epicondylar axis, the posterior condylar axis and a distal point that represents knee joint location.

2.1.1. Centreline

The approximation of the femoral shaft centreline is an iterative process that requires the input of the general location of the femoral head and the greater trochanter. By subtracting the sphere that represents the caput plus a margin from the femur model, the general shape of the femoral shaft remains. Starting from the most distal point of the shape a large sphere (r = 150 mm) intersects with the femoral shaft. The centre of gravity of the intersecting coordinates is considered to be the initial guess of the first coordinate of the centre line. The vector between the past coordinate and the initial guess is used to generate a new sphere that intersects with the femoral shaft. The centre of gravity of these coordinates is considered to be the best guess for a coordinate on the centreline. This process is repeated until the intersection sphere intersects with the greater trochanter. This process is also visualized in Figure 1.

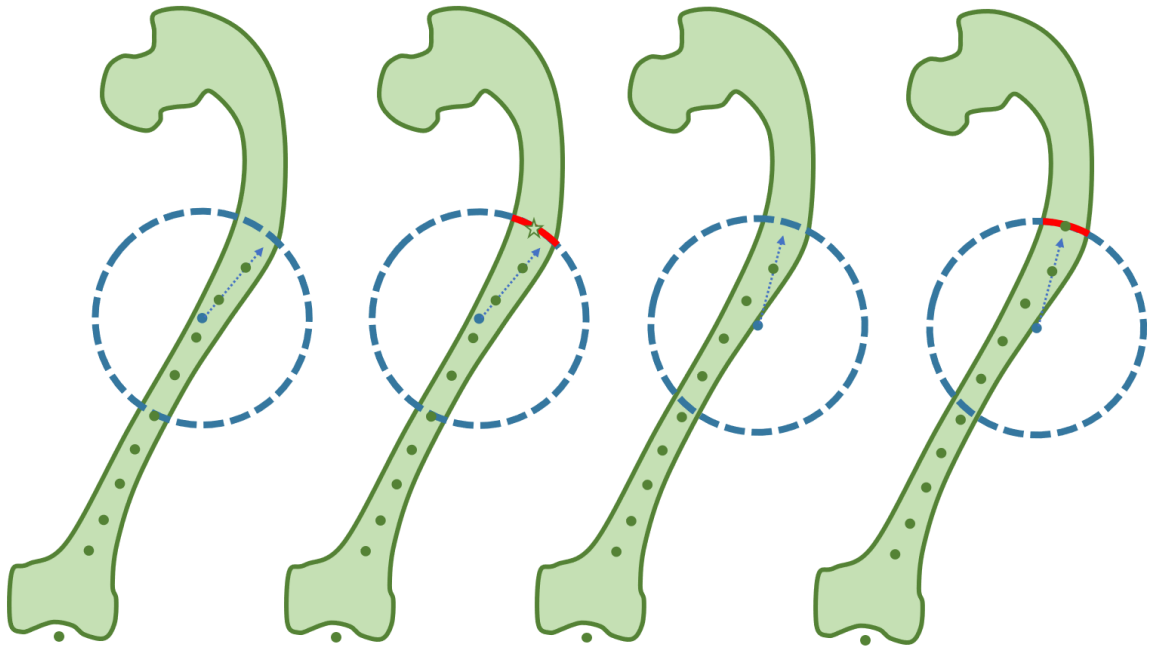

Figure 1: The iterative process of finding the centreline of an oblong object. From left to right: 1) Draw a sphere with a large diameter and direction in line with the slope of the most proximal two coordinates. 2) calculate the mean of the intersecting coordinates. This is the initial guess, 3) draw a sphere with large diameter in the direction of the last known centre coordinate and the initial guess, 4) calculate the mean of the intersecting coordinates. This is the new centreline coordinate.

Completing this iterative process results in a good estimate of the centreline with relatively few datapoints. Now that the general shape of the centreline is found, new datapoints can be interpolated from the known datapoints. These points are generated by creating planes that intersect with the femur in between two datapoints. The normal of the plane is in line with the vector spanned by the two surrounding datapoints. This process is visualized in Figure 2.

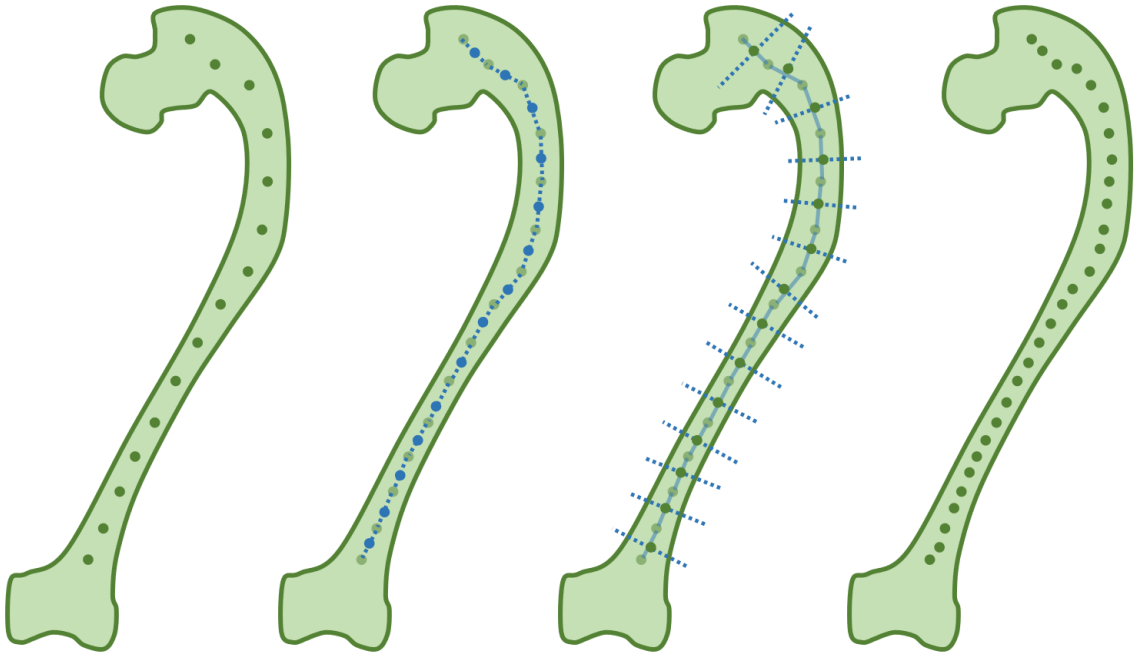

Figure 2: The interpolation algorithm for a given low sampling frequency centreline. From left to right: 1) An image of the low sampling frequency centreline, 2) The mean of every two centreline coordinates is calculated, 3) Lines perpendicular to the local centreline slope and through these mean points are drawn, 4) The mean of the intersecting coordinates with the planes are added to the centreline.

2.1.2 Greater trochanter

The greater trochanter is an important bony landmark in the placement of the intramedullary nail. The user is prompted to select a region in which the greater trochanter is present. The distance from each of the coordinates in this region to the most proximal coordinate of the centreline is calculated. The coordinate that is furthest from the centreline is considered to be the most proximal bony edge and thus the location of the tip of the greater trochanter.

2.1.3 Posterior condylar axis

The user is prompted to select two regions that encase the lateral and the medial condyle respectively. The single coordinate from each of these regions that is the most posterior and thus has the lowest global y-coordinate value is considered the posterior condyle point. The vector spanned from the medial to the lateral posterior condylar point is considered the posterior condylar axis.

2.1.4 Epicondylar axis

The epicondylar axis, is similarly extracted from the annotated regions mentioned in the previous paragraph. However, instead of finding the largest y-coordinate value, the coordinates are projected on the posterior condylar axis by performing a dot product. The highest negative and positive values are considered to be the medial and lateral epicondyle respectively.

2.1.5 Distal point

The distal point is a single coordinate that is used to represent the centre of the knee joint. The coordinate is calculated by taking the datapoint furthest from the most distal point of the centreline within the medial and lateral condylar region. These coordinates represent the most distal point of the femoral condyles. The mean of these two coordinates is defined as the distal point.

2.1.6 Caput centre and caput radius

The user selects a region that encompasses the femoral head. The mean of these coordinates is the centre of the caput. The mean distance from the centre to the coordinates within the region is the radius of the caput.

2.1.7 Collum axis

To define the collum axis a centreline through the collum should be calculated. This is done by generating several spheres with incrementing size from the caput centre with diameter slightly larger than the caput radius. For each sphere the mean of the intersecting coordinates is considered to be a point on the collum centreline. The mean of these coordinates is the middle of the collum centreline. The collum axis is the vector spanned between the collum centre and the caput centre. The process of acquiring the collum axis is visualized in Figure 3.

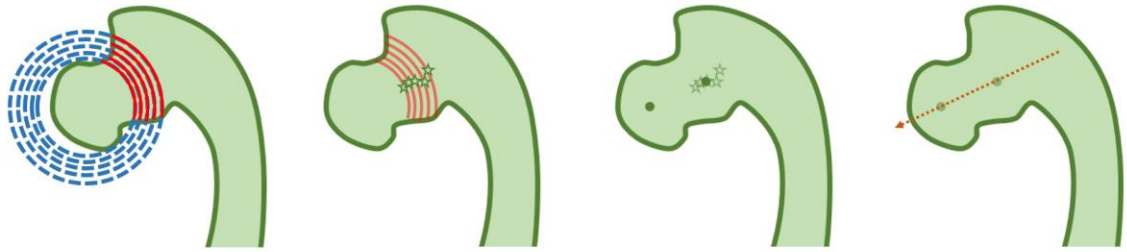

Figure 3: The calculation of the collum axis given the caput centre. From left to right: 1) Multiple spheres are drawn around the caput with increasing size, 2) The mean of the intersecting sphere coordinates are calculated, 3) The mean of these points mean point is calculated, 4) the caput centre and mean intersection point represent the collum axis.

2.2 Defining the osteotomy

2.2.1 Osteotomy function parametrisation

In order to find the shape of the deformity centreline post-surgery a mathematical definition of an osteotomy has to be defined. The osteotomy algorithm consists of several steps:

- Finding the locations of the osteotomy planes from their parameters
- Finding the remaining bony parts after osteotomy
- Transformation of the bony parts to their post operative configuration
- Calculation of the dissimilarity score, post-operative deformity against target shape
- Performing a single cut osteotomy on the target shape
- Inverse transformation of the target shape
- Calculation of the dissimilarity score, preoperative deformity against inverse target shape

These steps are also visualized in Figure 4, Figure 5.

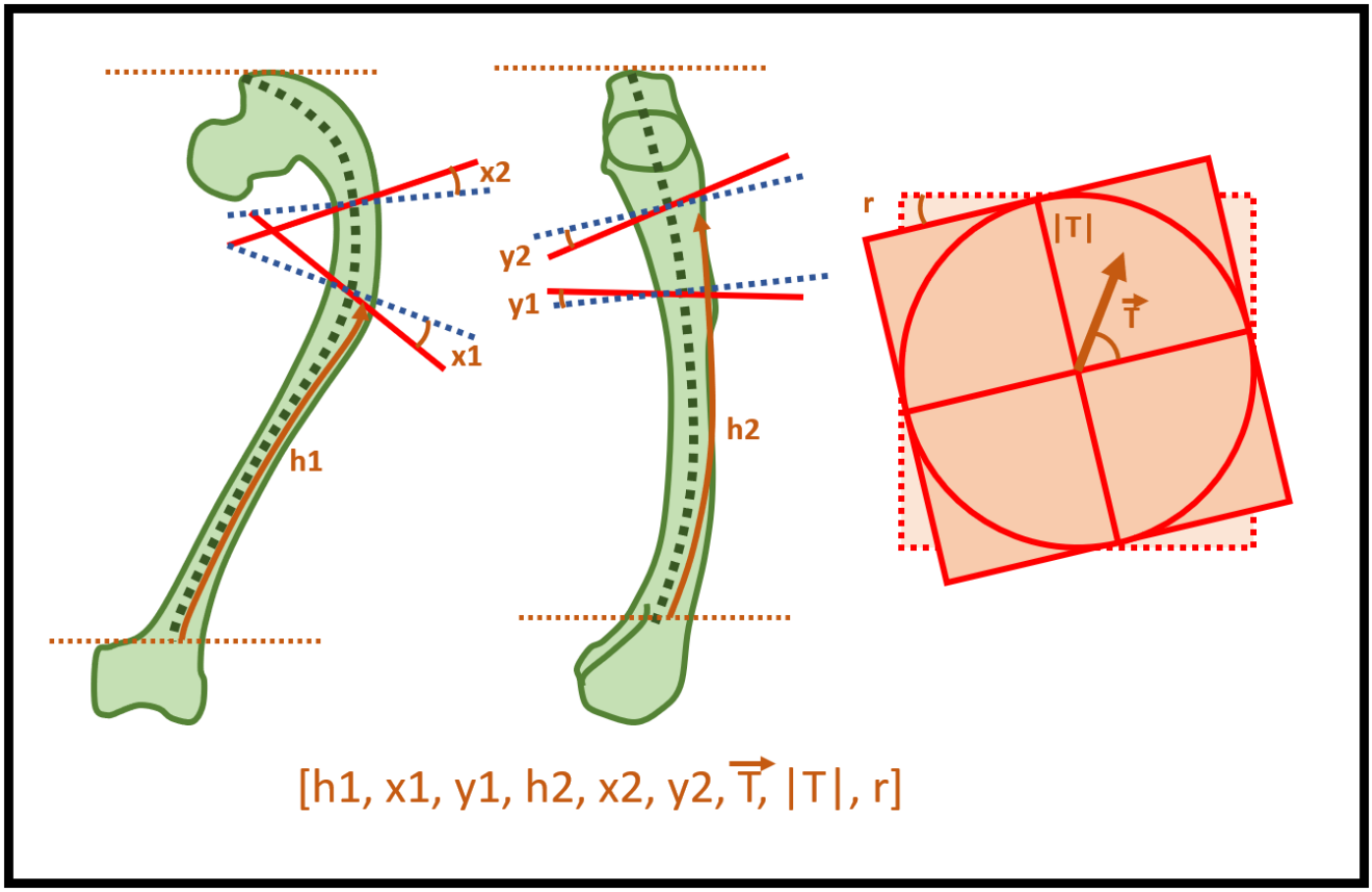

Figure 4: A visual representation of the translation from parameters to osteotomy planes. The first six parameters are the plane parameters. The last three parameters are the wedge parameters.

Two categories of parameters for a single osteotomy exist: 1) plane parameters, 2) wedge parameters. The plane parameters consist of the location defined as a single coordinate <x,y,z> and direction, defined as normal vector <x,y,z>. The wedge parameters are parameters that are defined per two planes, that represent the realignment of two adjacent bony parts. These parameters describe the translation and rotation of the proximal part in relation to the distal part. The rotation is defined as a single radian value. The translation is defined in polar coordinates, as this facilitates the expression of translation in the global x, y and z axis, using two parameters.

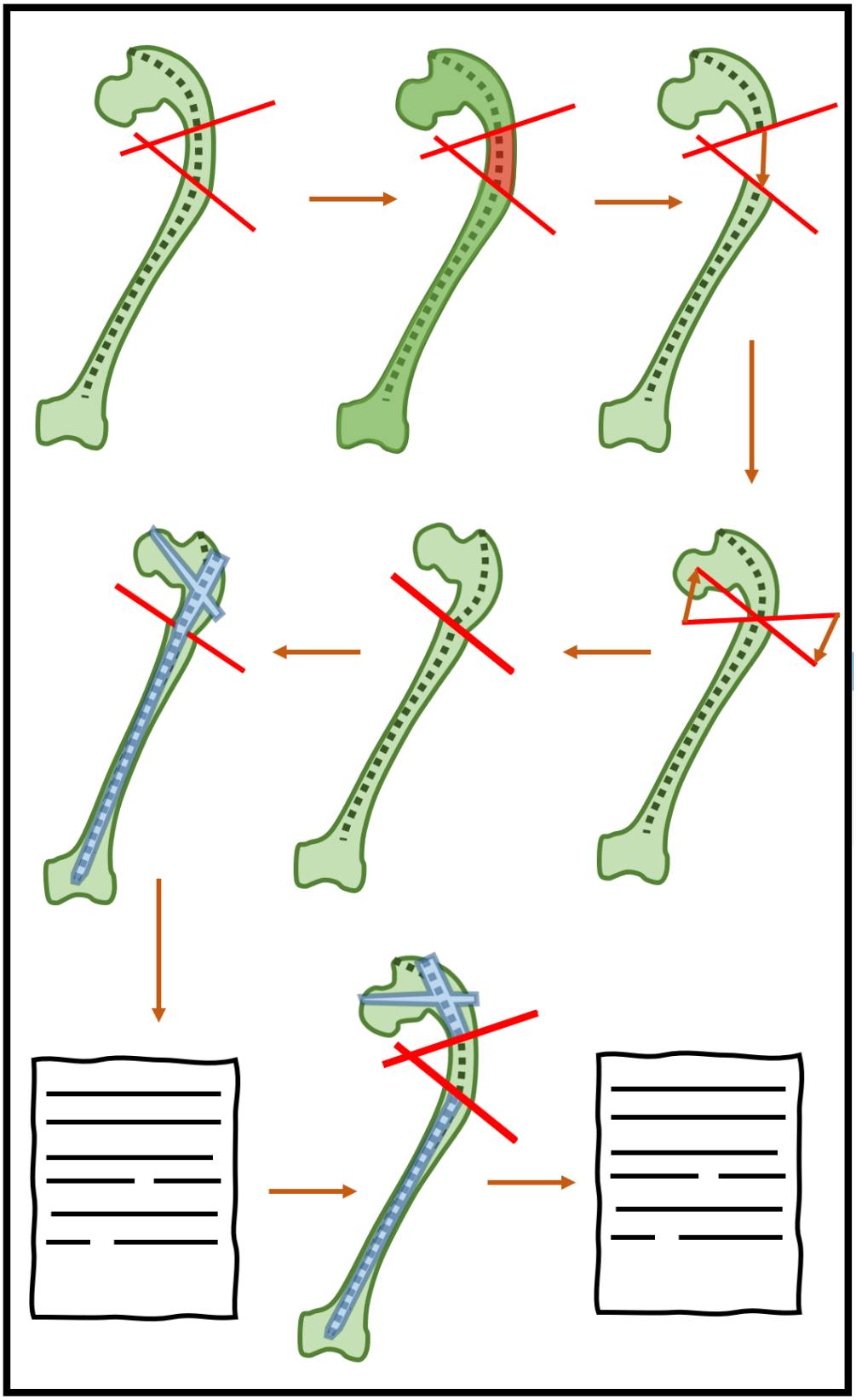

Figure 5: A schematic representation of a single cycle of osteotomy execution and quantification. Following the arrows from top to bottom. 1) Generating the osteotomy planes, 2) removing the bony part excised in osteotomy, 3) finding the proximal and distal bony part, 4) translating the distal part to the proximal part, and perform additional proximal segment translation, 5) aligning the normal vectors of the osteotomy planes, 6) registering the target shape the post operative shape, and performing proximal segment rotation, 7) calculating the dissimilarity score for the postoperative configuration, 8) performing the inverse osteotomy on the target shape, 9) calculating the dissimilarity score for the preoperative configuration.

Interpretation of the parameters result in the creation of osteotomy plane pairs. In order to perform the osteotomy the distal and the proximal centreline part of the deformity shape are identified. Coordinates of the centreline belong to the proximal part post-osteotomy if the dot product of the vector spanned by the centre of the proximal osteotomy plane to the centreline coordinate and the normal vector of the plane is positive. Coordinates of the centreline belong to the distal part post-osteotomy if the dot product of the vector spanned from the distal osteotomy plane centre to the centreline coordinate and the normal vector is negative. The proximal part of the deformity centreline should be transformed in space to represent its post-operative situation. The matrix used for this transformation is a combination of a rotation matrix to align the normal vector of the proximal plane to the normal vector of the distal plane and the translation matrix to align the centre of the proximal and distal osteotomy planes. After this realignment of the planes, the proximal part is translated orthogonal to the normal vector of the distal plane, and rotated around the distal plane normal. The amount of rotation and translation in the latter two steps are defined by the wedge parameters.
Using algorithms explained in the further sections, the dissimilarity score between the post-operative situation and the target shape are calculated. Using the distal plane the target shape can be cut in a proximal and a distal part. The proximal part is now realigned to the preoperative situation using the inverse matrix of the transformation matrices described above. The centreline of the deformity shape is reset to its original shape. This leaves us with the original deformity shape and the inverse target shape that corresponds with the performed osteotomy. The dissimilarity score of the preoperative deformity and inverse target shape is calculated. All shapes are reset to their original to facilitate a next osteotomy iteration.

2.2.2 Closed domain parameter definition

In the definition of the osteotomy parameters close attention was paid to achieving a closed domain in which all osteotomies exist and all osteotomies are unique. A domain in which not all solutions are unique, will lead to unnecessary calculations. A domain in which parameter combinations exist that do not correspond with a feasible osteotomy, will lead to the need of an additional constraint violation check. All possible cutting planes must conform to the following two rules: 1) all feasible osteotomies pass through the femur shaft, 2) an osteotomy is not feasible if the angle of the blade to the shaft is sharper than 45 degrees. This last statement is defined as making a sharp angle with the blade on the surface of the femur shaft will lead to slipping of the blade in the direction of the cut. Note that another motive to minimize the slope of the distal plane is that the vertical load on a sloping osteotomy plane, will lead to shear forces on the bone contact area, which might cause delayed bone-union or non-union.
Note that the common centre coordinate and normal vector representation of a plane does not offer unique solutions only. The translation of the centre coordinate in any direction orthogonal to the normal vector will produce the identical plane. To overcome this problem the centre coordinate of the cutting plane is defined as the relative location on the centreline of the femur. Where the most distal point is 0 and the most proximal location is 1.
The angle of the cutting plane to the femur is defined as the angle between the local direction of the femur and the direction of the cutting plane. As the femoral direction influences the angle, one cannot calculate the angle from the cutting plane normal vector alone, and no closed domain can be defined. However, defining the cutting plane direction relative to the femoral centreline overcomes this problem. In other words, the used coordinate system to generate the osteotomy planes has its origin on the femoral centreline. The x-axis of the coordinate system is in plane with the global XZ plane and its vector is orthogonal to the local direction of the femoral shaft, pointing in the positive global x-axis direction. The y-axis of the coordinate system is in plane with the global YZ plane and its vector is orthogonal to the local direction of the femoral shaft, pointing in the positive global y-axis direction. The z-axis is orthogonal to the local coordinate system x- and y-axis. Using this parametrization of the cutting plane, the parameters
[h1 = 0.5, x1 = 0, y1 = 0, …] correspond to a proximal plane that cuts the femur in equal halves perpendicular to the shaft.

2.2.3 Height sorting

An important factor in the optimization of an osteotomy is the sorting of the plane parameters. The height parameters, representing the relative distance from the most distal centreline point, for a single wedge are defined in such a way that the first three parameters, location and tilt, represent the proximal plane and the second three parameters represent the distal plane. This is problematic if within the parameters of a single wedge the first height is smaller than the second height. This would be interpreted as the proximal cut being more distal than the distal cut and thus the osteotomy is invalid. There are some ways to overcome this problem. One method is to define the height of the proximal plane relative as the distance to the distal plane. This creates two additional problems: 1) How can you define the bounds for the distance between the proximal and distal plane? Setting it to a high value would result in a lot of proximal osteotomy planes that are to proximal to intersect with the shaft. Setting it to low would result in certain large osteotomies that cannot be found by the model. 2) Changing the height of the distal plane automatically changes the height of the proximal plane. These two problems are especially problematic when scaling to multiple osteotomies.
The currently implemented method is to perform sorting of the parameters based on their height. In practice this means that the height, x tilt and y tilt of the proximal plane is swapped with these parameters of the distal plane in case of an invalid osteotomy. This means that some parameter configurations have identical outcomes. Note that the solution space for this sorted situation is perfectly symmetrical, as the solution space with h1 > h2 has the identical shape as the solution space with h2 > h1. Therefore, the problem of duplicate solutions is attempted to overcome by initializing the optimization with sorted data, meaning that all initial samples are in the search space of h1 > h2.

2.2.4 Multiple osteotomy

The sections above describe the workflow for a single closed wedge osteotomy. It should be noted that in the creation of the osteotomy planes they are all placed on the centreline of the preoperative deformity shape. Performing the osteotomies iteratively from distal to proximal means that all osteotomy planes generated more proximal to the current osteotomy should be transformed to keep matching the femur centreline after performing the distal osteotomy. This should also be kept in mind while performing the inverse osteotomy on the target shape.
The height sorting in case of multiple osteotomy is a little more extensive in multiple osteotomy. It is possible within the bounds of the optimization to generate a proximal osteotomy plane of a distal wedge that is generated above the distal plane of a more proximal wedge. This too is an invalid osteotomy. Therefore, all planes should be sorted in such a way that in these scenarios the distal plane of the proximal wedge and the proximal plane of the distal wedge are swapped. This however leads to even more duplicate solutions. Where a single osteotomy had only two duplicate results, in multiple osteotomy however this leads to (n*2)! duplicates. There are however no clear signs that this hampers the optimization, possibly due to the symmetric nature of the duplicates, in combination with the initialization in one symmetric search space. It is hypothesized that a parametrization that overcomes this problem, without introducing additional complications might improve convergence to the global minimum.

2.3 Nail and femur shape dissimilarity

2.3.1. Nail registration algorithm

The nail fitting function starts with the registration of the centreline of the nail with the centreline of the osteotomized femur. The registration process consists of three registration stages. Starting with the registration of the nail collum screw with the femur collum axis. The result of this first registration is a global fit of the centrelines purely fixed on the fit of the collum screw in the femur. The steps are shown in Figure 6. First the direction of the collum screw vector is placed in line with the vector of the femur model vector. Secondly the top of the nail is placed at the location of the femoral entrance point. Viewing the nail and femur in plane with the screw, there is still a rotation apparent in the lateromedial plane. After correcting this rotation the collum screw, femur collum axis, greater trochanter and femoral nail entrance point are on the same plane. To fully align the nail screw and collum axis a final translation is performed.
Fixing the collum screw to the femoral collum, fixes the femoral neck shaft angle as well as the depth that the nail is placed in the femur. In clinical practice the collum screw and femoral collum need not perfectly align. Besides this, a different collum screw angle might be used to compensate for a change in collum angle. In order to give a little more latitude in the collum registration three additional steps in nail registration are added in the second registration stage. Firstly the direction of the nail shaft is aligned with the direction of the femur shaft to let go of the fixed femoral neck shaft angle. Besides this an extra optimization parameter is introduced, namely the nail end cap size. This parameter is used for the final stage of nail registration. This single float between 0 and 30 defines the extra depth the nail should be placed in the femur for an optimal fit and thus clinically the size of the end cap to compensate for the extra placement depth in the femur. These extra steps are visualized in Figure 7.

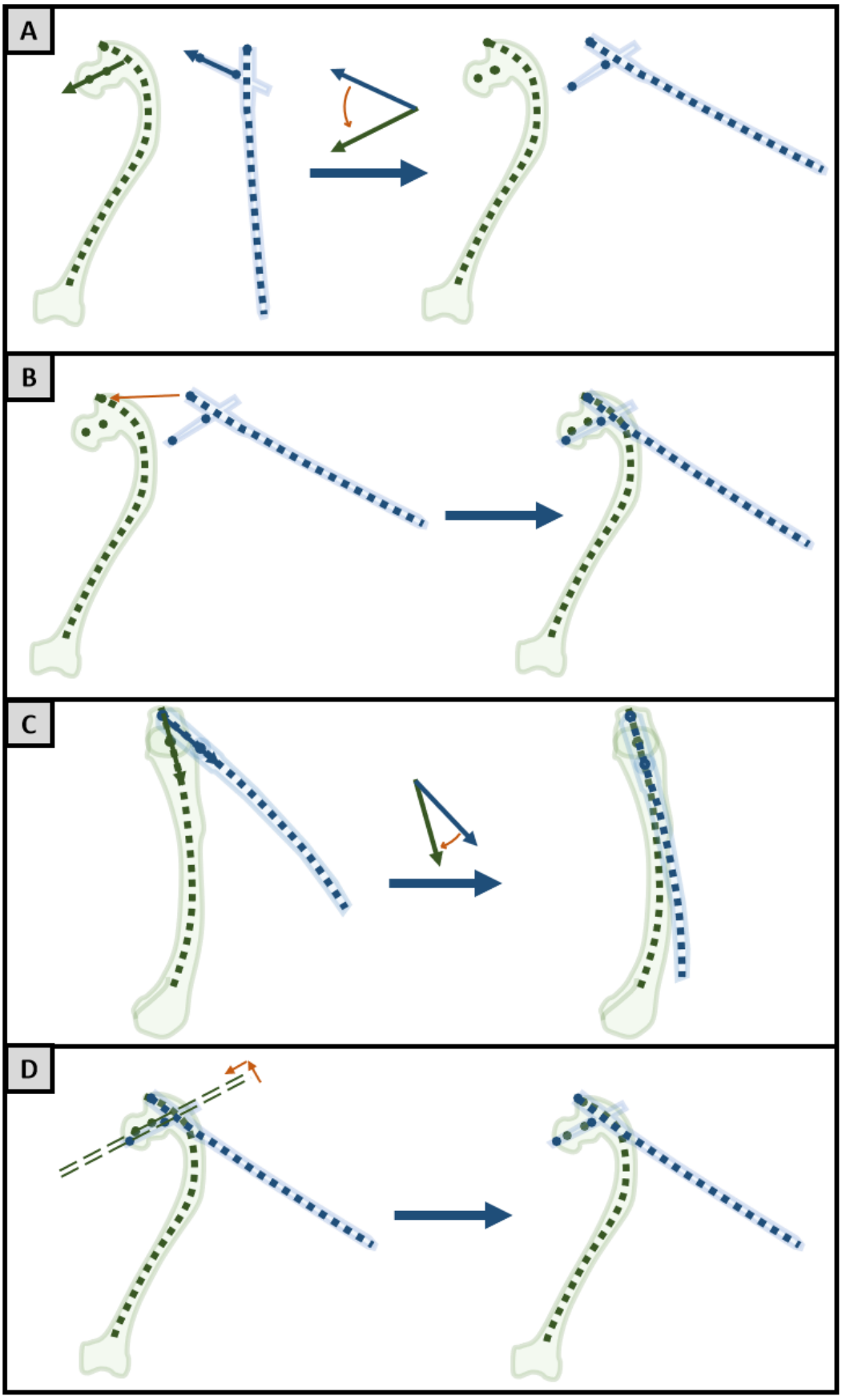

Figure 6: The first steps of the nail alignment. These steps show the fit of the nail in the femur with a fixed collum screw. A) The screw axis is aligned with the femoral collum axis, B) The top of the nail is translated to the trochanteric entry, C) The nail shaft is pivoted around its top, perpendicular to the collum direction, D) Two translations are performed to perfectly align the collum screw and femoral collum axis.

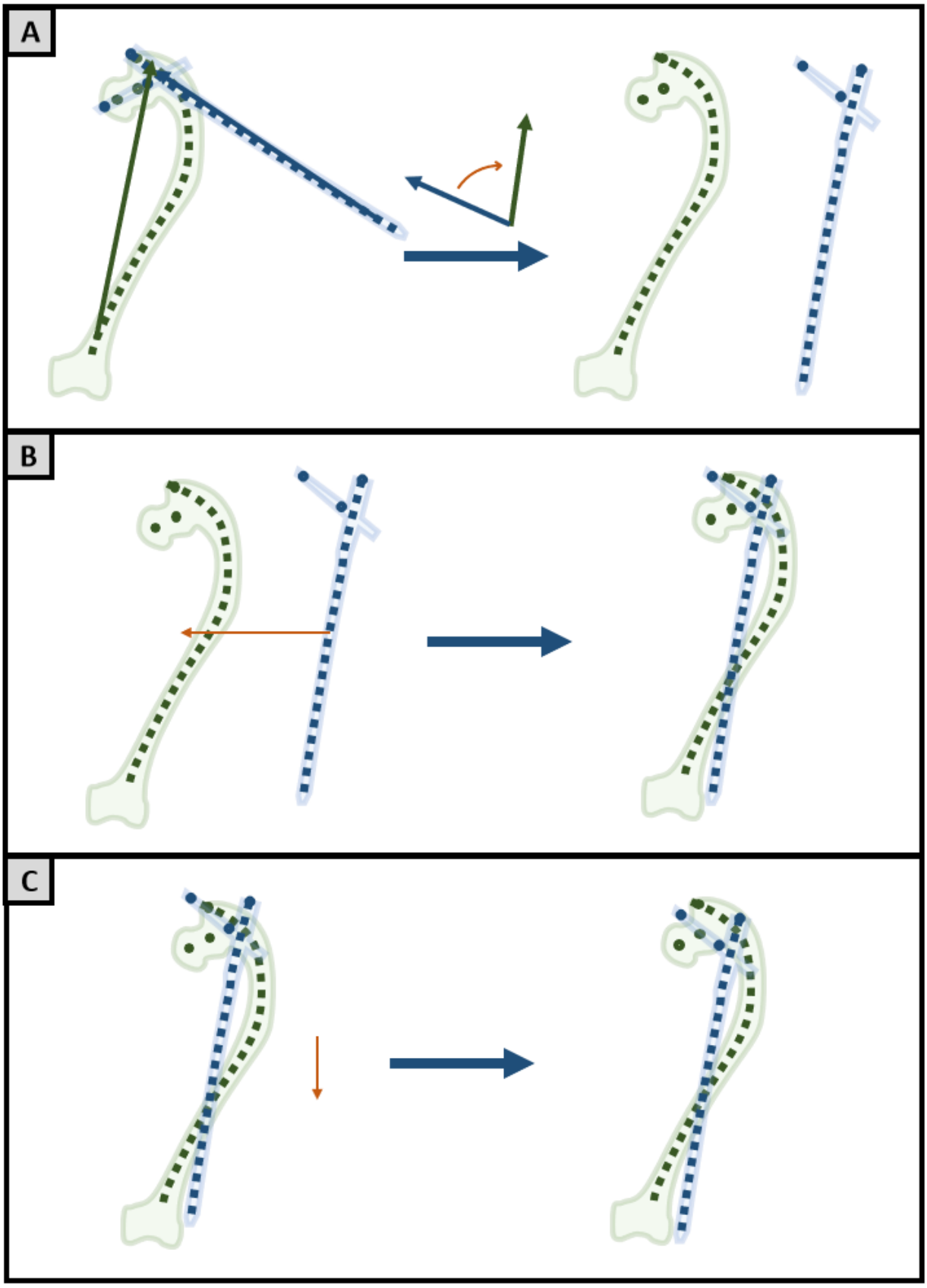

Figure 7: These additional extra steps find the fit of the gamma nail with focus on the shaft fit instead of collum fit. A) Align the nail shaft axis with the femur shaft axis, B) Translate the nail to match the centre of gravity of the femur. C) Translate the nail in the nail shaft direction to optimize fit.

2.3.2 Shape dissimilarity measure

Calculating the dissimilarity between the centreline of the nail and the centreline of the femur, is done by defining a single dissimilarity score. Common scores for quantifying the dissimilarity of two shapes are the Hausdorff distance (HD), root mean square error (RMSE) and dice score similarity. As the shape does not have a closed border the dice score is challenging to define and computationally heavy. The two remaining scores have their pros and cons that are demonstrated in simplified cases in Figure 8. Crucial are the clinical consequences of the solution. The focus of the dissimilarity score outcome should always be in which of the scenarios the nail fits the intramedullary canal of the femur.

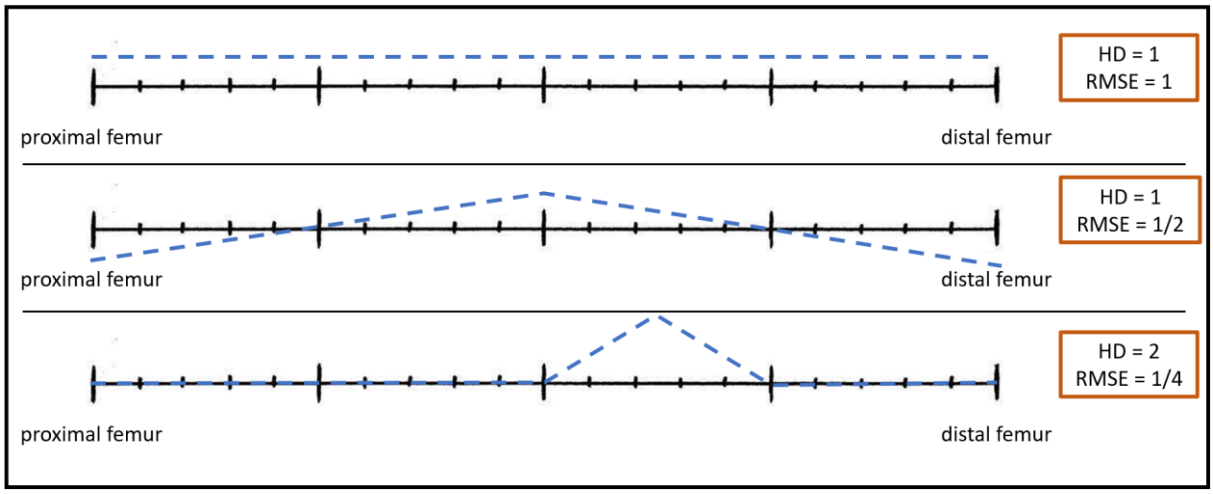

Figure 8: The HD and RMSE in abstract scenarios, showing the drawbacks of the HD and RMSE as cost function. HD = Hausdorff distance, RMSE = root mean squared error.

The HD of the first and second simplification are identical. However in the first scenario there is not a single point where the nail fits the femur and in the second scenario there are at least two locations where the nail fits the femur. The second scenario is the preferred of the two, which is not reflected in the HD. The RMSE however is lower in the second scenario compared to the first. The third scenario has a lower RMSE than the second scenario and would be regarded as the better solution if this metric was used. There is however a single peak in the middle which would make the insertion of the nail in the intramedullary canal impossible. Thus a reduction in RMSE does not necessarily result in a better gamma nail fit. It should be noted that the HD is larger in the third scenario compared to the second scenario. These simplified scenarios point to the use of a combined metric of the HD and the RMSE.
Small deviations between the centrelines, will not result in the gamma nail not fitting the intramedullary canal. Therefor small deviations between the centrelines should not be penalized in the shape dissimilarity metric. The RMSE metric benefits from being capped. This means that a value lower than a certain threshold is set to zero. A simplified scenario is shown in Figure 9. Here it is demonstrated that the RMSE in the upper scenario is significantly lower, yet the fit of gamma nail is similar in both cases. The capped RMSE is identical in both scenarios and demonstrates the better representation of actual nail fit in the capped RMSE compared to the regular RMSE. In the current model this threshold is set to 2 mm.

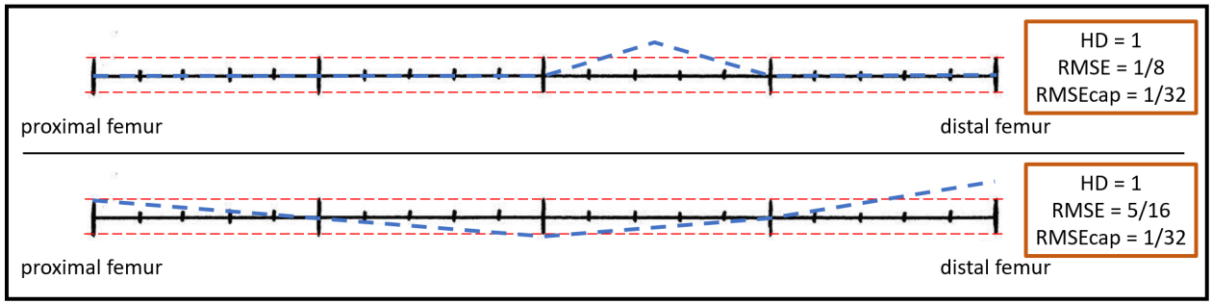

Figure 9: The HD, RMSE and capped RMSE in two simplified scenarios, showing the improvement of the capped RMSE over the regular RMSE.

2.3.3 Reversed osteotomy fit

In the centreline simplifications of the femur model and the nail model, both centrelines are of the exact same length. In practice however the nail and femur centreline post osteotomy are not of the same length. The metric is influenced by which of the two centrelines is considered the reference and which is considered the difference line. This means that the HD from the femur centreline to the nail centreline is not the same as the HD from the nail centreline to the femur centreline if the length of the centrelines is not the same. This means that the length of the femur after osteotomy influences the shape dissimilarity metric. This phenomenon is shown in Figure 10. The first scenario is the nail fit before osteotomy. It can be seen that the nail does not fit the intramedullary canal and the HD is located at the CORA of the femur. An osteotomy is proposed which straightens and slightly shortens the femur. In the second scenario the centrelines are shown post osteotomy. The nail now perfectly fits the intramedullary canal. However because of shortening of the bone the HD in the second scenario is larger than the HD in the first scenario if the HD is calculated as the largest shortest distance from the nail to the intramedullary canal. If in this post operative scenario the HD is calculated as the largest shortest distance from the femur to the nail, the HD is zero.

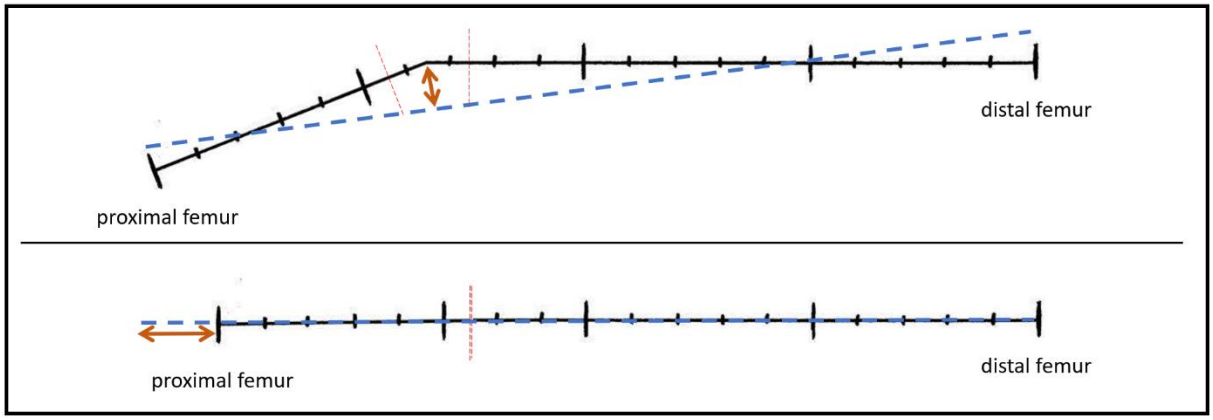

Figure 10: A simplified osteotomy, showing a growing one sided Haussdorff distance after performing a perfect osteotomy. Above the situation pre-osteotomy, below the situation post-osteotomy.

However if the metric would only consist of the distances calculated from the intramedullary canal to the nail, the metric would converge to a femur centreline with no length, as this post operative result consisting of a single sample point will always have an HD and an RMSE of zero.
For this reason, the complete metric used to calculate dissimilarity consists of the $RMSE_{nail \rightarrow femur}$, $HD_{nail \rightarrow femur}$, $RMSE_{femur \rightarrow nail}$ and the $HD_{femur \rightarrow nail}$.

2.3.4 Cost function composition

The cost function that is minimized to quantify the dissimilarity of the two shapes is defined by the multiplication of a modified Hausdorff distance and a modified RMSE, Equation 5. The modified Hausdorff distance is calculated as the maximum minimum distance from the transformed deformity shape to the target shape plus the maximum minimum distance from the transformed target shape to the original deformity shape, Equation 1. The modified RMSE is the mean minimum distance from the transformed deformity shape to the target shape plus the mean minimum distance from the transformed target shape to the original deformity shape, Equation 2. The minimum distances are capped using a threshold Θ, Equation 3, 4.

$$d_H = d_{YX} + d_{XY} = \max_{y \epsilon Y} \min_{x \epsilon X} d(x_T, y) + \max_{x \epsilon X} \min_{y \epsilon Y} d(x, y_T) \quad (1)$$

$$d_{Mean} = \frac{\sum_{i=1}^{n} D_X(x)}{n} + \frac{\sum_{i=1}^{n} D_Y(y)}{n} \quad (2)$$

$$D_X(x) = \begin{cases} \min_{x \epsilon X} d(x_T, y), & \text{if } D_X(x) \geq \theta \\ 0, & \text{otherwise} \end{cases} \quad (3)$$

$$D_Y(y) = \begin{cases} \min_{y \epsilon Y} d(x, y_T), & \text{if } D_Y(y) \geq \theta \\ 0, & \text{otherwise} \end{cases} \quad (4)$$

$$f_{CostShaft} = d_H * d_{Mean} \quad (5)$$

Equation 1-5: The equations used to build the cost function. In which d_H = modified Hausdorff distance, d_{Mean} = modified RMSE, d(x, y) = the distances from all points on shape x to all point on shape y, x = deformity shape, y = target shape, x_T = transformed deformity shape, y_T = transformed target shape, Θ = RMSE cap threshold

2.3.5 Centreline interpolation

In the past sections, the centreline shapes of the nail fixation and the femur were regarded to be continuous shapes. In reality however, the centreline shapes are a discrete set of coordinates that are spaced on the shape with equal distance to each other. Meaning that, for calculating the dissimilarity metric, the first step is to calculate the distances from each point on the first shape to the second shape and from the second shape to the first shape. This matrix of distances is then processed to a single value that represents shape dissimilarity. The higher the sample frequency on the shape the more accurate the calculation of dissimilarity metric. Having more datapoints in the centreline objects, does increase the computational cost needed to calculate the optimal preoperative plan. The accuracy of the dissimilarity metric as influenced by the sampling frequency of the shape is displayed in Figure 11.

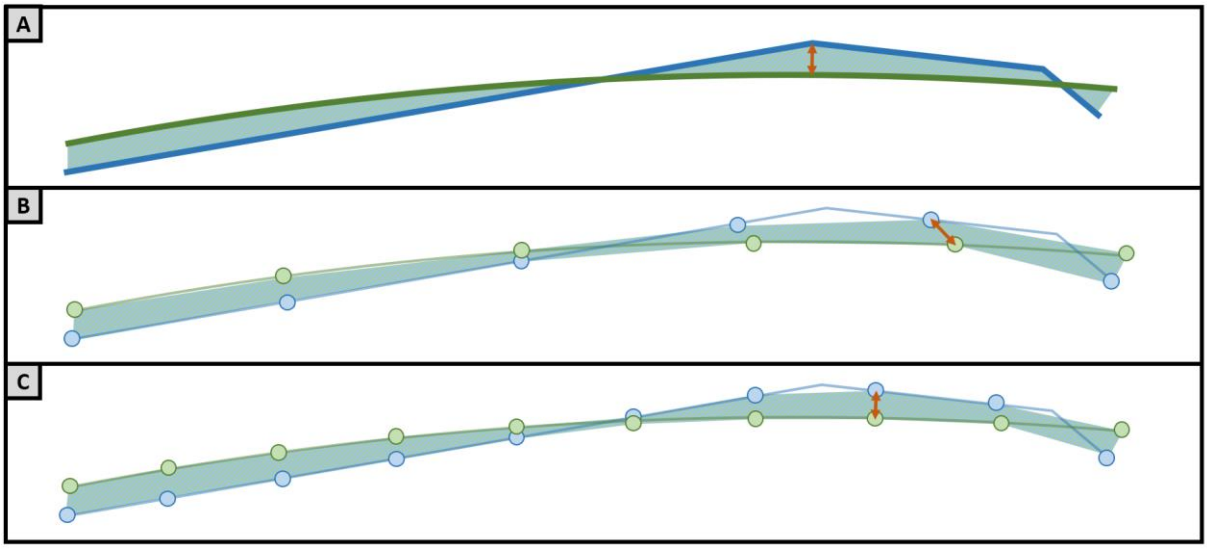

Figure 11: The HD and RMSE in the case of A) continuous, B) low frequency, C) high frequency sampling.

These slight miscalculations of the actual metric can lead to incorrect final results of the osteotomy model as well as noise during optimization of the osteotomy. In order to investigate the impact of the sampling frequency of the shapes on the convergence of the model, optimization of the same case has been performed with different sampling frequencies. The results for a single and a double osteotomy can be seen in Figure 12.

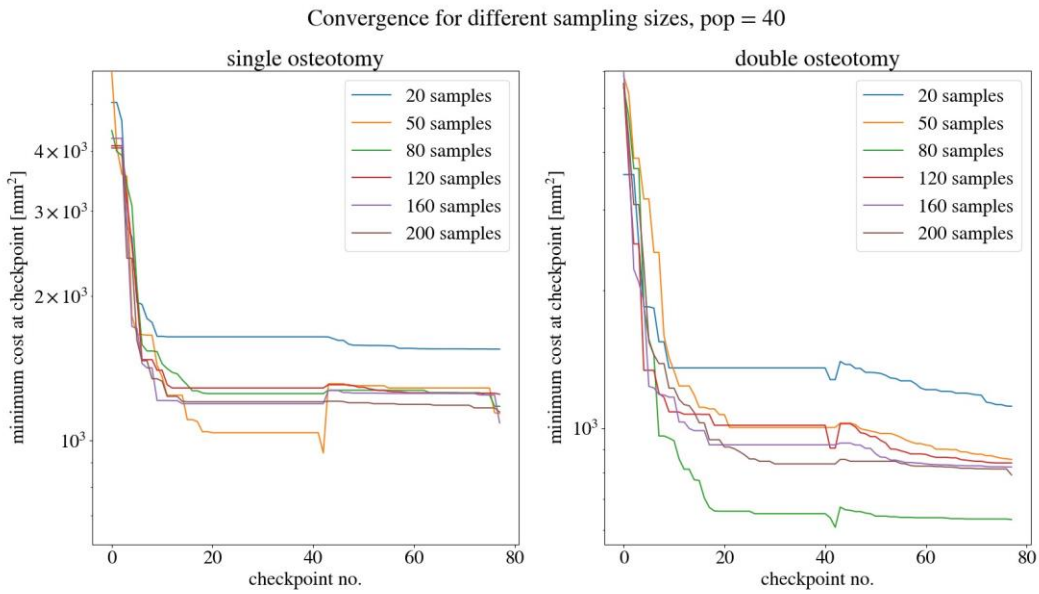

Figure 12: The convergence of the cost function for single (left) osteotomy and double (right) osteotomy, for different sampling frequencies.

This figure shows the convergence of the cost function to an optimum. The model optimizes the same femoral deformity case, with the same optimization parameters, accept for a varying sampling frequency. Note that higher sampling frequencies tend to converge faster and to a lower overall dissimilarity score. This vouches for using a high sampling frequency in the model. As said, the higher sampling frequency will lead to higher computational times which is displayed in Figure 13. It can be seen that the computational time is linearly related to the sampling frequency of the two shapes.

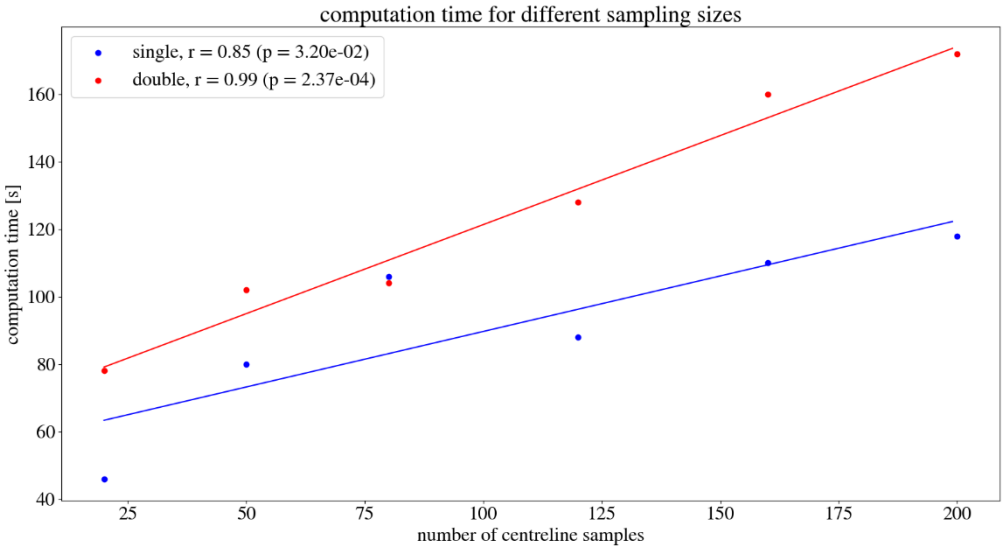

Figure 13: The time needed in seconds to perform a full optimization in relation to the sampling size of the gamma nail and femur object in a scatterplot. The blue and red line represent the linear correlation.

Weighing speed against accuracy, it was concluded that a sample size of 160 datapoints was a good compromise. Sampling frequency should be seen as a hyperparameter that can be tuned for specific use cases. An important notice, is that the comparison of the dissimilarity of very low sampling frequencies can be misleading as they are prone to lucky or unlucky metric calculations, meaning that very high or very low scores do not represent the actual fit of the nail in the intramedullary canal. An unlucky calculation occurs when the two shapes are sampled only in those locations that are most dissimilar. A lucky calculation occurs when two shapes are only sampled in those locations where the shapes are most similar.

2.4 Clinical constraints

The optimization of the femoral osteotomy is achieved by minimizing the cost function, which represents femoral shaft shape. To achieve a post-operative outcome that is useable in clinical practice the bone should be as anatomically correct as possible within the boundaries of several clinical constraints, including morphometric characteristics. These constraints are listed below.

2.4.1 Femoral length

The length of the femur post-operatively, should be within a window of preset values. Correction of angular deformities of the shaft can lead to lengthening in the post-operative setting. It is of crucial importance to limit this lengthening as too much lengthening can lead to peripheral neuro trauma caused by high nerve tension. The nervus ischiadicus is especially susceptible to this. Extensive lengthening can also cause functionally limiting muscle contractures. The high tension on the nervus ischiadicus, vascularity and musculature should especially be kept in mind for proximal and midshaft valgisation osteotomy, where large amounts of tension occur on the medial side of the femur. A shortening of the femur causes a decreased muscle tension, which leads to post-operative muscle weakness. These complaints will fade as the soft tissues shorten over time. An important notice in deciding on post-operative femoral length, is the leg length discrepancy. Post-operatively the leg length discrepancy should be minimized within the anatomical boundaries.

2.4.2 Collum anteversion

A patient with increased collum anteversion will present itself with an in-toeing gait. This in-toeing is a compensation of the increased collum anteversion attempting to reduce pain and hip instability. By rotating the leg inwards the collum anteversion angle normalizes relative to the acetabulum. This does change the femoral condylar direction, causing a misalignment in the knee joint, with eventual complaints of pain and arthrosis. This principle is shown in Figure 14. The normal range of collum anteversion angles is from 8 to 15 degrees. The functional and aesthetic impairment of in-toeing as well as the risk of early onset arthrosis, makes the collum anteversion a clinically important parameter.

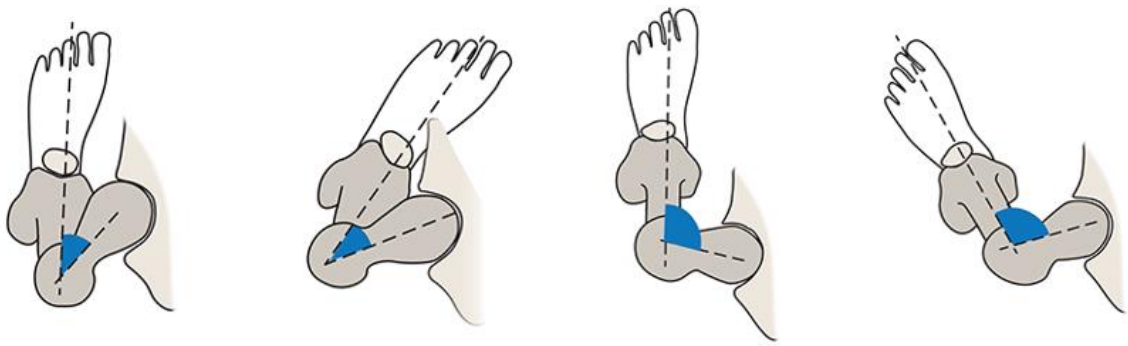

Figure 14: Anteversion and retroversion of the collum and its clinical presentation. From left to right: 1) collum with increased anteversion in foot neutral position, 2) collum with increased anteversion in collum neutral position, 3) collum with retroversion in foot neutral position, 4) collum in retroversion in collum neutral position. Illustration credit: Jake Pett, B.F.A. and Stuart Pett (2)

2.4.3 Total femoral rotation

As with femoral length, with femoral rotation the most important structures to consider are the vessels and nerves of the thigh. Adding rotations to the bone will lengthen the vessels and nerves. Large rotations can cause tension trauma and are avoided by setting the maximum total rotation of the femur to a preset value.

2.4.4 Mechanical axis

This constraint is optional and controllable in the GUI of the Blender environment. The mechanical axis deviation cannot be calculated based on the femoral shape alone as the mechanical axis is calculated as the angle spanned from hip joint, to knee joint, to ankle joint. In this model, the vector spanned between knee and ankle joint is not known. However, as this vector does not change by femoral osteotomy, the change in mechanical axis preoperative and post-operative can be extracted using the change in femoral shape. Bowing and shepherds crook deformities often come with genu varum or valgum deformity. These deformities might cause pain and arthrosis and should therefore be added to the morphometric constraints.

2.4.5 Maximum osteotomy angle

The constraint for maximum osteotomy angle is mainly of importance for practical feasibility of the osteotomy. Extremely tangent cuts on the femur are hard to perform and should therefore be avoided. The maximum angle of the saw blade to the normal of the bone should not exceed a preset maximum degrees in order to make the cuts possible intra-operatively. It should also be noted that the obliqueness of the cut line post-osteotomy is controlled by the tangent of the lower osteotomy plane. Having a large obliqueness of this cut will negatively affect the healing tendency of the femur. The angle of the osteotomy is controlled by the optimization bounds of the plane slope.

2.4.6 Wedge distances

In case of multiple osteotomy it is important to have a minimum wedge distance. The bone segments are vascularized via the periosteum. Smaller bony segments will have a larger change of losing their periosteal vascularization and become necrotic. The shortest distance between the proximal plane of a distal wedge and the distal plane of a proximal wedge should not be smaller than a preset value to prevent the scenario of osteonecrosis.

2.4.7 Wedge clearance

A closed wedge osteotomy involves the removal of a bony wedge at least the size of the bone width. The removal of a bony wedge with a width larger than 50% of the bone width, but smaller than the full width of the bone, is considered a closed hybrid wedge. In some cases a closed hybrid wedge with a small width is not desired because it reduces bone contact area between segments. The wedge clearance is defined as the largest size of two equally sized cutting planes that cause intersection. This is visualized in Figure 15. A larger plane clearance will restrict the optimization in creating hybrid wedges with a small osteotomy height

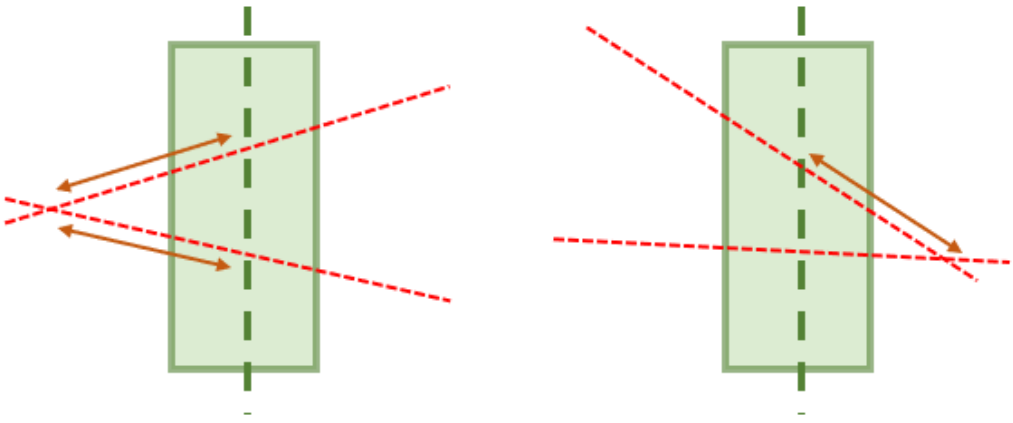

Figure 15: Two closed wedge osteotomies. The dotted red lines represent the cutting planes. The wedge clearance is the largest, shortest distance from the osteotomy planes intersection line to the femur centreline measured in line with the cutting planes.

2.4.7 No-cut and must-cut

In some cases the optimal cut location interferes with an anatomical structure one would not prefer an osteotomy to be performed. Examples of locations to avoid are the trochanter minor, regions close to the femoral neck or the atypical femoral fracture plane. Osteotomies close to the collum might increase the risk of osteonecrosis of the femoral head. Osteotomies in plane with the atypical femoral fracture plane, might result in a delayed union time in patients with long-term bisphosphonate use. These demands are mostly subjective and surgeon specific. Regions where a cut should not be performed can be selected in the Blender GUI using a lasso tool, Figure 16. A convex hull is created around the point cloud. The coordinates of this convex hull are saved. During optimization the no-cut zone constraint is violated if any of the coordinates on the surface of the convex structure are within any osteotomy zone.

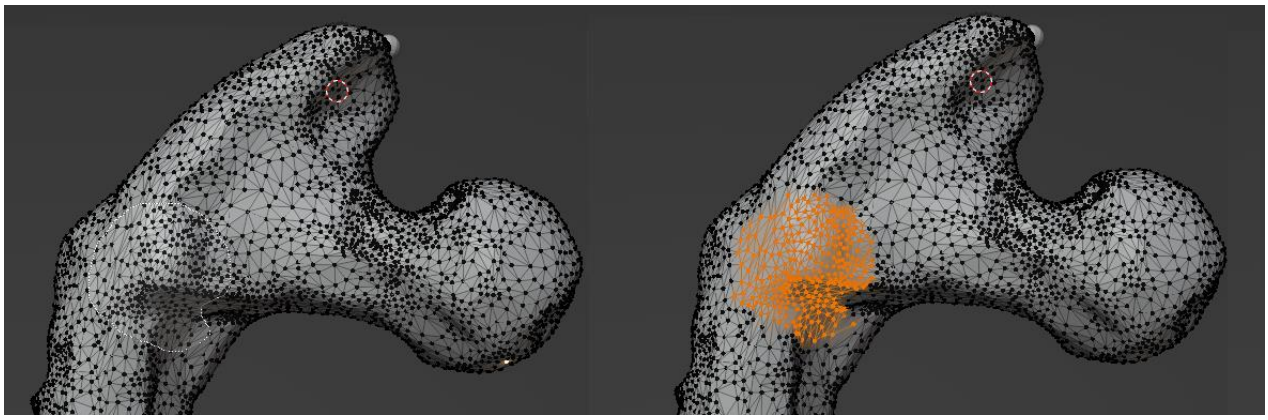

Figure 16: The trochanter minor of a femur is selected as a no-cut zone by using the lasso tool in the blender GUI.

A similar parameter is added if the surgeon has a preference where the osteotomy has to be performed. In some cases selecting a few vertices on a visible angulation speeds up the convergence of the model to a feasible solution. Besides this there might be clinical implications to use a must-cut parameter. An example of this might be placing an osteotomy around an existing non-union. In these cases the tool operator creates a convex must-cut object in a similar fashion to the creation of the no-cut object.

2.5 Optimization algorithms

Several optimization algorithms and strategies have been evaluated on performance. Important factors were the methods ability to generate useable surgical plans consistently, to minimize the clinical constraints and to get out of local optima generated by strict clinical constraints.
In the earliest testing of the model single objective optimization methods were implemented. In these methods the single objective was the cost function as described earlier and the clinical constraints were implemented as hard constraints. The implementation of a hard constraint means that a sample that violates the constraints is removed from the optimization. In these setups the optimization of the preoperative plans were visually poor and the optimization function stopped converging after adding more clinical constraints. It was hypothesized that the implementation of the hard constraints pushed the function to minimize to a local minimum.
To test this hypothesis, the clinical parameters were implemented as soft constraints, meaning that constraint violation is accepted as a solution, but adds a penalty to the cost function. This would give more freedom to the model to converge past clinically suboptimal plans and to the global optimum. This resulted in a visually better fit, within clinical feasible bounds. Using soft constraints however, means that the optimal result might include constraint violations. As the final result may not include any constraint violations a two stage optimization is created. In the first stage a multi-objective optimalization is used to calculate a set of preoperative plans with an even spread on the pareto-optimal line. This is done by adding the constraint violation score as a second objective to the optimization. After half of the iterations, the sample population in that iteration are used as initialization of a single objective optimization function with the clinical parameters as hard constraint. In Figure 15, the convergence of the cost function is shown for each of the three constraint handling methods. It should be noted that the convergence for the soft constraint and multi-objective constraint method is faster. Besides this the final half of the multi-objective method does not allow for a preoperative plan with constraint violation. For these reasons this two stage method is the superior form of constraint handling.

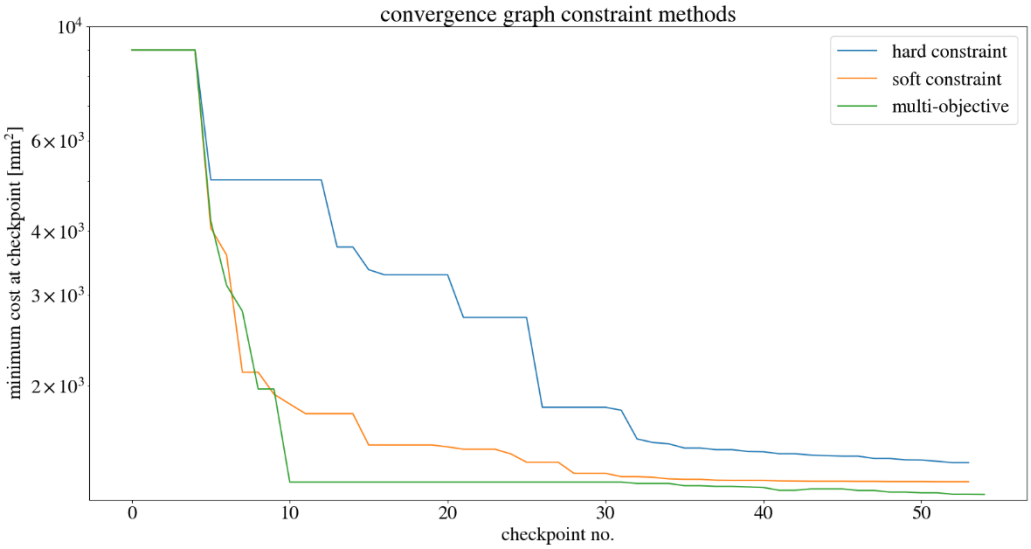

Figure 17: The convergence of the optimization with different methods of clinical constraint handling.

Particle swarm optimization and several genetic algorithms were considered for the optimization of this problem. The search space was visualized using a t-SNE representation of the parameters. This technique uses a non-linear distance between the osteotomy parameters to show a two dimensional visualization of the search space. The t-SNE feature space is used to plot the cost function and constraint violation scores at those specific points. This is shown in Figure 18. Interestingly, there is no pattern of clustering of feasible solutions in the search space. This implies that optimization techniques based on gradient search or linear optimization are not feasible. After thorough testing of different optimization methods. The SMS-EMOA method showed greatest potential in producing consistently good results upon visual inspection.

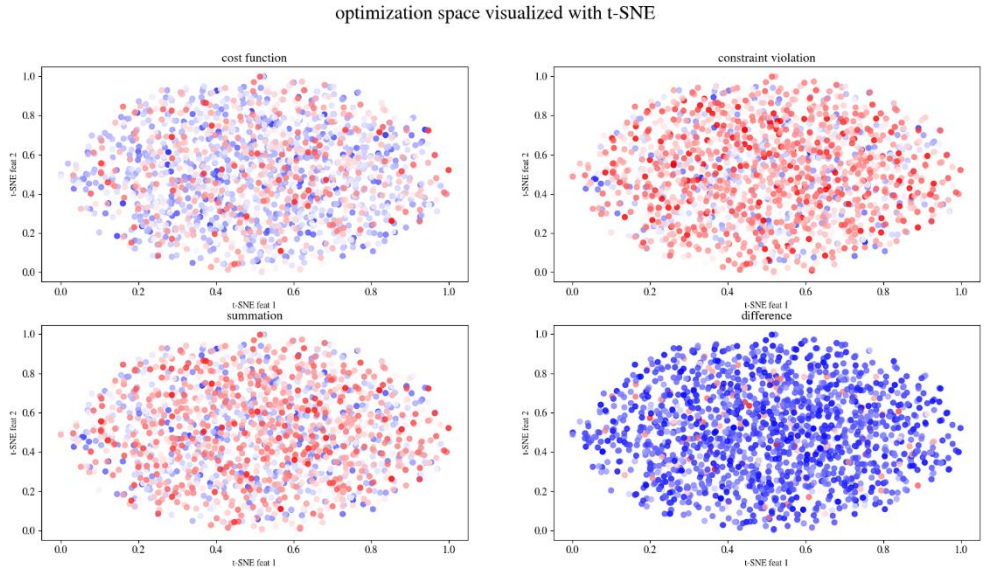

Figure 18: A clustering representation of a set of random samples. Samples with similar parameters are close to each other. Red dots represent high values, blue dots represent low values.

2.5.1. SMS-EMOA

The SMS-EMOA optimization method is a genetic algorithm (3, 4). A genetic algorithm is an algorithm inspired by the evolution theory. The keystones on which these algorithms are build are: 1) reproduction, 2) survival, and 3) mutation. The iterative process starts with a population of random samples. These samples reproduce, which means that they share information in order to generate offspring samples. These samples are than sorted based on a fitness score. The fittest individuals of the offspring are kept and the rest of the samples are discarded. This gives us the next generation of samples. This process is repeated until termination requirements are met. Mutation is a concept in which noise is added to the samples in order to create new samples.
The SMS-EMOA defines fitness in two different ways, both of which attempt to find solutions that lie on the Pareto-optimal front. The first fitness measure is the hypervolume measure, which is the volume spanned by the points on the estimated Pareto-front, Figure 19.

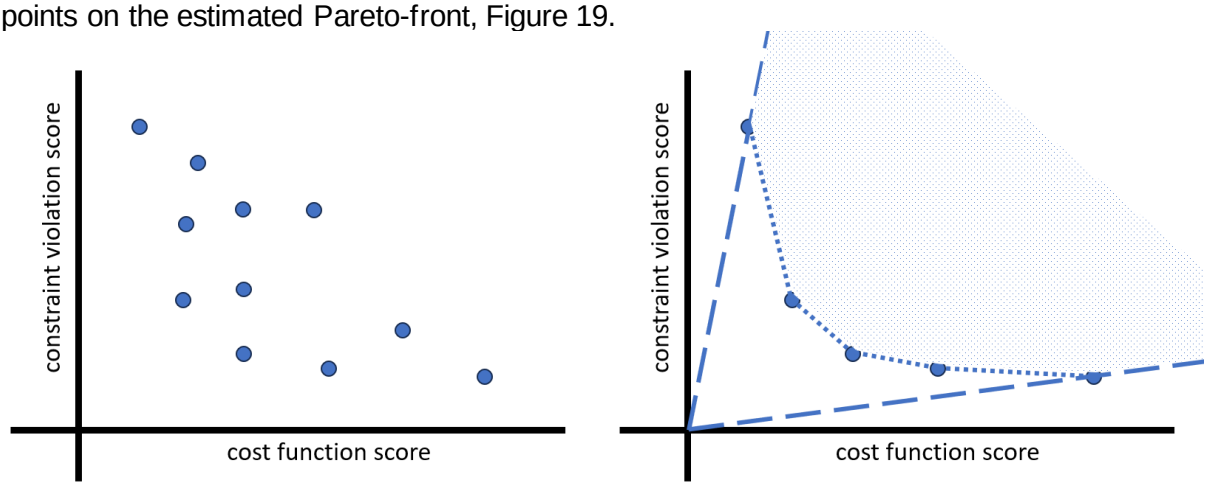

Figure 19: A visual representation of the hypervolume. Notice how maximalization of the hypervolume leads to a good spread approximation of the pareto-optimal front.

The second fitness measure is the non-dominated sorting algorithm in which samples are sorted based on the amount of samples that they are dominated by. A sample is dominated by another sample if it is further away from the estimated Pareto-front.
In the basic algorithm of SMS-EMOA new samples are generated from the current population by means of random variation. Samples from this mutated population replace samples from the current population if it would result in a larger hypervolume measure. After this, offspring is generated. Samples are sorted using non-dominated sorting, after which the best individuals are kept and the process is repeated. Using the hypervolume measure, a widespread of samples on the Pareto-optimal are found.

2.5.2 Random vs structured initialization

The initialization of the algorithm is regarded to be an important factor in the optimization. A random initialization in an optimization with many different parameters and only a small population might lead to the fast convergence to a local optimum. In clinical practice the location of the osteotomy impacts the final result more than the other parameters such as rotation of the plane and slope of the plane. Besides this in most cases in clinical practice the distal cut is never tilted. For this reason the model was initialized randomly either with all parameters non-zero or randomly with only the height parameters non-zero. The results are displayed in Figure 20. This shows that the initialization using only the height as a non-zero parameter results in more consistent osteotomy outputs and an overall lower cost function value.

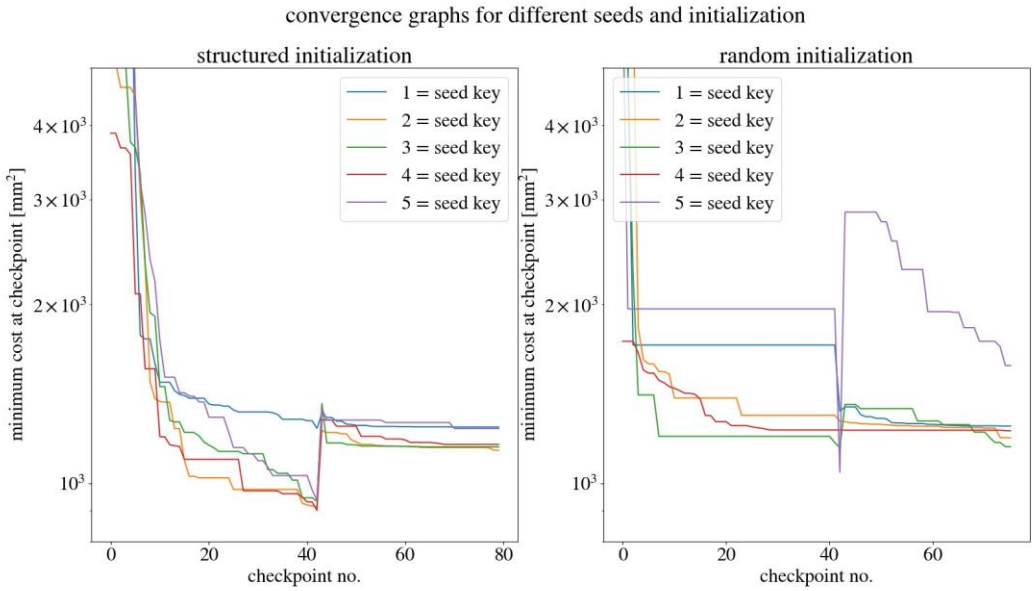

Figure 20: The convergence of the cost function for different random seeds. Left a structured initialization in which only the height of the plane is a non-zero value. Right a completely random initialization in which all parameter values are non-zero.

2.6 Visualization

The visualization of the surgical plan and post-operative outcome is an important factor in the validation of a surgical plan. To evaluate the surgical plan all steps of the osteotomy: pre-, intra and postoperative should be well visualized. These visualizations are integrated into the Blender GUI to enable a tight feedback loop and full evaluation of the plan without the need for additional software. Three visualization methods are used to communicate the preoperative plan to the surgeon. After calculation of the preoperative plan, these visualizations are displayed in the blender GUI after evoking the underlying code using one of the visualization buttons, Figure 21.

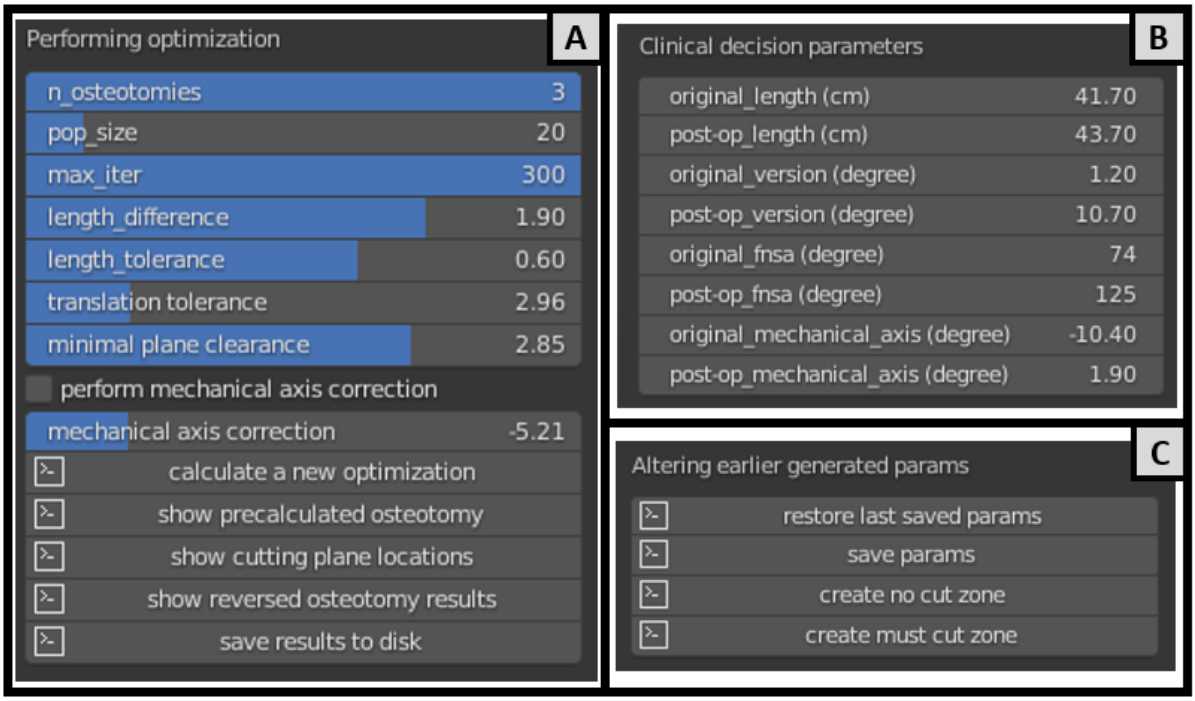

Figure 21: The control panels embedded in the Blender GUI. A) Sliders to change clinical and optimization parameters. Buttons from top to bottom, perform a new optimization, show the postoperative situation for the last optimal parameters, show the cutting planes for the last optimal parameters, show the inverse osteotomy on the target shape and save the STL files of the three visualizations to the disk. B) The preoperative and postoperative clinical parameters. C) Buttons that are used to create no cut zones, must cut zones and save the location of bony landmarks after manipulation.

The three visualization methods are the cutting planes in the preoperative situation, Figure 22, the postoperative situation with the target shape registered to the bone model, Figure 23, and the inverse osteotomy on the target shape registered to the preoperative situation, Figure 24.
The visualization of the cutting planes, shows the surgeon which bony parts are resected, and aides in assessing the interoperative feasibility of the cut. The postoperative visualization, shows the postoperative femoral anatomy as well as osteosynthesis fit. The inverse osteotomy is used to visualize the nail trajectory in the preoperative situation. This can be particularly useful after importing the osteotomized nail to the preoperative CT scan.
To ensure that the cutting planes produced by the software indeed lead to the postoperative situation as visualized in the Blender environment, all visualizations should be analysed in additional software. The cutting planes must be verified before creating cutting guides for intra-operative use. The software generates separate STL files for the gamma nail fitted in the original bone. These files can be imported in a slide viewer and in computer-aided design software to visualize the fit of the nail in the preoperative CT scan and to validate the postoperative result.

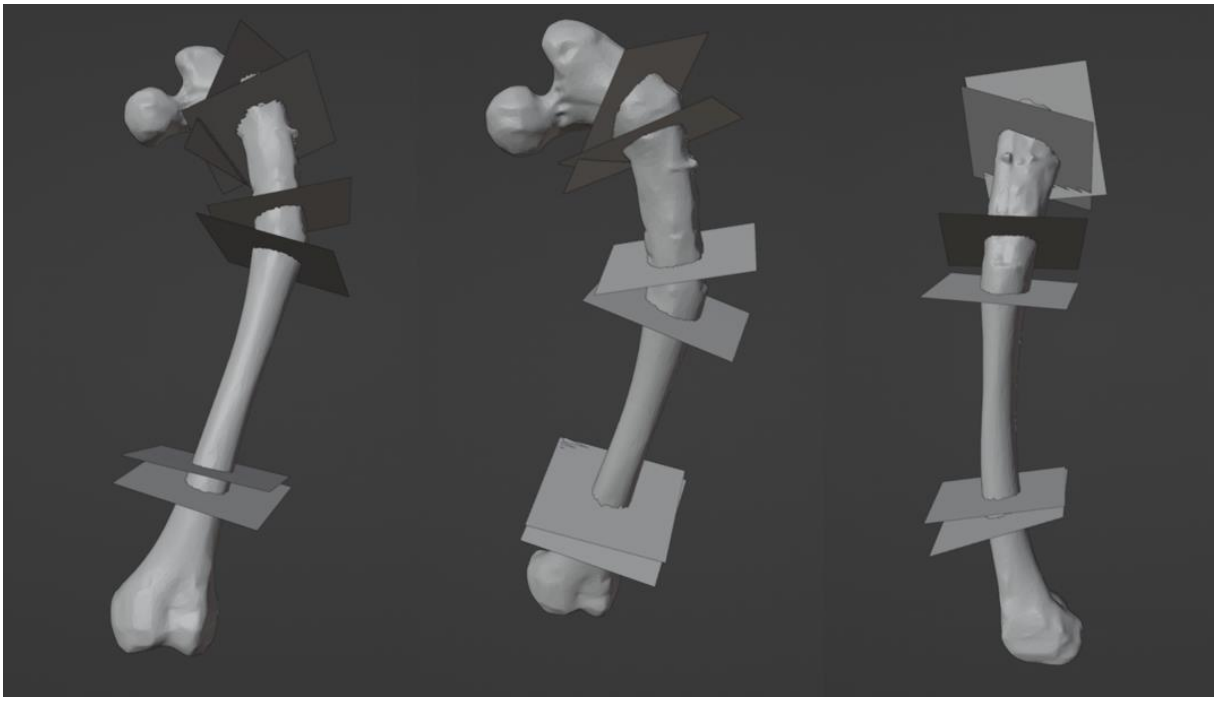

Figure 22: The automated visualization of the cutting planes in the preoperative situation in Blender.

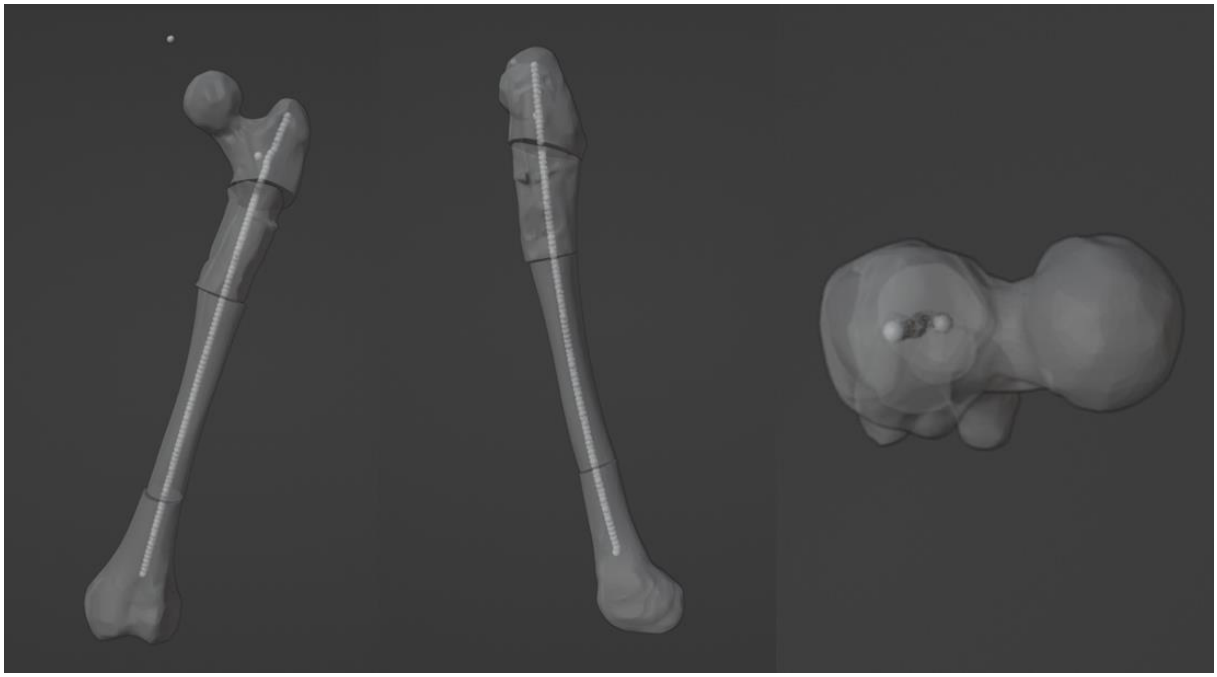

Figure 23: The automated visualization of the postoperative situation with the registered target shape in Blender.

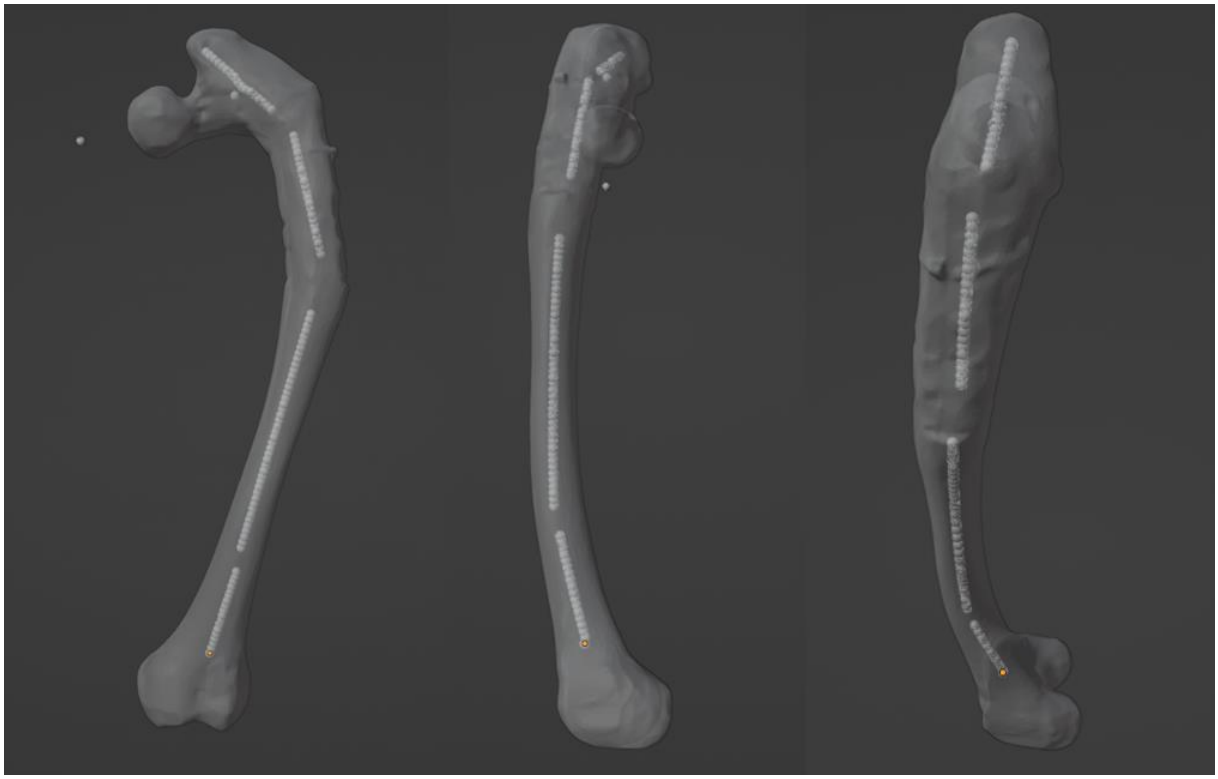

Figure 24: The visualization of the inverse osteotomy on the target shape registered to the preoperative situation in Blender.

2.7 Discussion and conclusion

In this technical document, the algorithm development and use is discussed in detail. Parametrisation, quantification and optimization of the osteotomy are defined and clarified. This document aims on demystifying development choices and inspire readers to develop their own applications.
The process of algorithm development has mostly been based on visual inspection of the algorithm output. For this the visualization tools have been of most value. Figures presented in this document, have been created for a single randomly selected case. Thus, it should be noted that recreation of these figures using the proposed algorithm can slightly differ from those presented in this document. This will be caused by the unique presentation of non-traumatic bony deformities.
The algorithm has several hyperparameters that can be tuned for specific use cases. The parameter bounds of the optimization are an important tuneable hyperparameter. For example, the bounds of the slope of the distal plane can be narrowed. This would reduce obliquity of the bony contact surface, which has impact on bone union.
The centreline resampling frequency and method are important hyperparameters, as they strongly influence preoperative plan optimization. In the current algorithm a linear interpolation with 160 samples is used. To represent the actual femoral centreline with more accuracy, it might be of interest to investigate other methods of resampling, such as b-spline interpolation.
Currently, the registration of the target shape is performed with a fixed set of steps. This approach is fast and reliable. However, the optimal preoperative plan is dependent on the trochanteric entry location chosen as anatomic landmark. By introducing a few extra parameters, the registration of the target shape can be added to the optimization as an extra objective. Using this method, the optimization is less dependent on the location of specific bony landmarks, such as collum axis and trochanteric entry point. This method was introduced by Carillo et al., by setting the orientation of osteosynthesis of antebrachii osteotomies as an added objective to the optimization function (5).
In conclusion, this document describes the reasoning behind the most important decisions in the development of the algorithm. The understanding of the algorithm is of importance when tuning hyperparameters, such as the optimization bounds and centreline resampling. In future research, adding the registration of the target shape to the optimization might improve the generated preoperative plan.

2.8 Bibliography

1. Paley D. Principles of deformity correction: Springer Science & Business Media; 2002.
2. Wilmerding V, Krasnow DJIAfDM, Paper SR. Turnout for dancers: hip anatomy and factors affecting turnout. 2011.
3. Beume N, Naujoks B, Emmerich MJEJoOR. SMS-EMOA: Multiobjective selection based on dominated hypervolume. 2007;181(3):1653-69.
4. Blank J, Deb KJIa. Pymoo: Multi-objective optimization in python. 2020;8:89497-509.
5. Carrillo F, Roner S, von Atzigen M, Schweizer A, Nagy L, Vlachopoulos L, et al. An automatic genetic algorithm framework for the optimization of three-dimensional surgical plans of forearm corrective osteotomies. Medical image analysis. 2020;60:101598.

3 Workflow Documentation

The general architecture of the software is embedded in the scripting module of Blender 3.1 (Blender Foundation, The Netherlands). For the use of the software, the Blender file “main.blend” must be present, as well as a set of 4 python scripts. These scripts contain functions and classes that handle: 1) basic functions needed for all scripts, such as performing shape generation or vector calculations, 2) the calculation and adjustment of bony landmarks, 3) the optimization and visualization of preoperative plans, 4) the use of these functions through the Blender GUI. Blender makes use of an in-build Python interpreter so the installation of an independent Python interpreter is not needed. The “main.blend” file contains a section that, when executed in administrator mode, will install the needed packages to the in-build Blender environment. Bone specific parameters and optimization solutions are stored using a .xlsx file and a .txt file respectively. The schematic workflow and the communication paths between files and scripts are displayed in Figure 1.

On the basis of a set of images, the workflow for preoperative planning of a single case will be elaborated upon. Note that the workflow consists of two parts. The internal validation of the model, which consists of inspecting the model within the Blender GUI, and the external validation. For the external validation Mimics 25.0 (Materialise, Belgium) and 3Matic 17.0 (Materialise, Belgium) are used.

In this workflow example, a preoperative planning for a shepherds crook deformity is designed and validated. The steps emphasize on the use of the tool as well as some common clinical decision making.

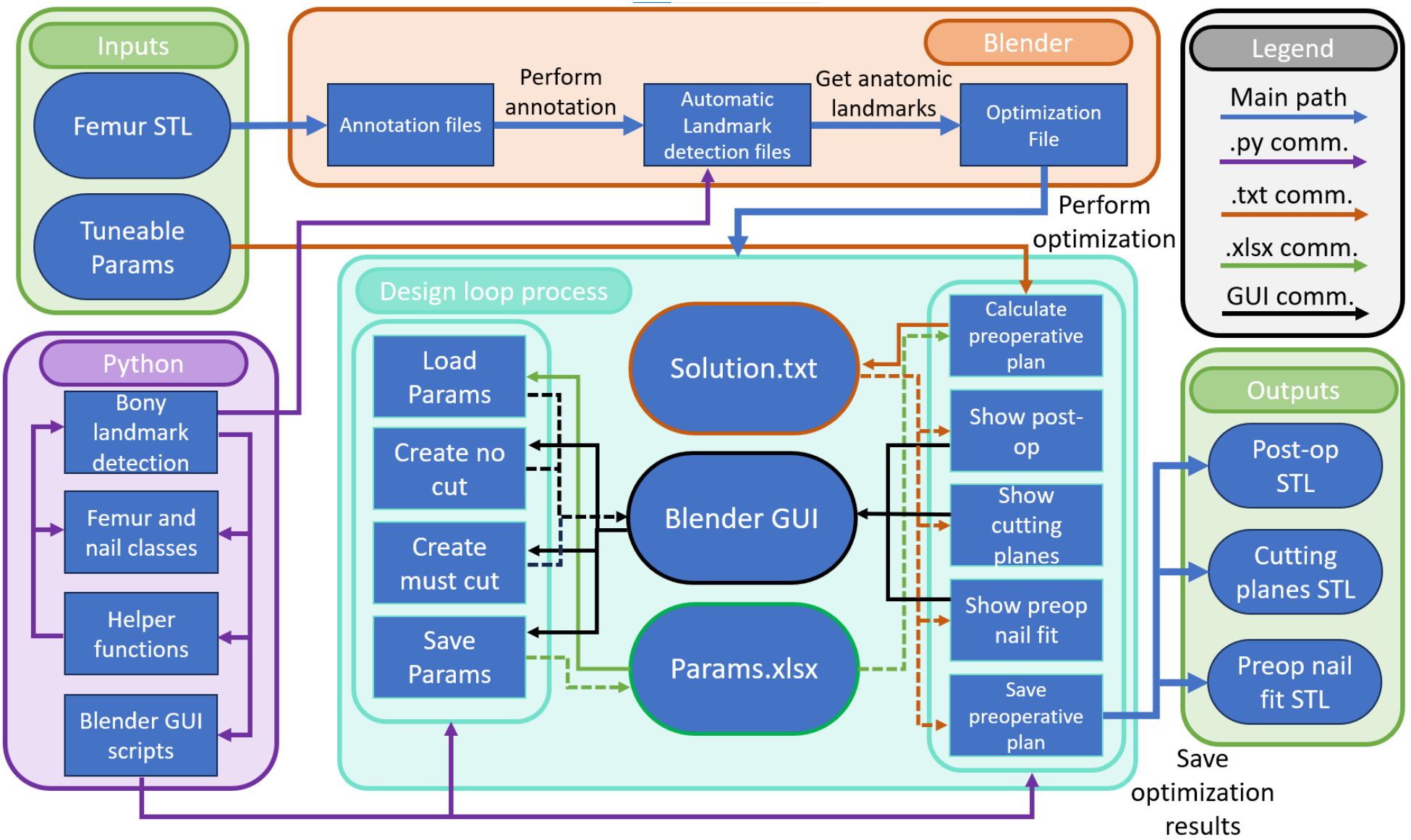

Figure 1: The workflow of the software solution and its communication paths visualized schematically. The main path follows the blocks: 1) Femur STL, load the model, 2) Annotation files, annotate the femur model, 3) Automatic landmark detection files, automatically calculate the location of the bony landmarks, 4) Optimization file, this opens the design loop process and its corresponding buttons in Blender enabling the semi-automatic design of preoperative plans, 5) Outputs, save the final results as STL files.

3.1 Internal validation

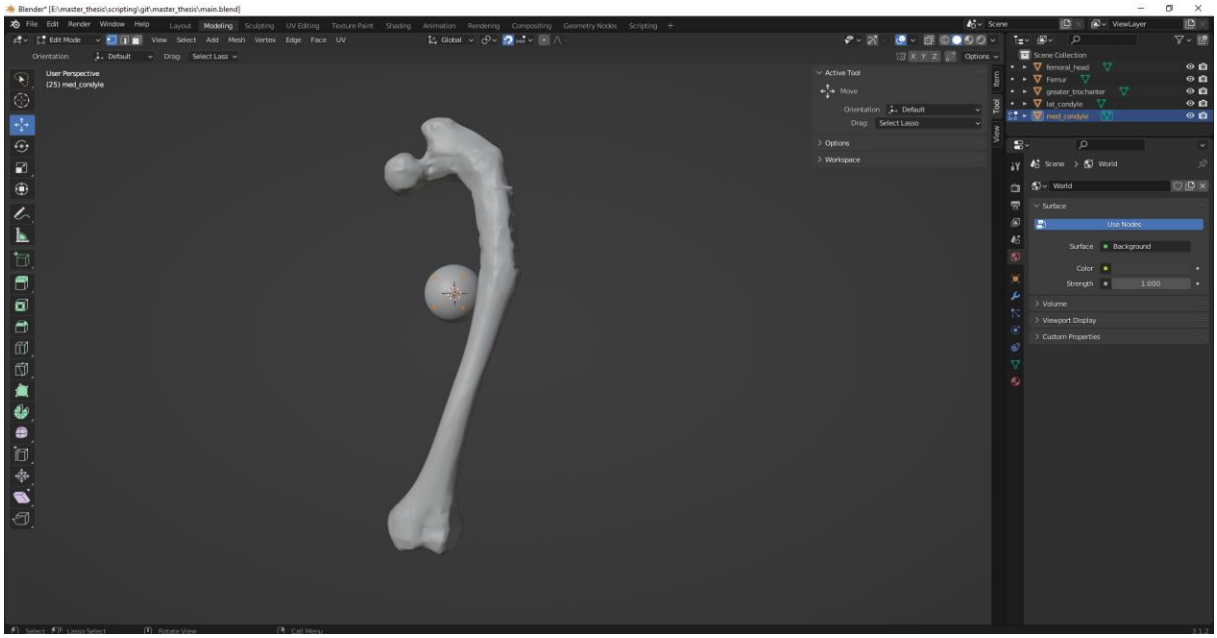

1, Import the STL model of the deformed femur in Blender (Blender Foundation, The Netherlands), by selecting the file location of the desired femur. The software will create 4 objects. Two spheres that will be used to annotate the caput femoris and the trochanter major and two cubes that will be used to annotate the region encasing the lateral and the medial condyle.

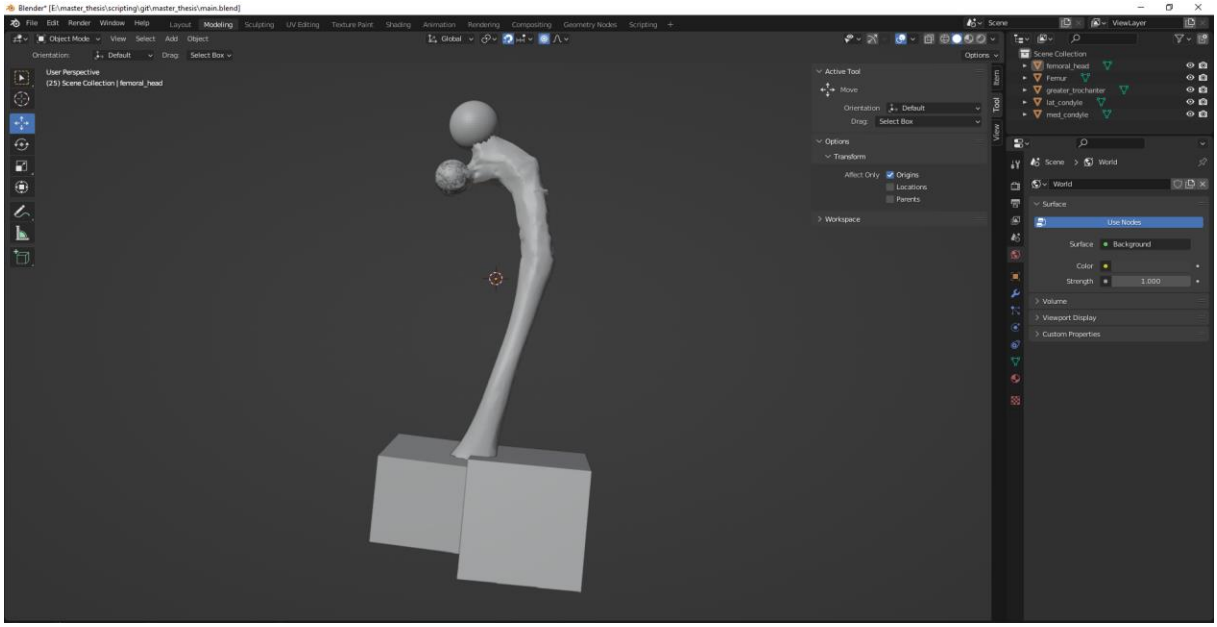

2, The shapes generated in the first step are used to roughly annotate the caput femoris, greater trochanter, medial condyle and lateral condyle. This is achieved by scaling, rotating and translating the shapes to their desired location.

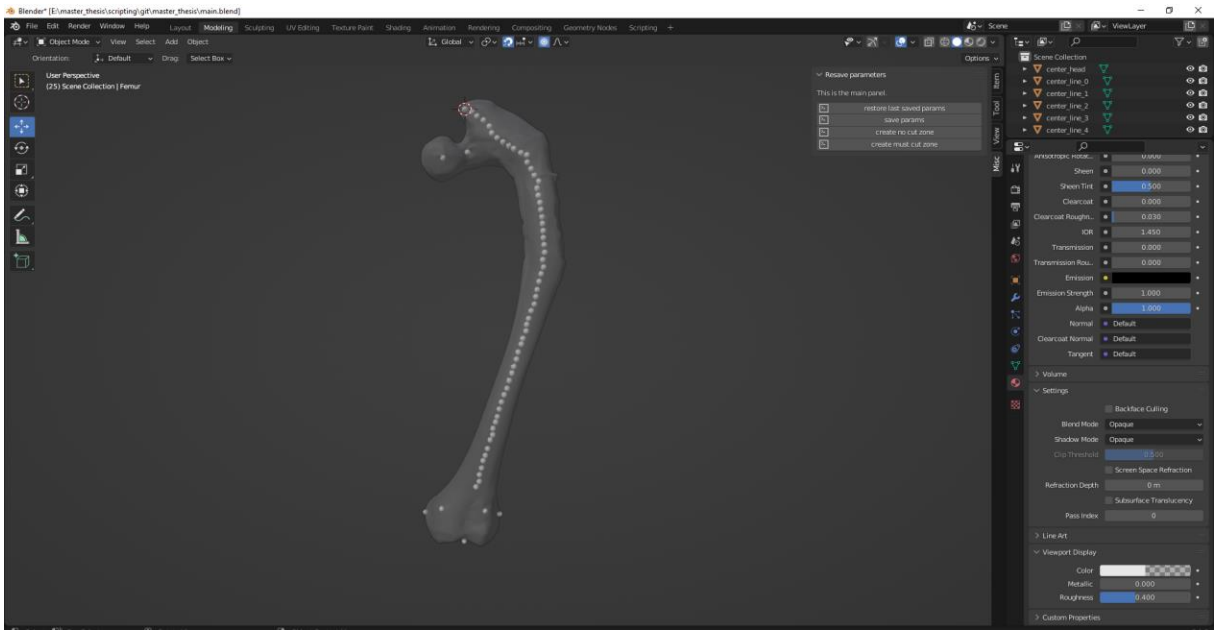

3, After satisfactory placement of the regions, the bony landmarks are extracted from the bone model. By executing the code in the calculate landmark section in Blender.

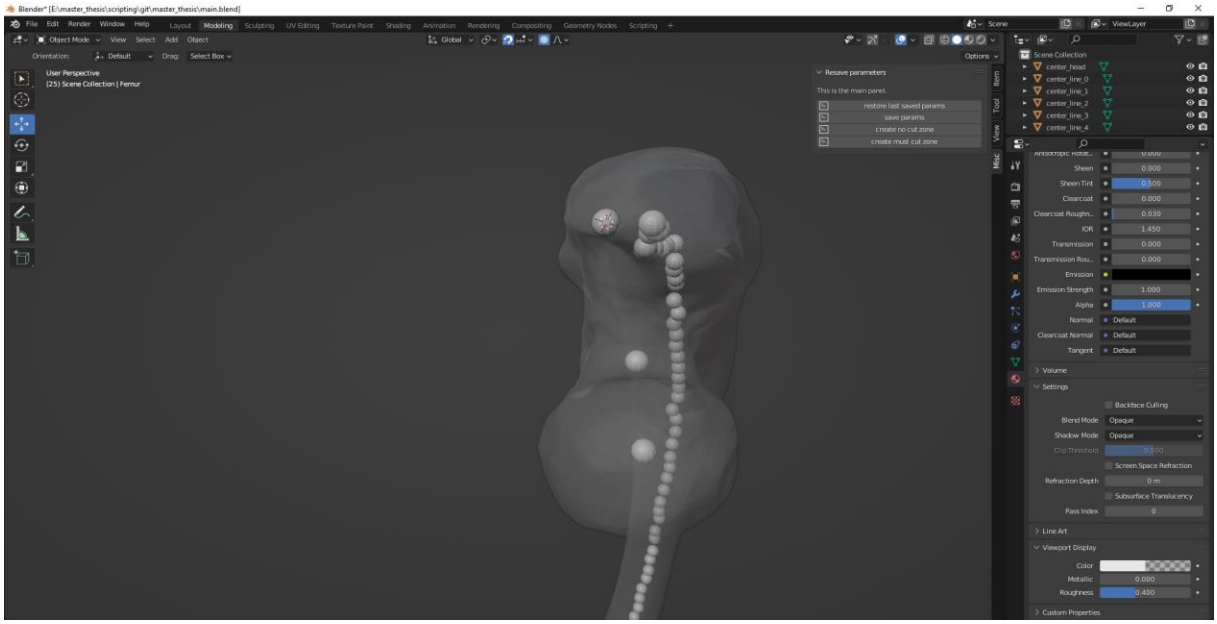

4, The landmarks are evaluated by visual inspection. This figure shows the inspection of the trochanteric entry point. One might say this entrance location is placed slightly too posterior.

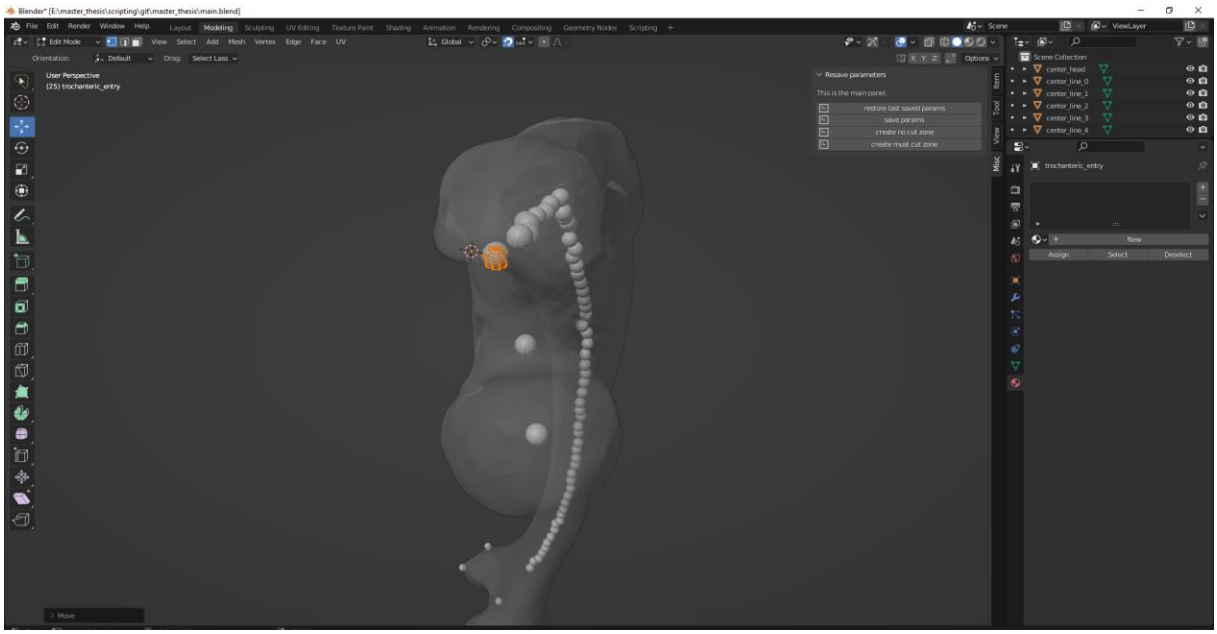

5, Using Blender's edit mode, the landmarks can be translated in three dimensions, until its location is deemed satisfactory.

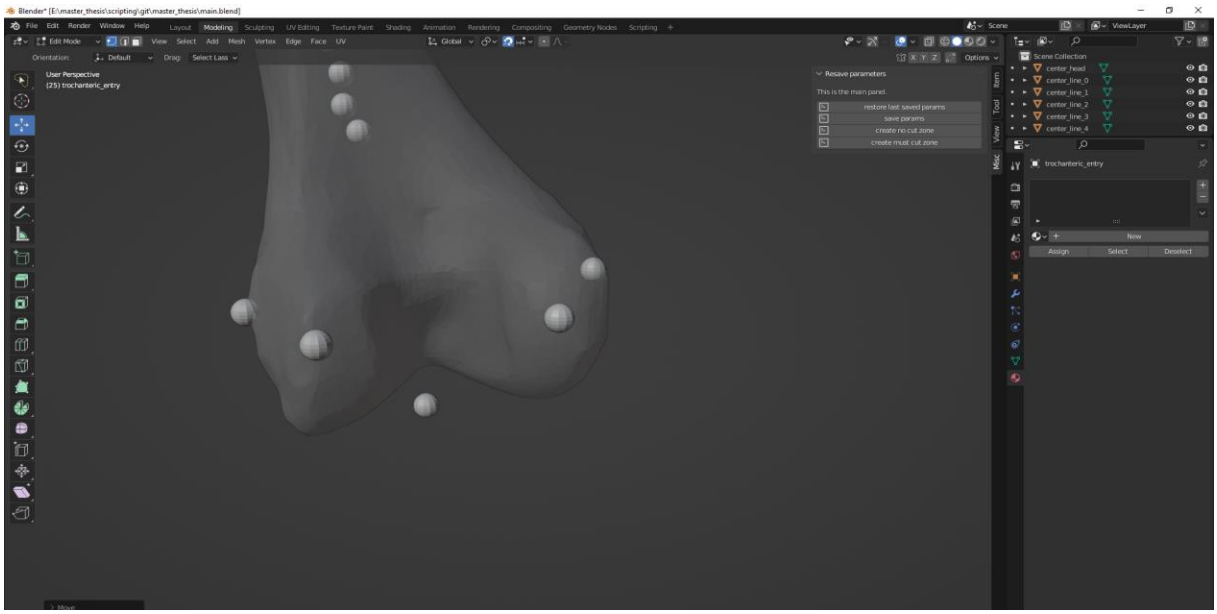

6, The landmarks distally are inspected and found satisfactory.

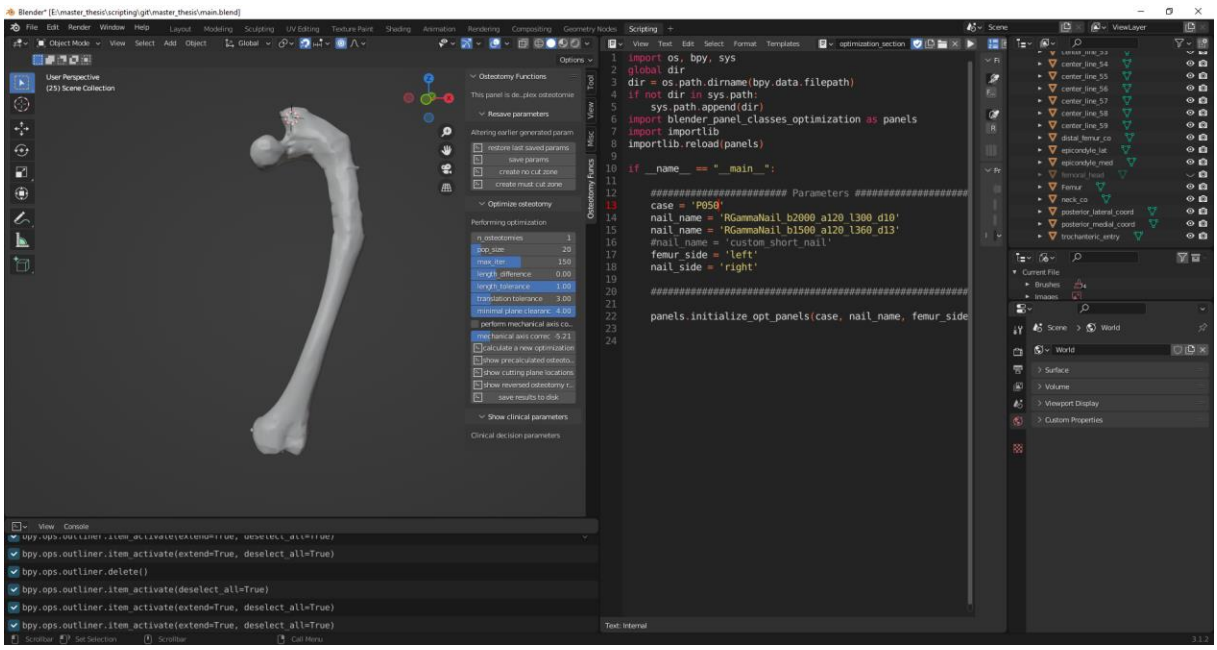

7, The landmarks are saved and the 'optimization section' of the Blender scripting module is opened. Running the script in this section makes a new set of operations and control panels in the graphical user interface (GUI) available.

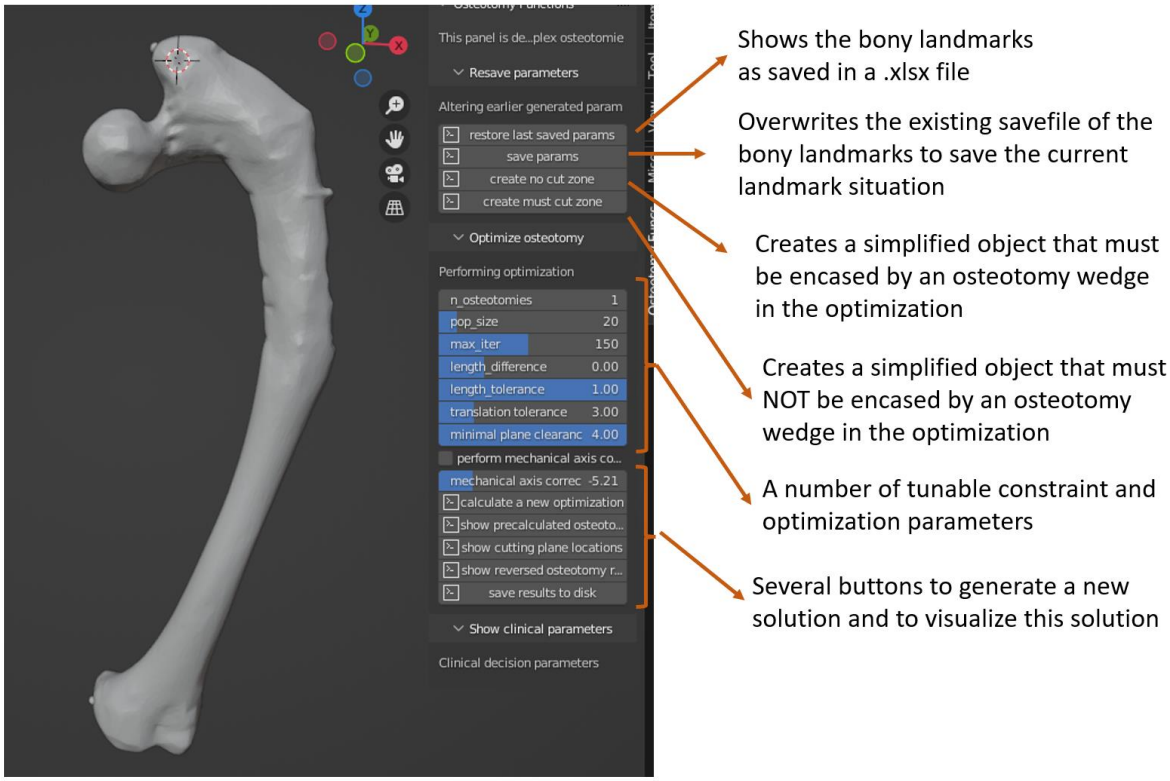

8, An overview of the newly made available operations and parameters.

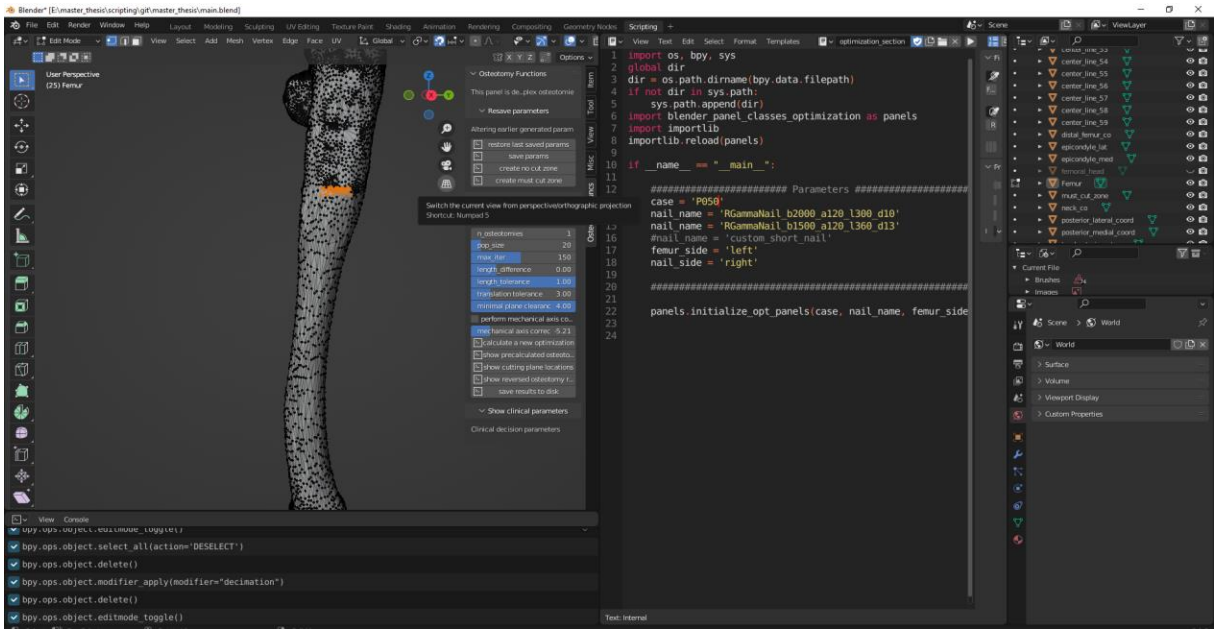

9, In Blender's edit mode several vertices are selected, after which the "create must cut zone" button is clicked. This will generate a simplified object of the region that during optimization must be encased by an osteotomy wedge. Note that only one must-cut zone per osteotomy wedge can be optimized successfully. Besides this a must-cut zone, partially or fully, encased by a no-cut zone cannot be optimized successfully.

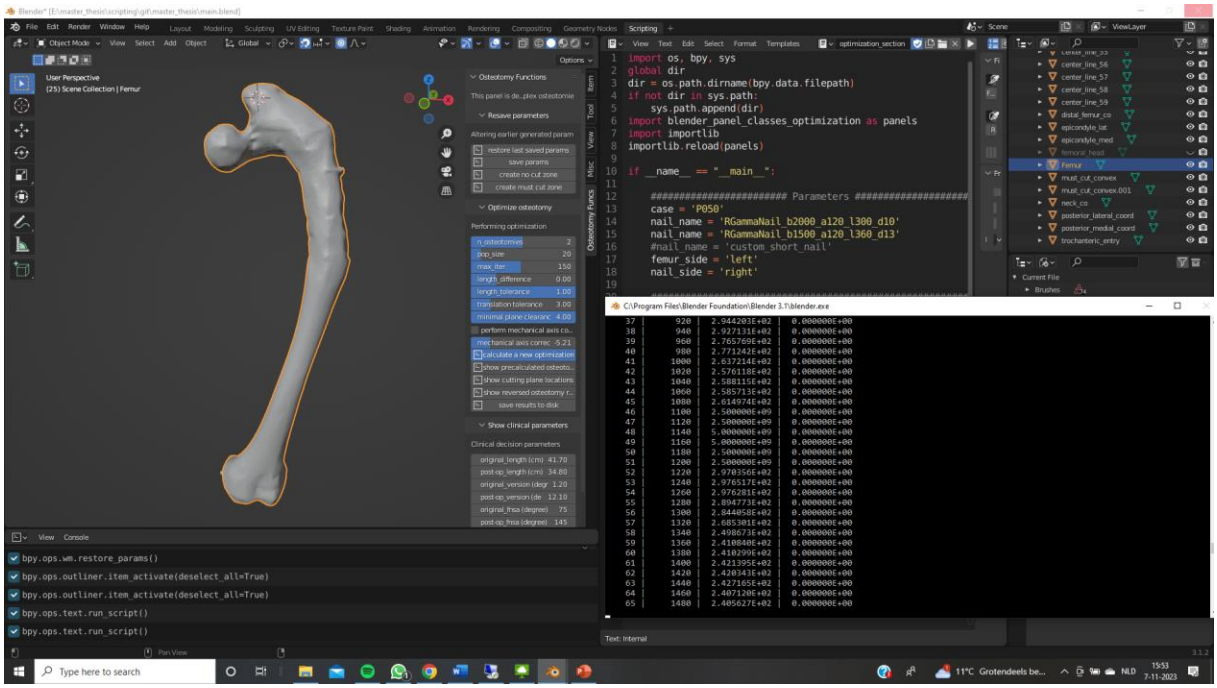

10, The parameters are set to create a preoperative plan with two osteotomies. The "calculate a new optimization" button is clicked.

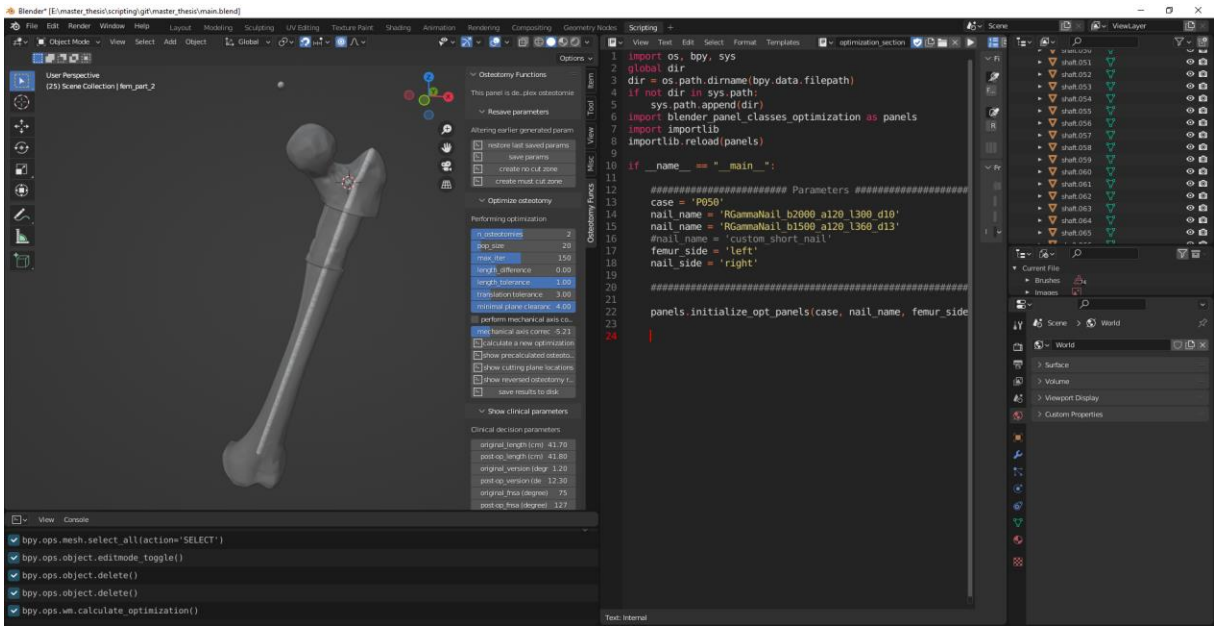

11, After calculation, the post-operative result is displayed in the GUI and a pre- and post-operative summary of bone specific properties are displayed.

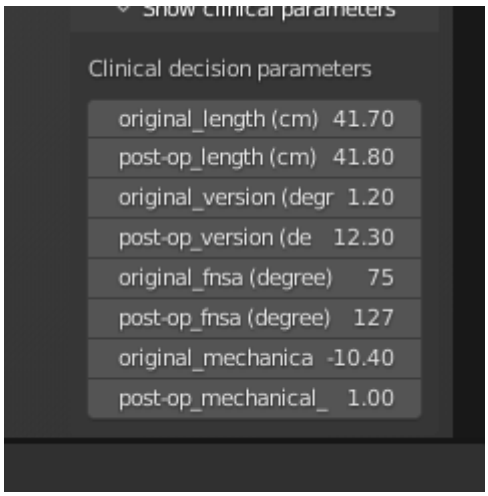

12, The femoral length, anteversion angle and femoral neck shaft angle are critical parameters that can help the decision making on the quality of the preoperative plan.

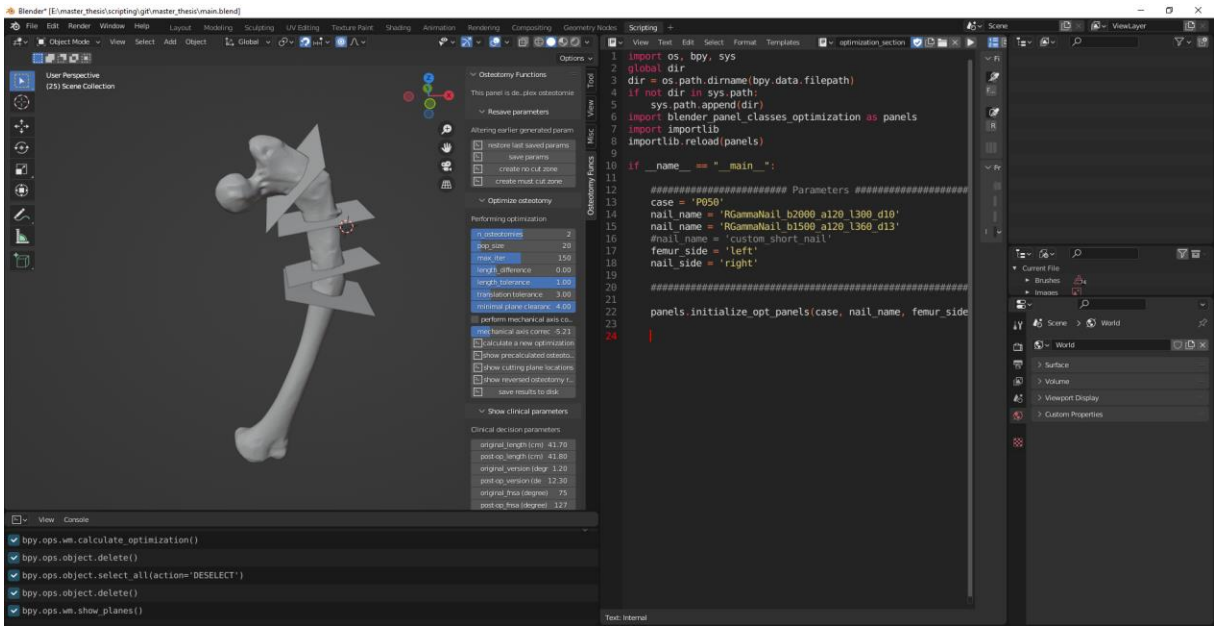

13, By clicking the "show cutting plane locations" button the location of cutting planes in the preoperative plan can be evaluated.

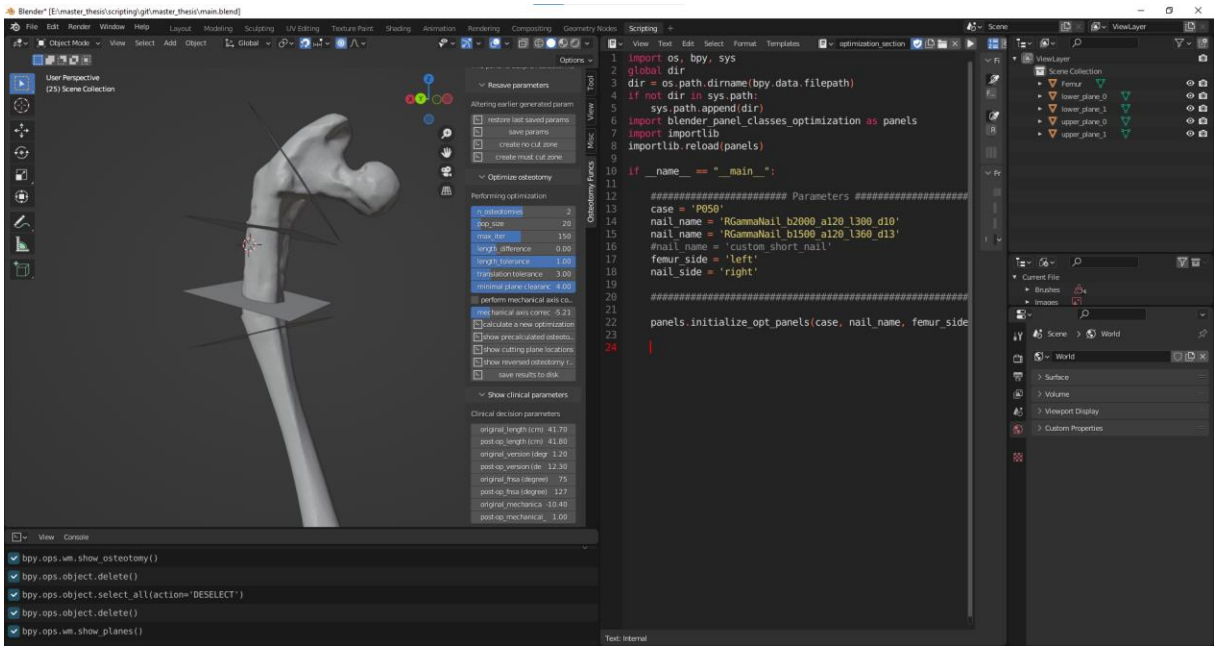

14, While inspecting the preoperative plan, it is noted that the trochanter minor is within the osteotomy wedge. It makes this preoperative plan undesirable. A new plan should be generated.

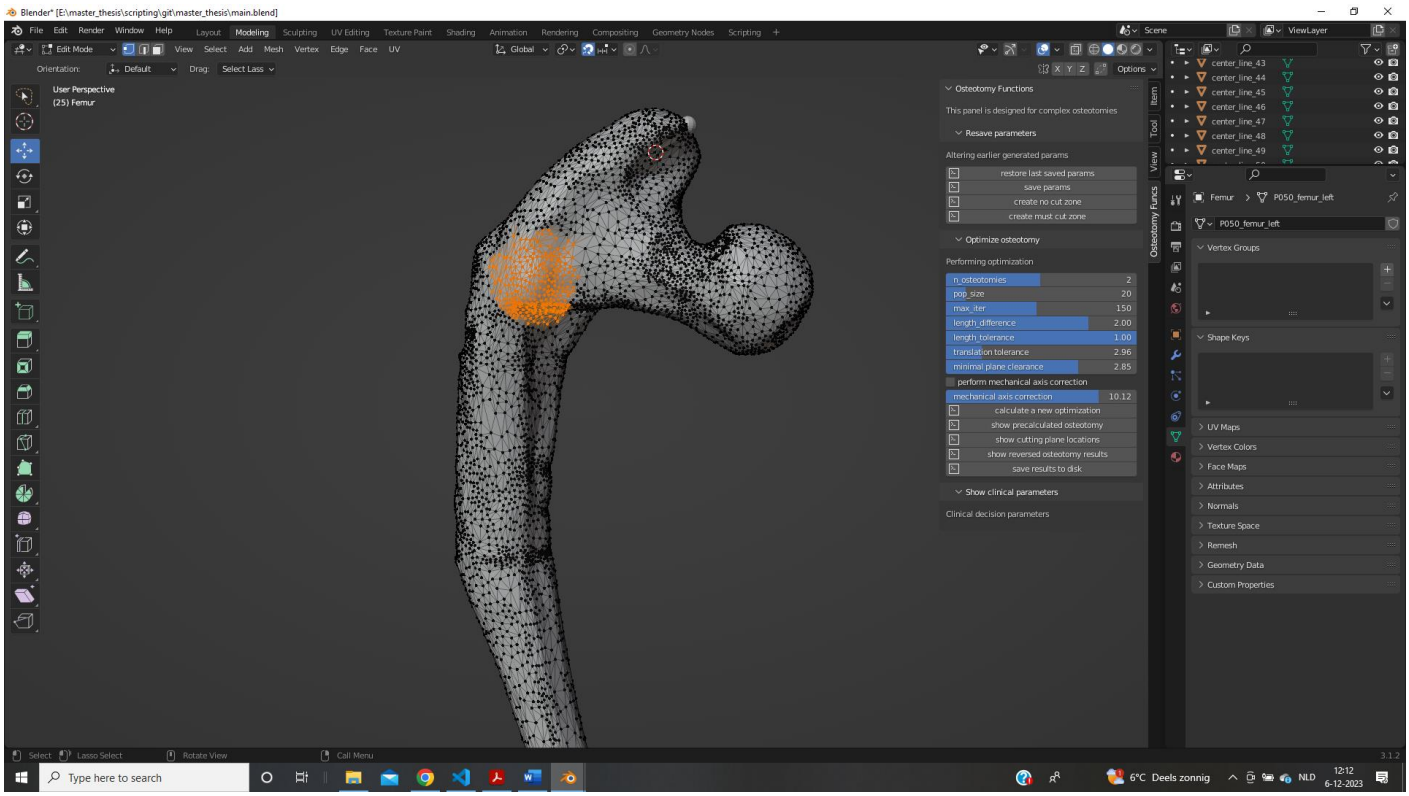

15 The trochanter minor is selected in edit mode and the “create no cut zone” button is clicked. This saves the simplified object of this region to the optimization parameter .xlsx file. This data will be used in the calculation of a new preoperative plan.

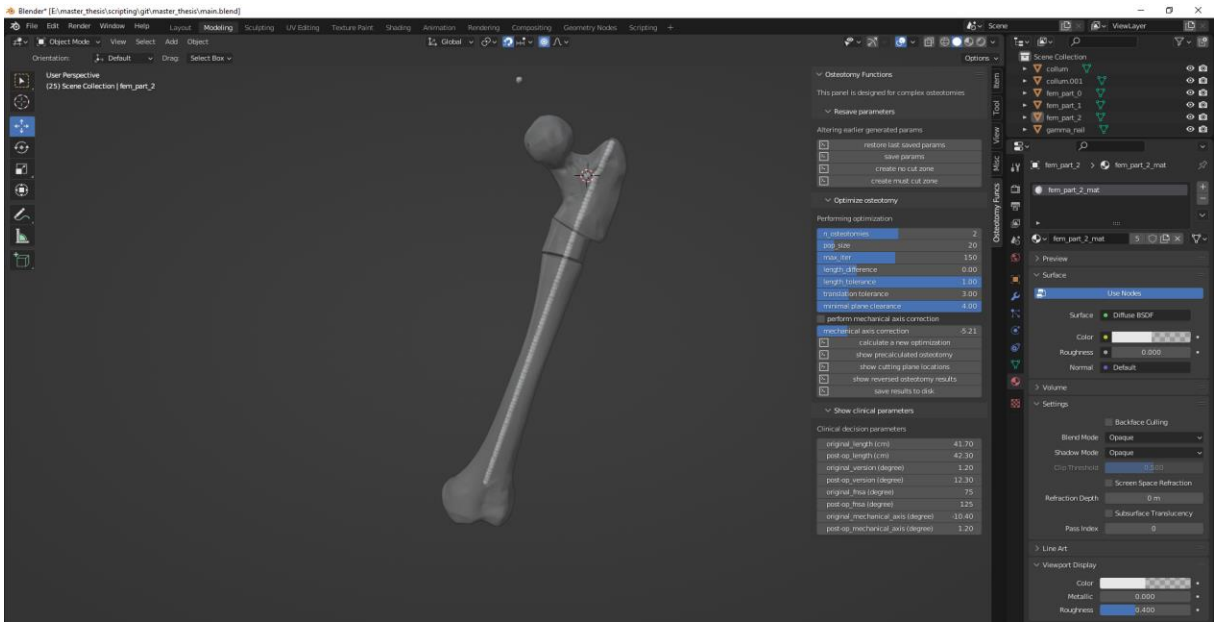

16, After calculation a plan is generated in which the trochanter minor is preserved.

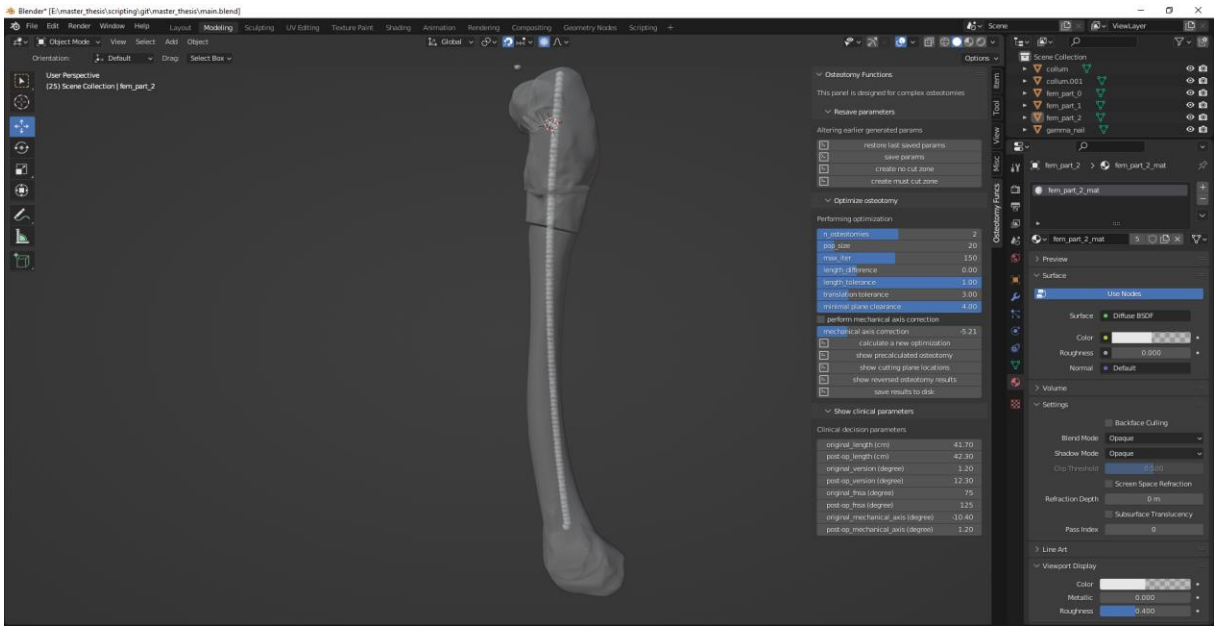

17, Inspection shows a poor fit of the gamma nail in the distal femur. It is decided that a preoperative plan with 3 osteotomies might give a more optimal solution.

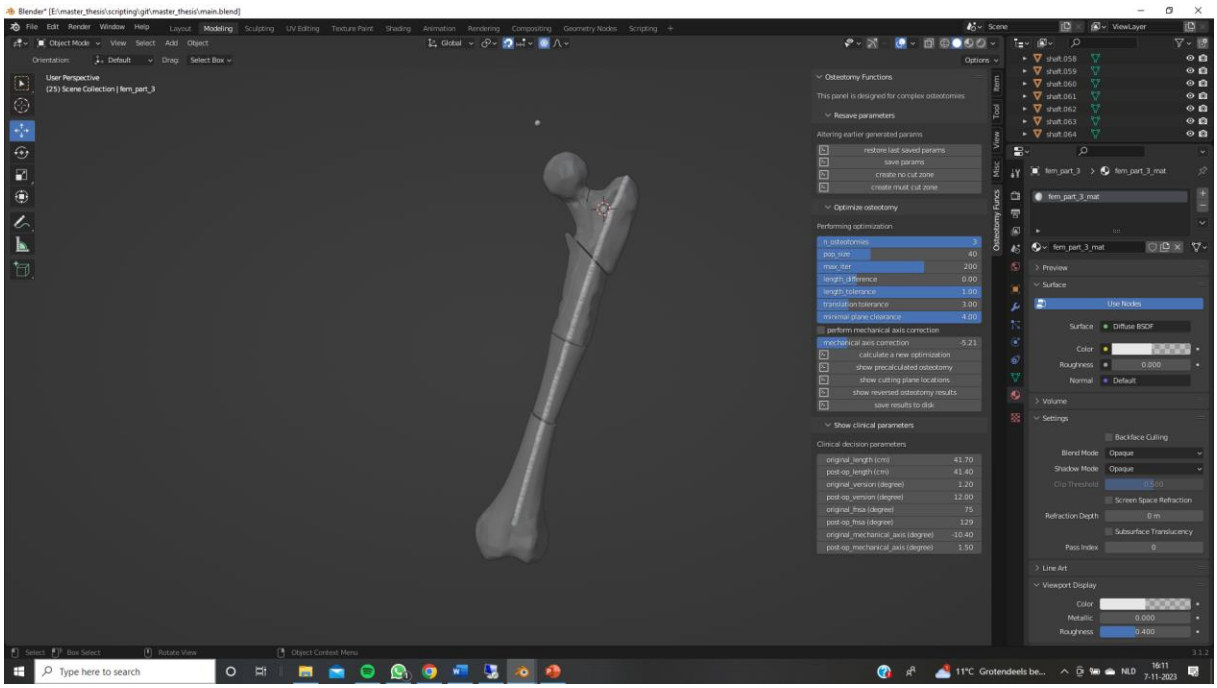

18, The number of osteotomies is changed in the parameters and a new calculation is performed. The result shows a preoperative plan with a good gamma nail fit and an intact trochanter minor.

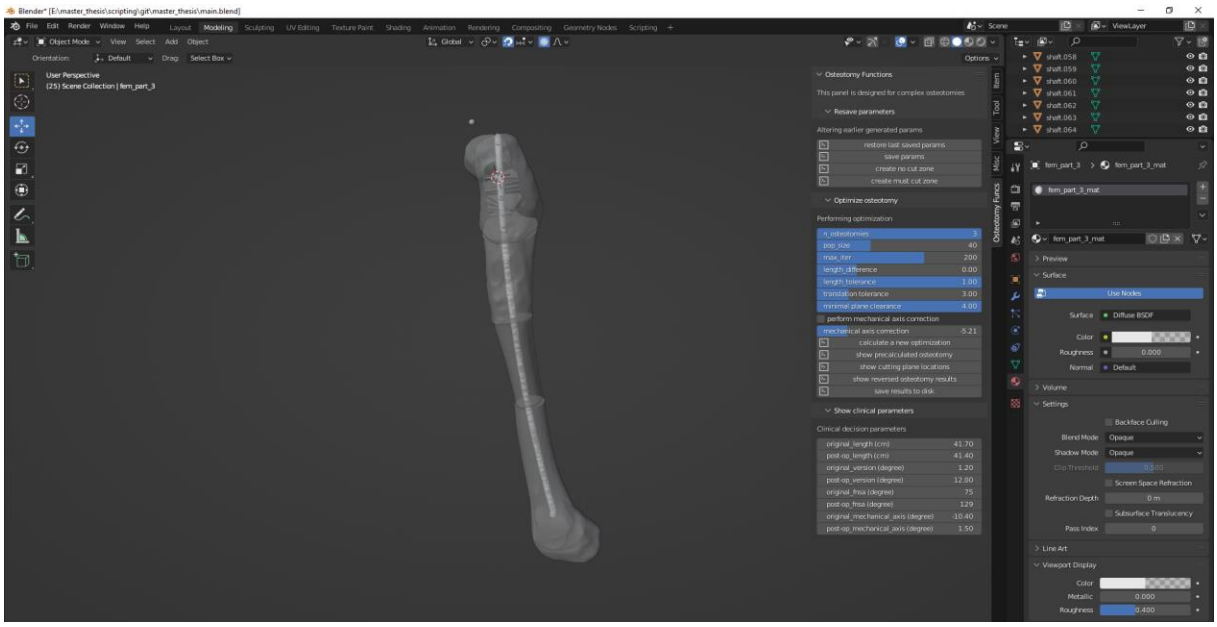

19, The anteroposterior fit of the gamma nail is excellent after the introduction of the third osteotomy.

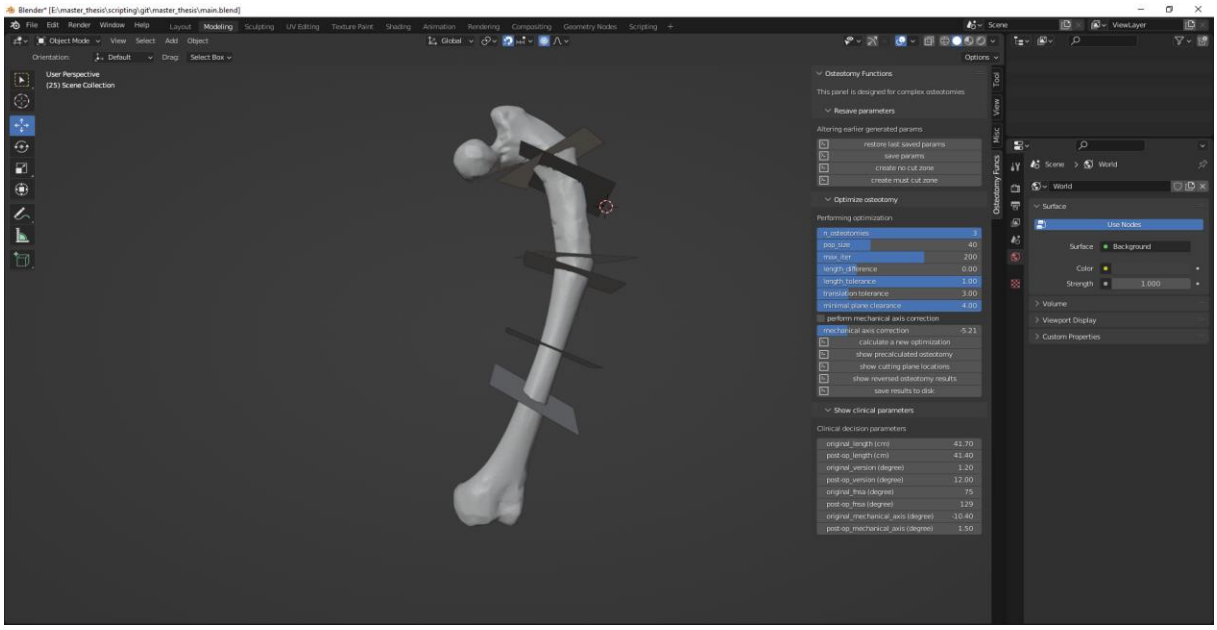

20, However, the distal wedge is considered to be very large. Possibly the preoperative plan will benefit from femoral lengthening.

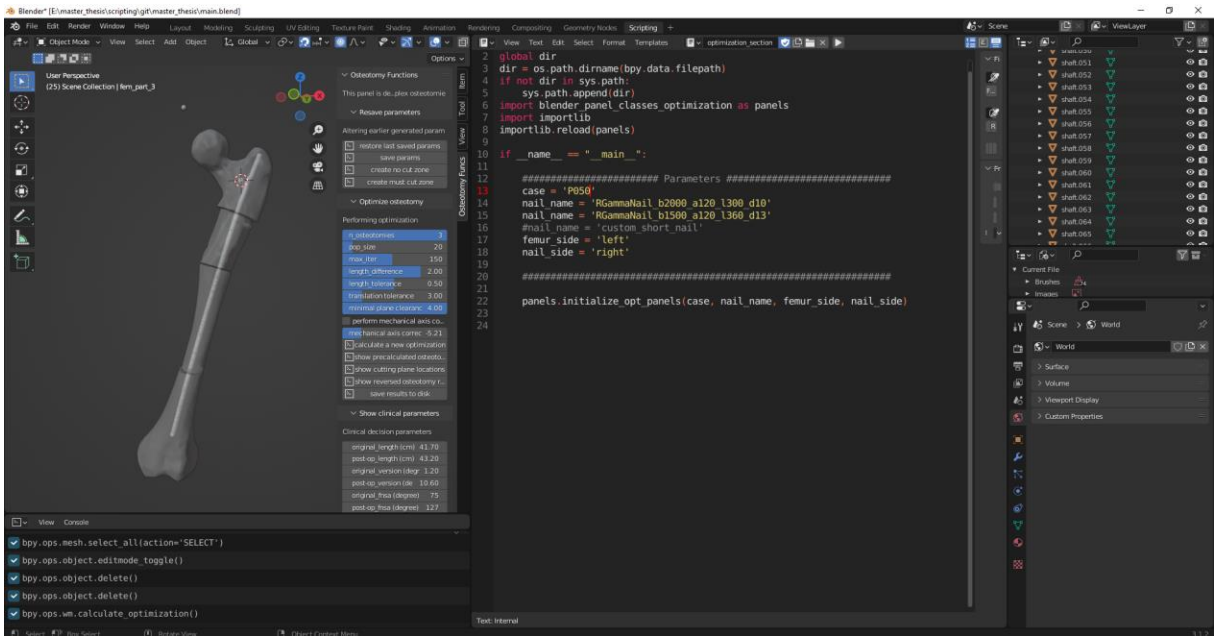

21, The "length difference" parameter is set to +2 meaning that the final result of the femur will have 2 cm of femoral lengthening. The post-operative result of this plan is displayed in the Blender GUI after recalculation.

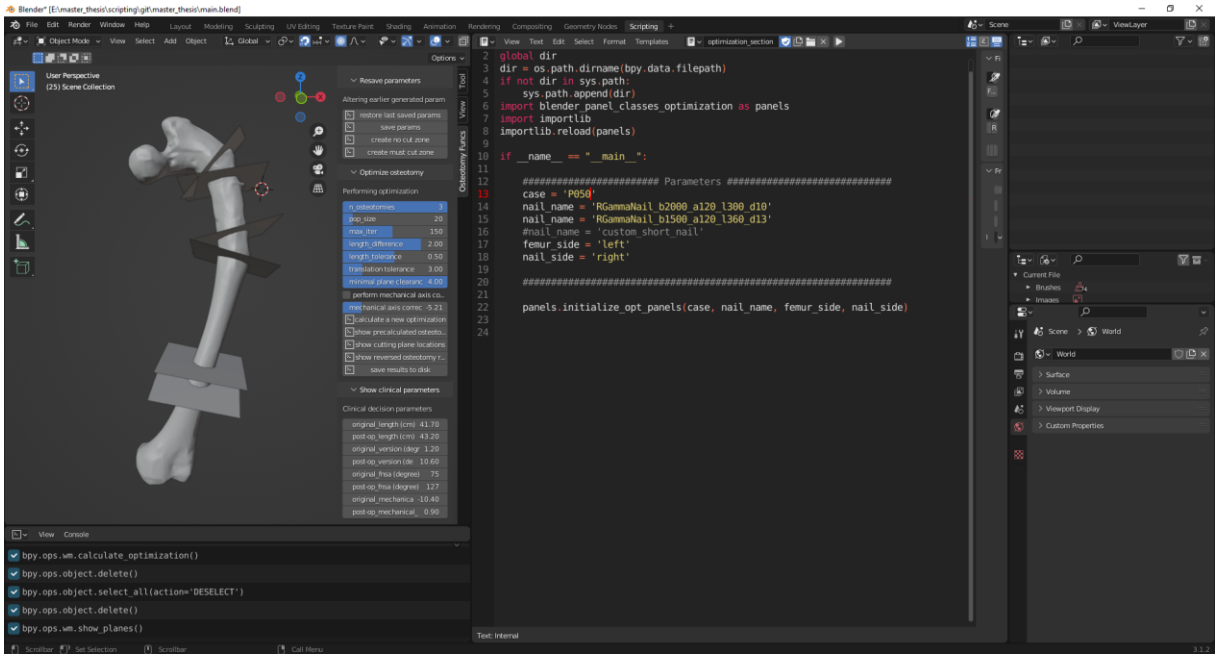

22, The cutting planes show a significantly smaller osteotomy wedge distally.

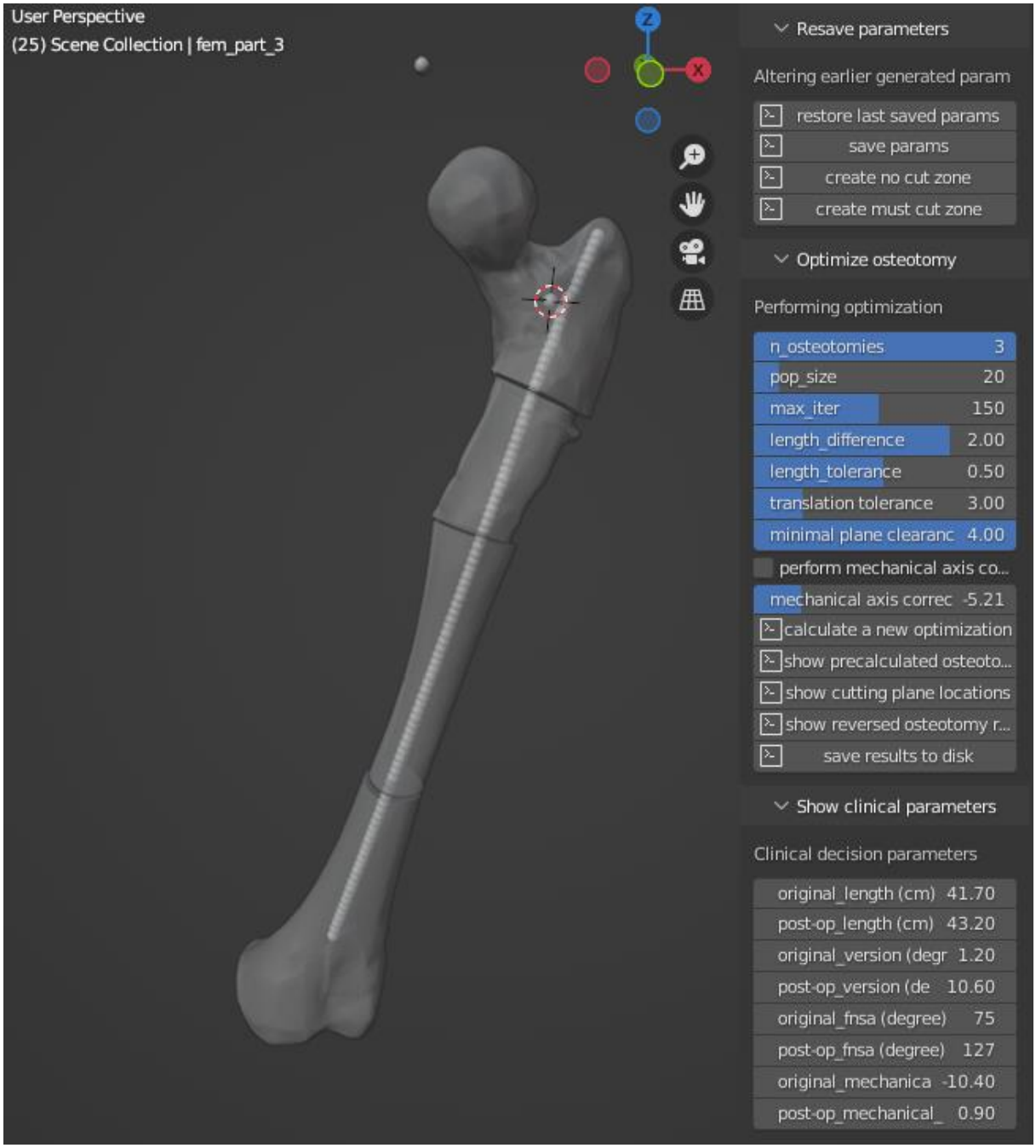

23, The final result and clinical decision parameters are visualized and deemed acceptable for surgery. The preoperative plan is complete and the STL files of this plan are exported by pressing the “save results to disk” button.

3.2 External validation

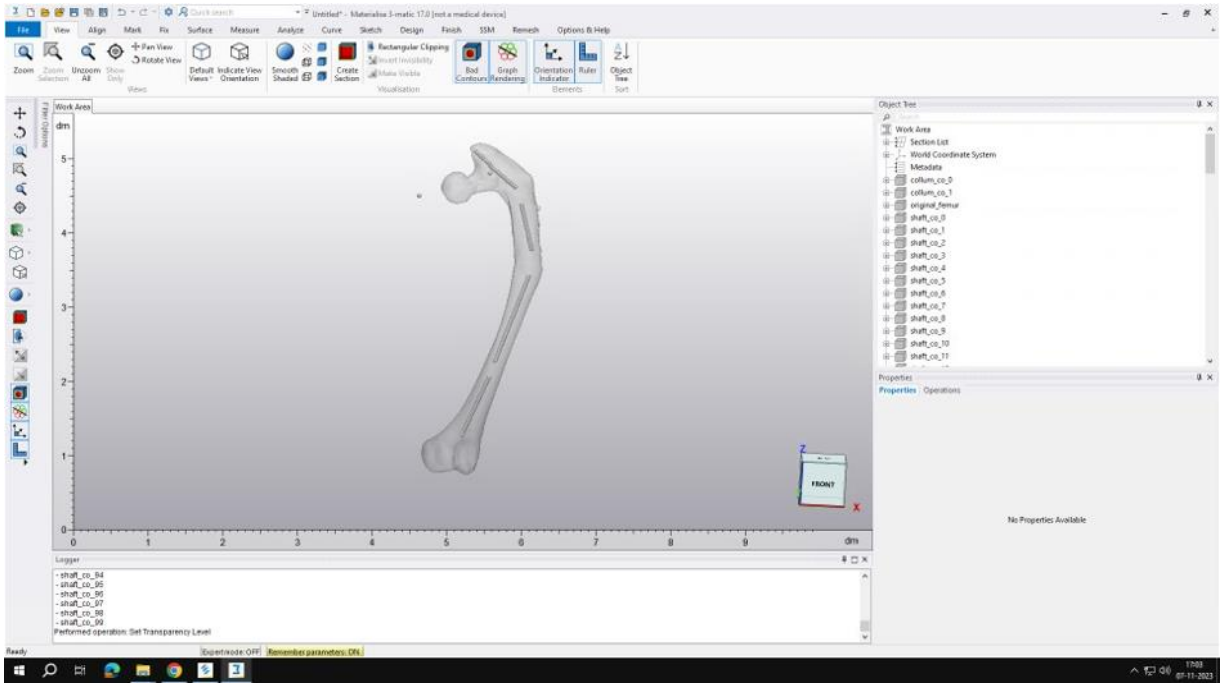

24, The STL files exported in the final step of the creation of the internal validation are imported to 3Matic.

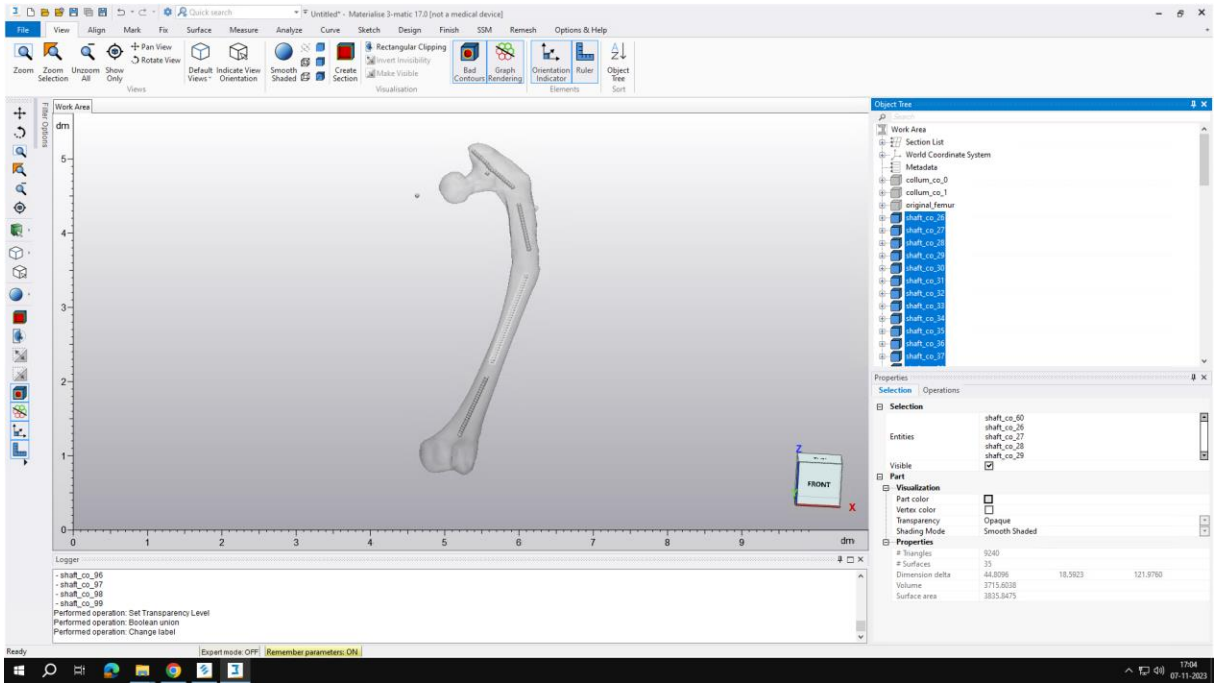

25, All separate nail coordinates belonging to the same nail part are fused using a Boolean union operation. This gives a better overview of the imported nail parts.

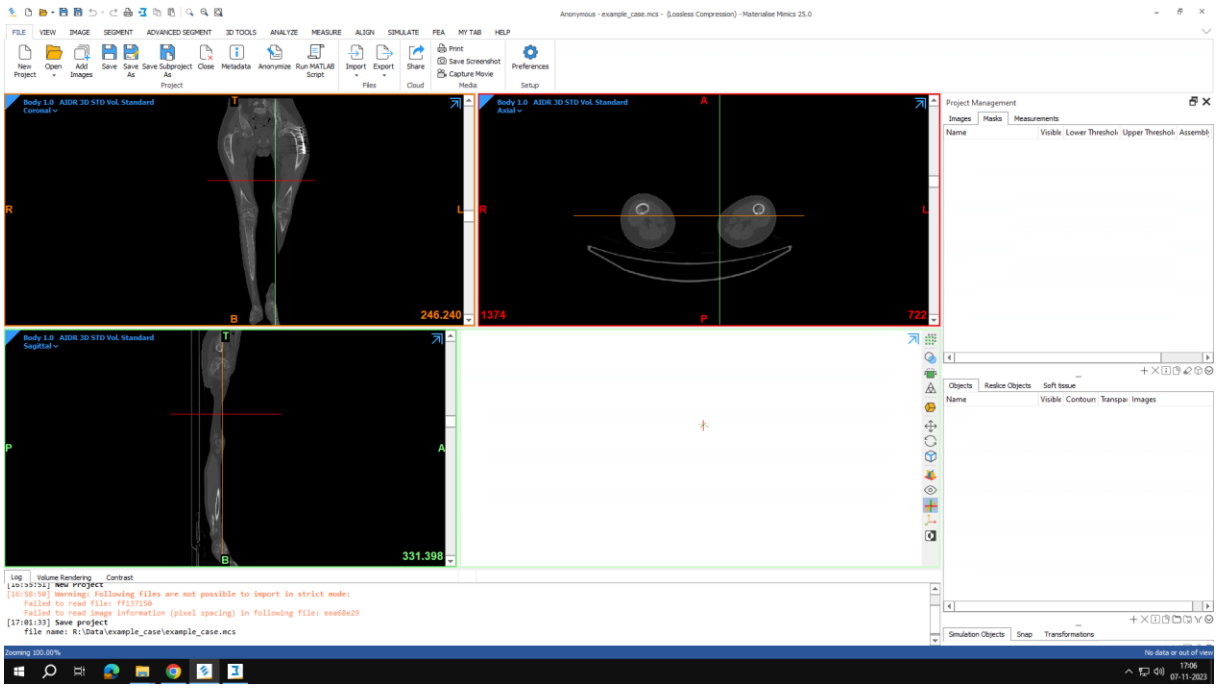

26, The CT scan of the corresponding patient is loaded to Mimics.

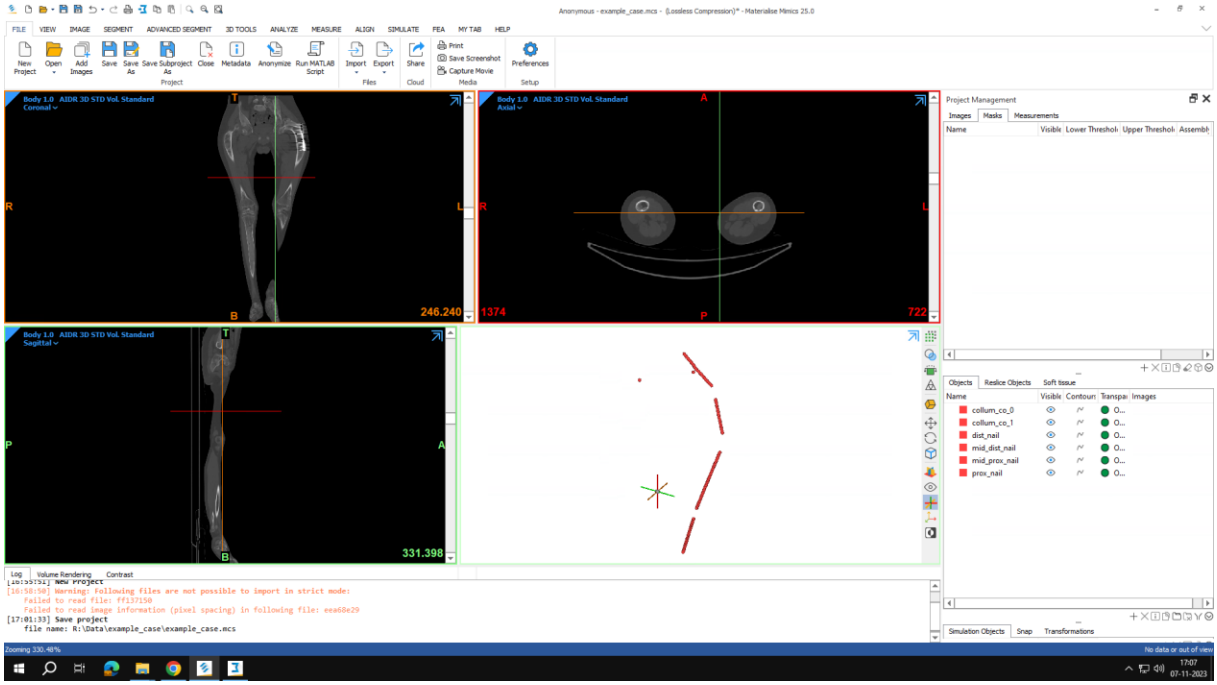

27, The parts of the nail generated from the union operation in 3Matic are imported to the Mimics environment, to check the fit of the nail intra-operative on the preoperative scan.

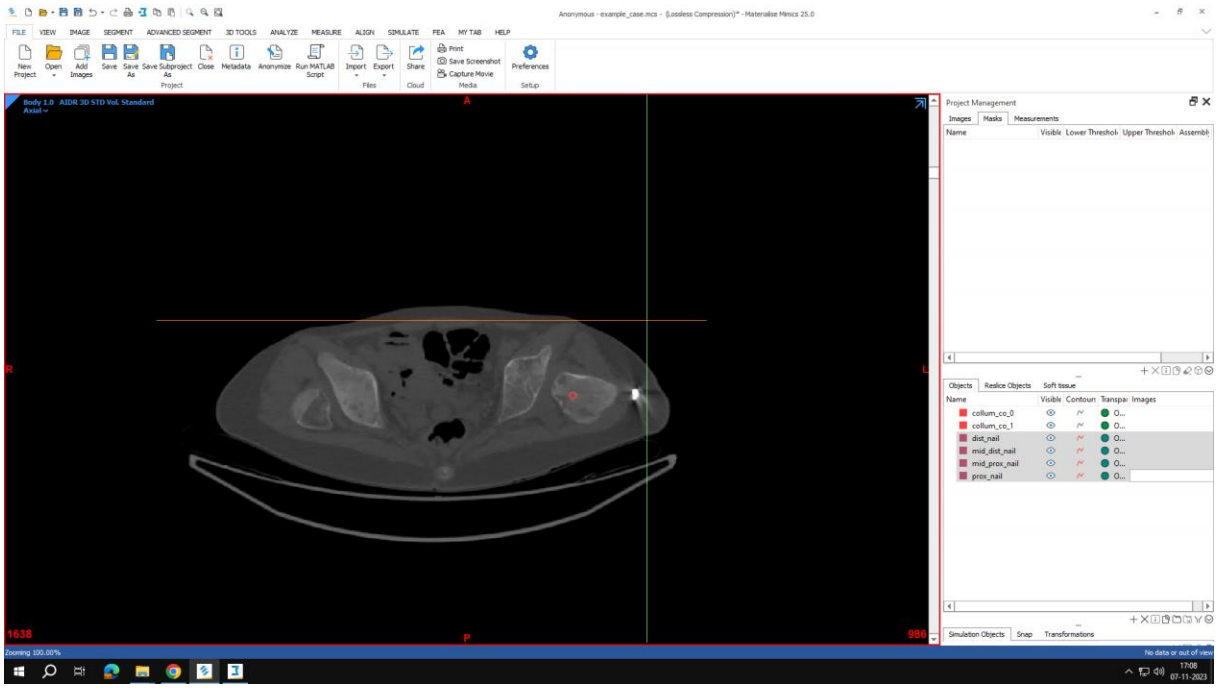

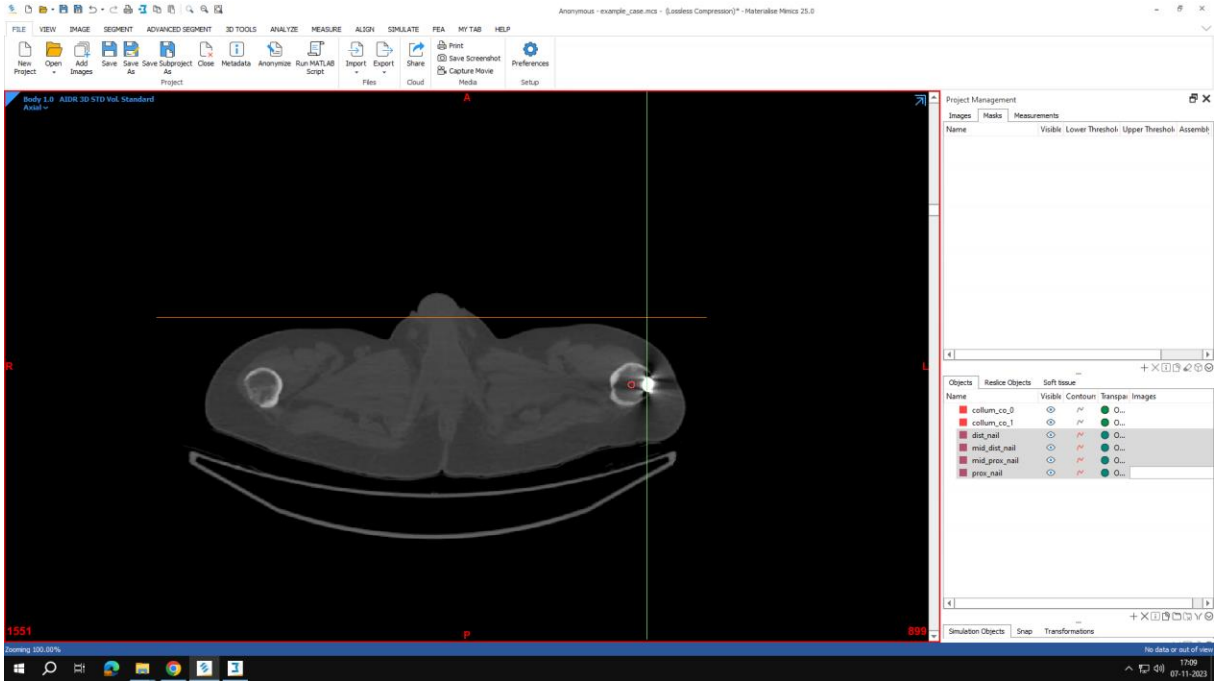

28, The fit of the nail is checked on all axial slides. Two slides are shown here as example.

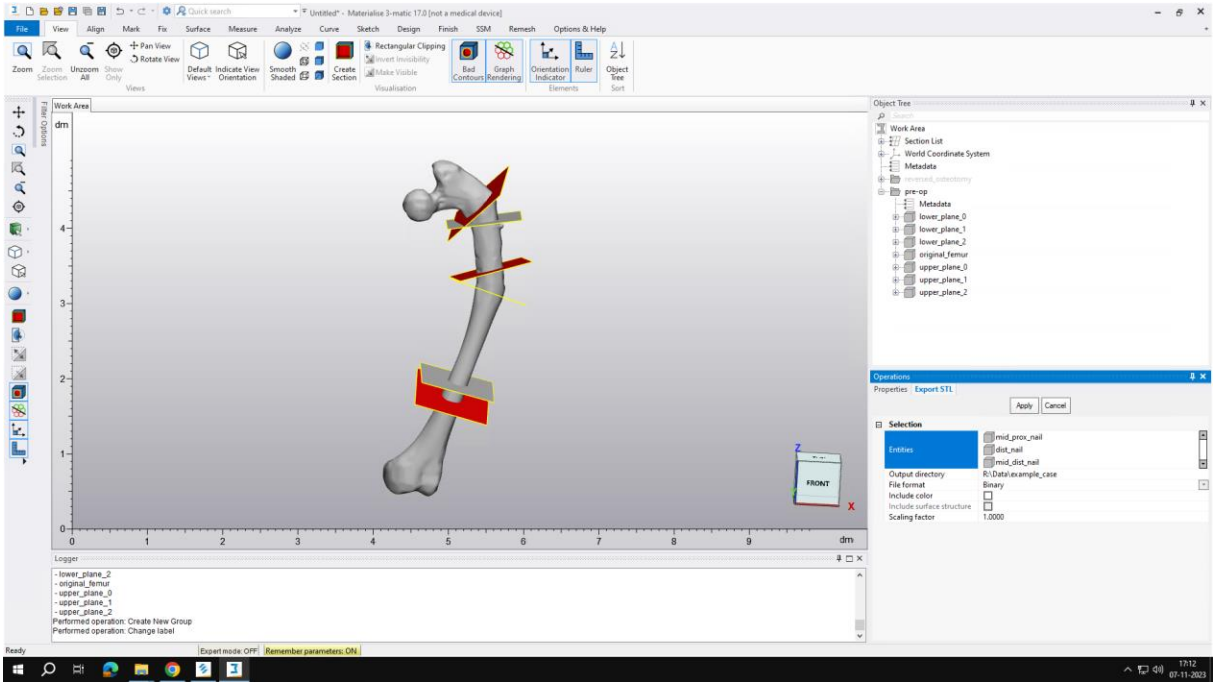

29, The cutting planes generated by the Blender software are loaded to 3-Matic.

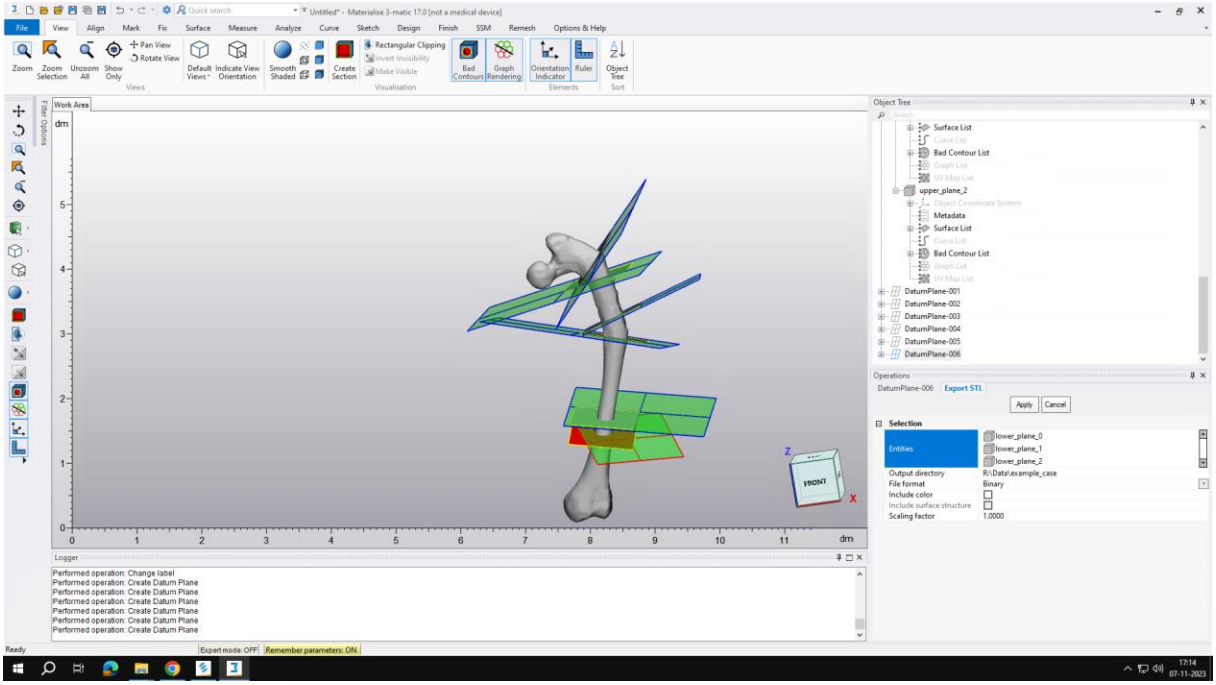

30, Datum planes are created for each cutting plane object.

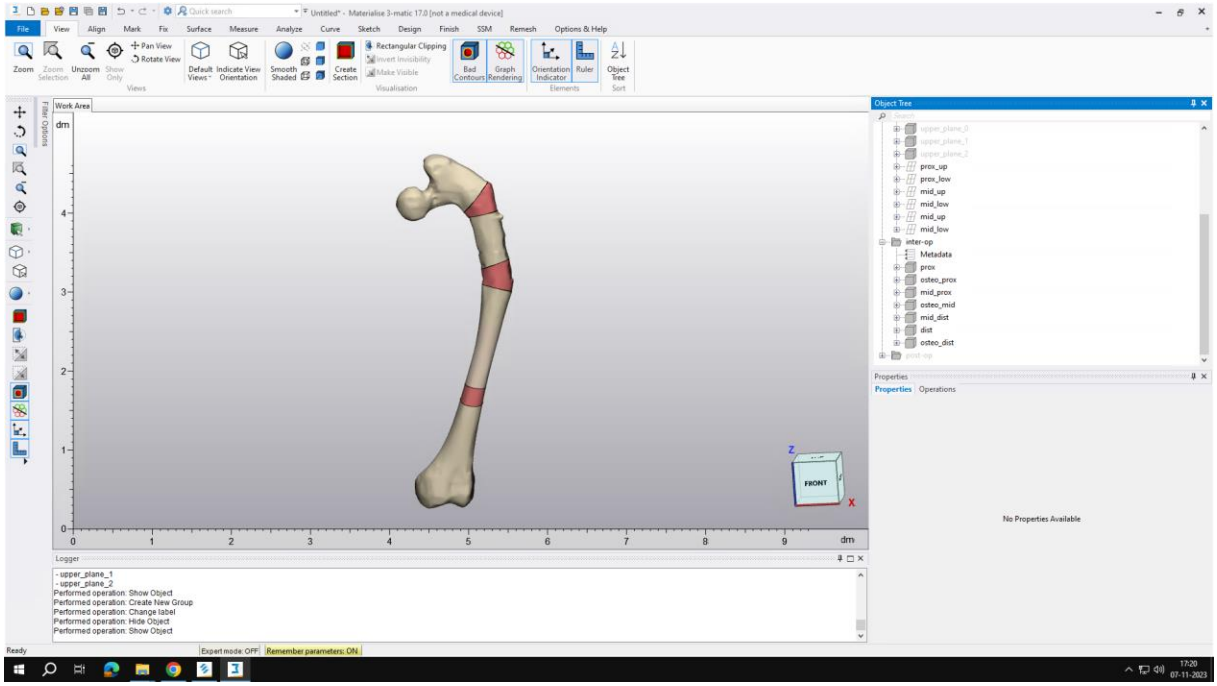

31, The datum planes are used to visualize the intra-operative situation.

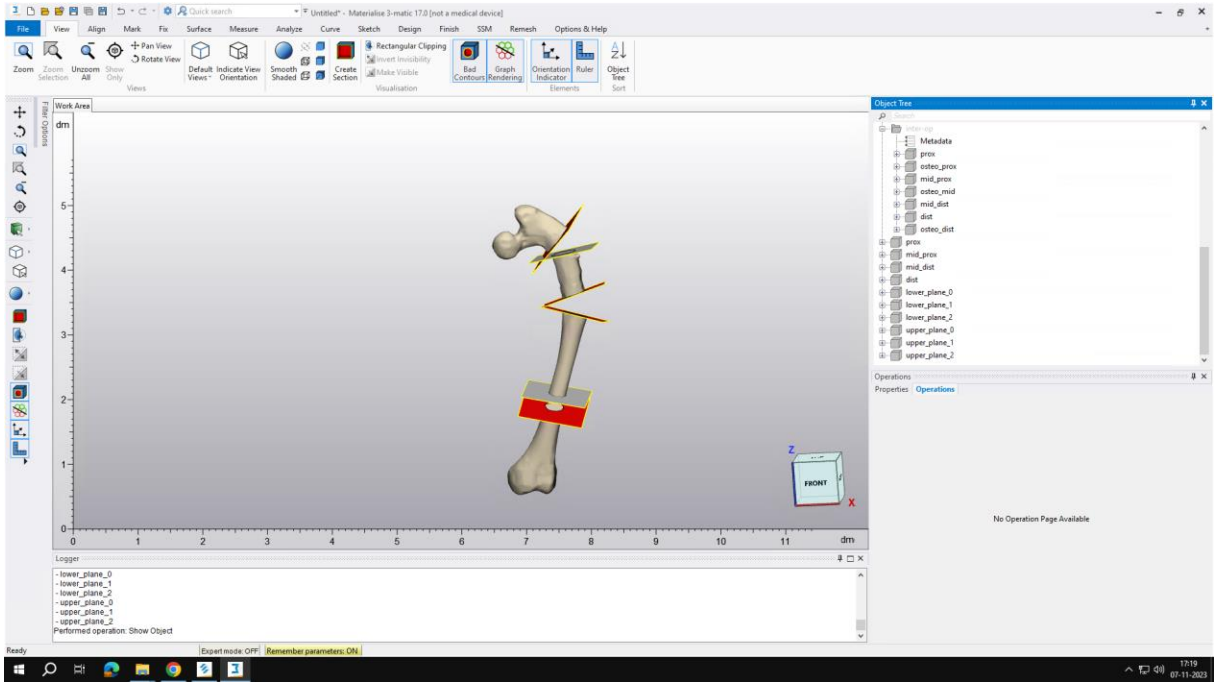

32, The osteotomy wedges are removed from the collection of objects and only the cutting planes and the remaining bony pieces after osteotomy are shown.

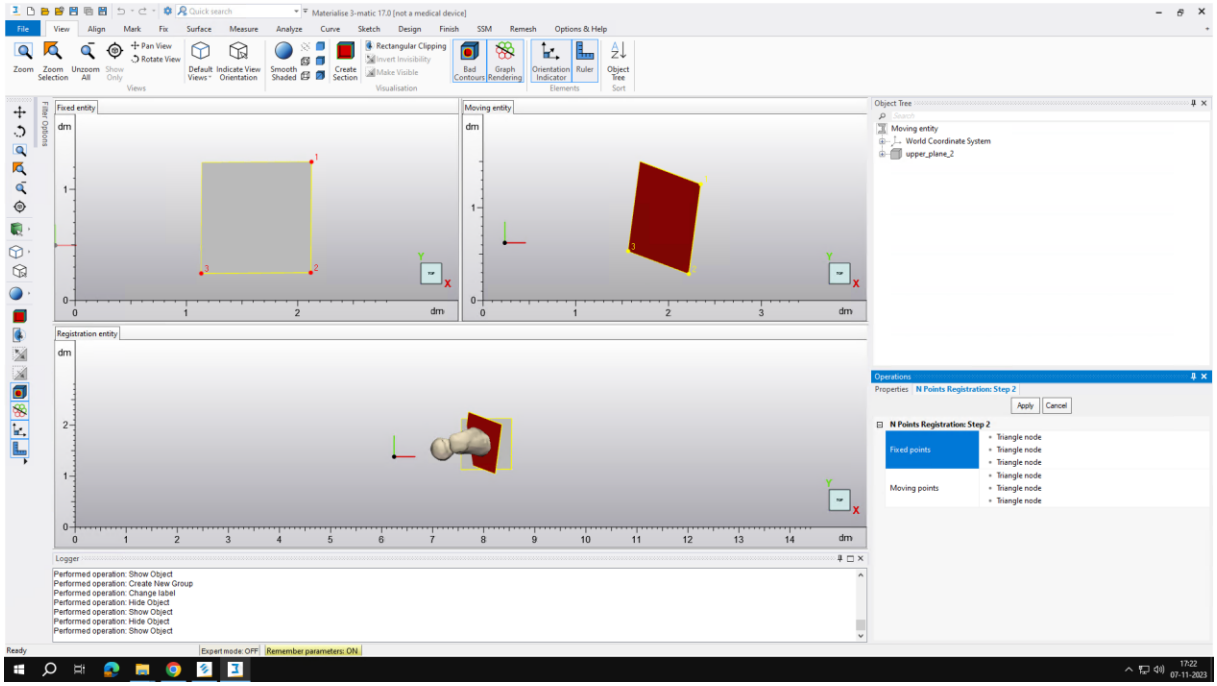

33, Using the N-points registration method in 3Matic the bony pieces can be translated and rotated to show the post-operative configuration.

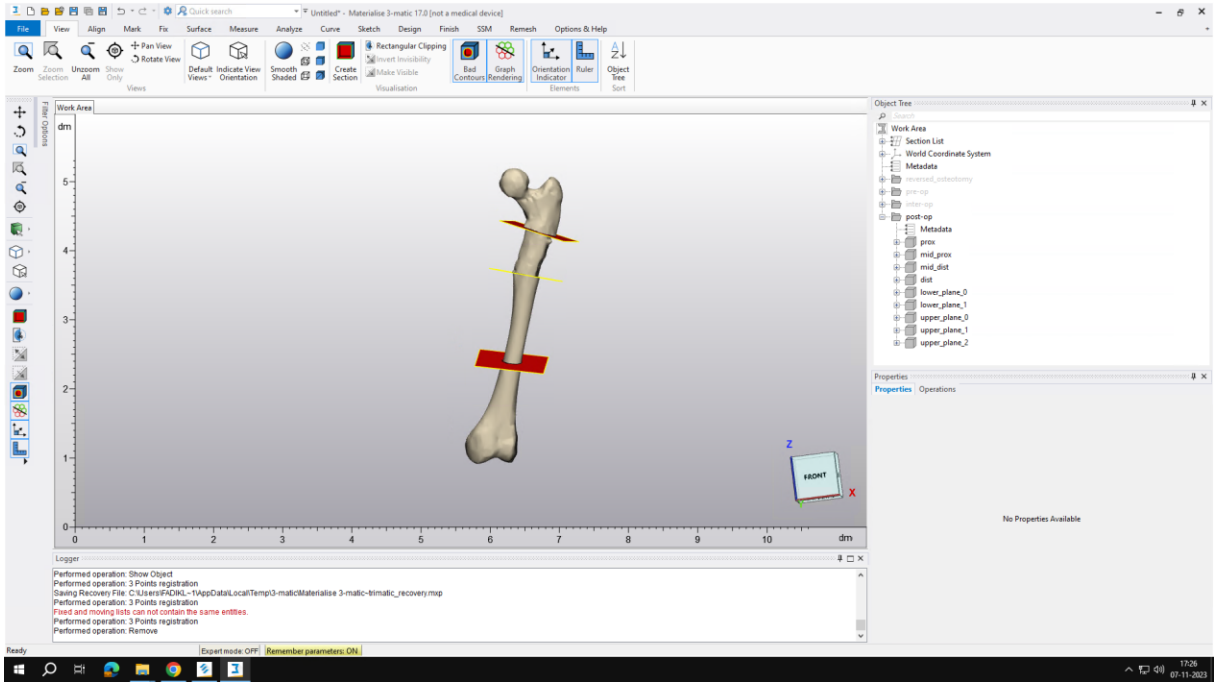

34, Repeating the registration method for all osteotomies gives the final post-operative result.

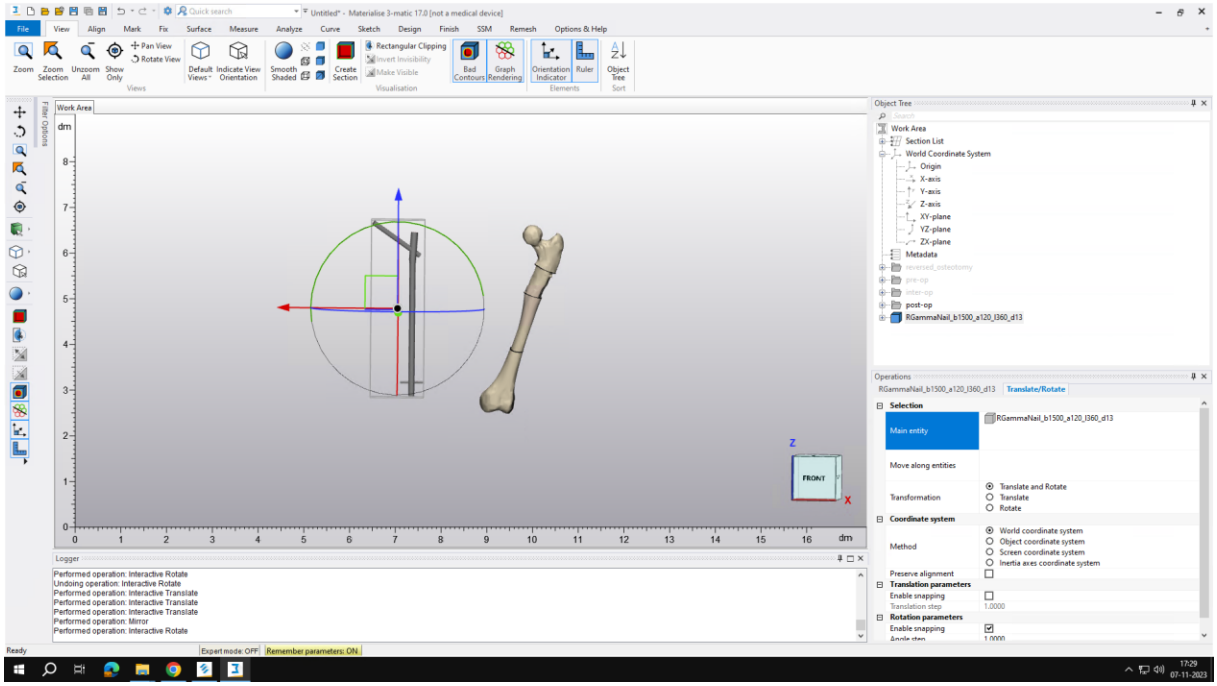

35, The STL model of the intramedullary nail that will be used during surgery is imported to the 3Matic project.

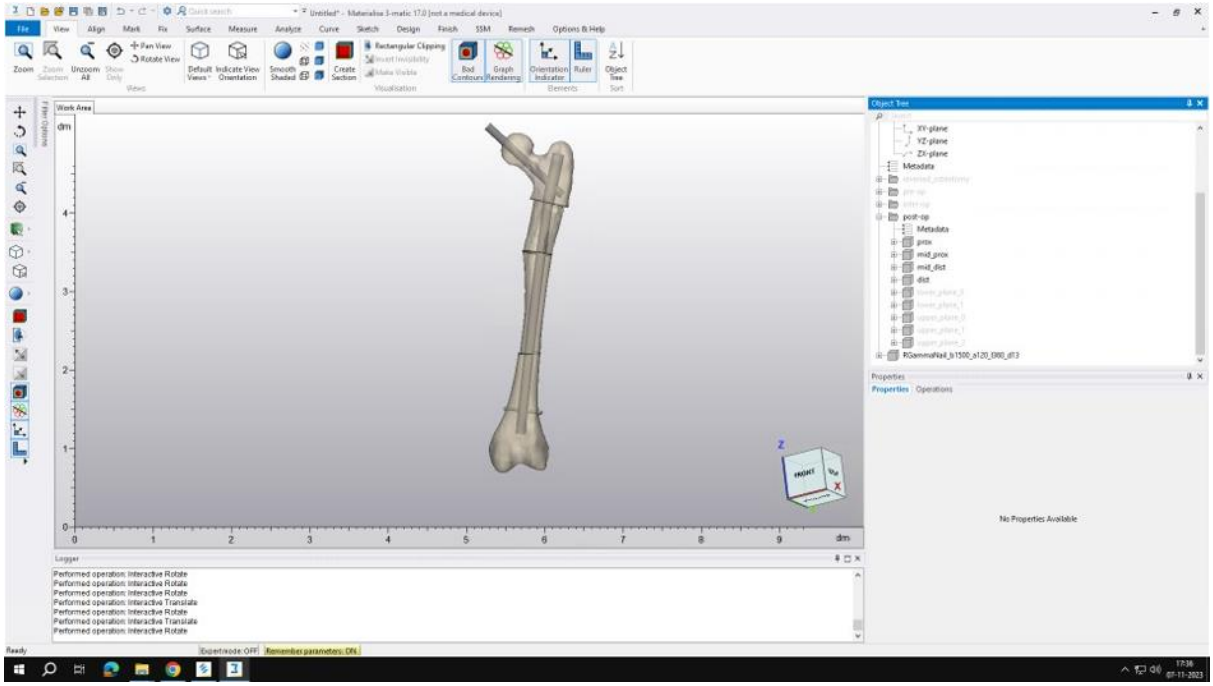

36, The nail can be fit manually in the post-operative result to evaluate the fit of the nail in the 3Matic validated post-operative result.

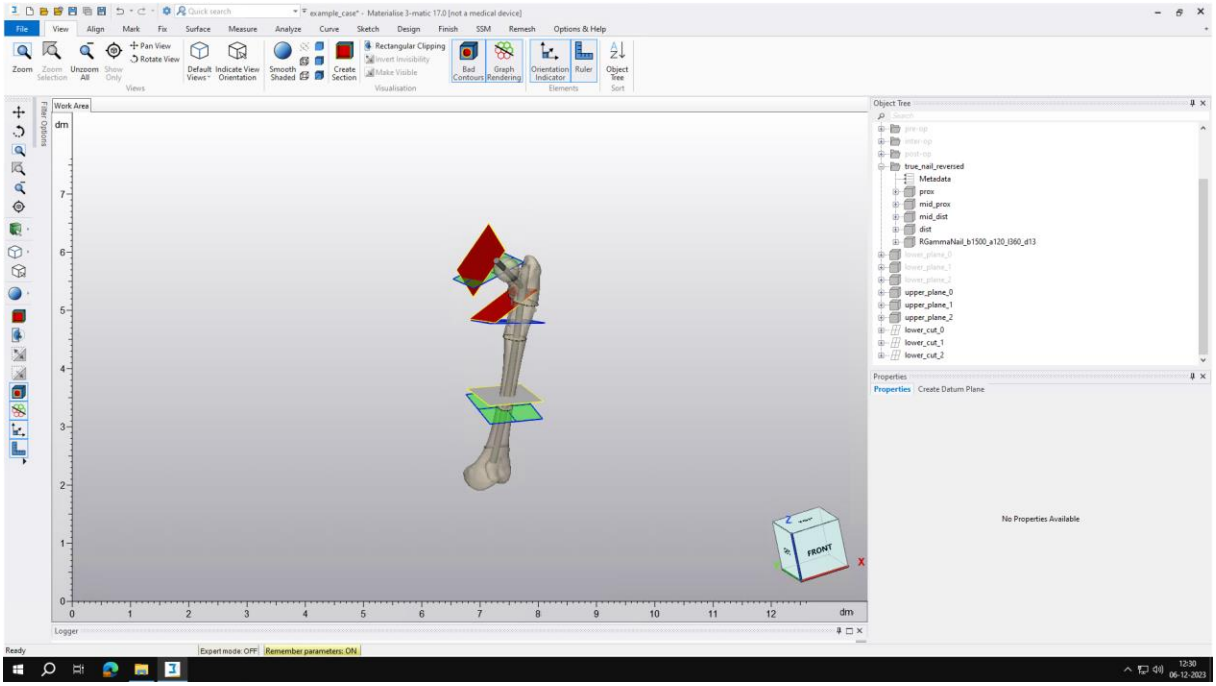

37, Starting from the most distal wedge, the distal plane of the wedge is used to cut to manually fit intramedullary nail.

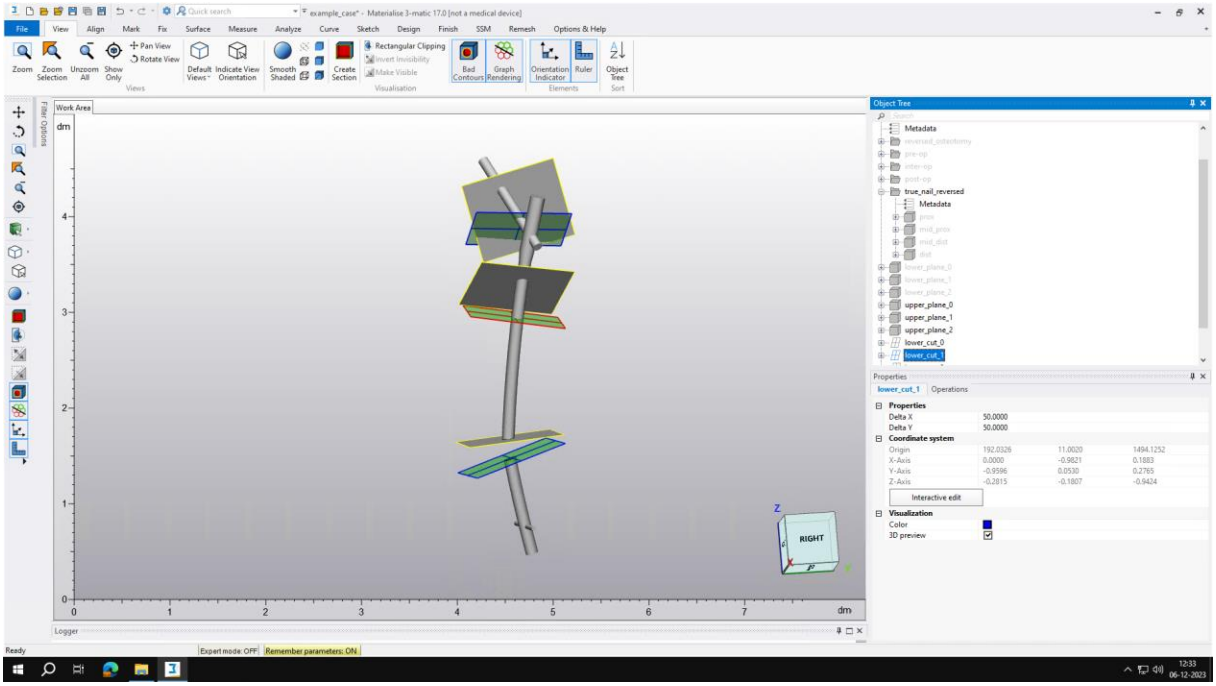

38, Again, using the N points registration tool the nail is transformed, performing an open wedge osteotomy on the intramedullary nail, corresponding to the closed wedge osteotomy on the femur.

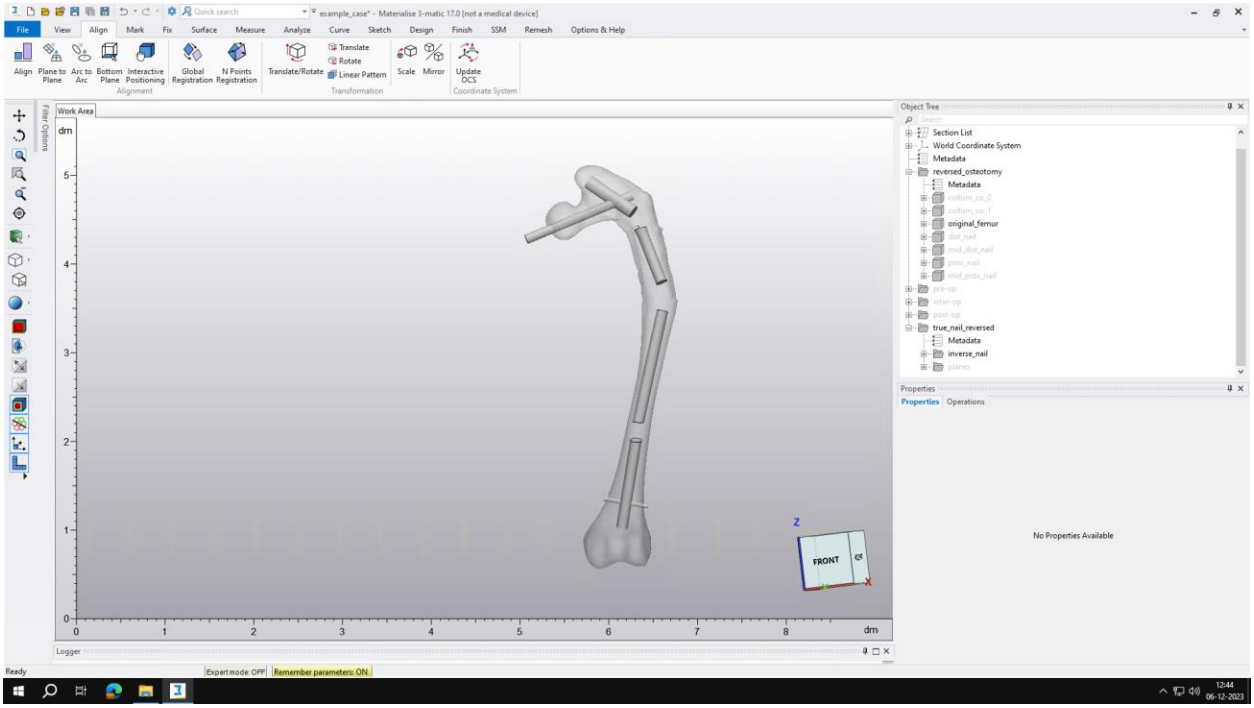

39, Performing the cut and transformation steps iteratively from distal to proximal, will result in the inverse osteotomy on the femoral nail. This visualizes the manually placed nail model on the preoperative bone model.

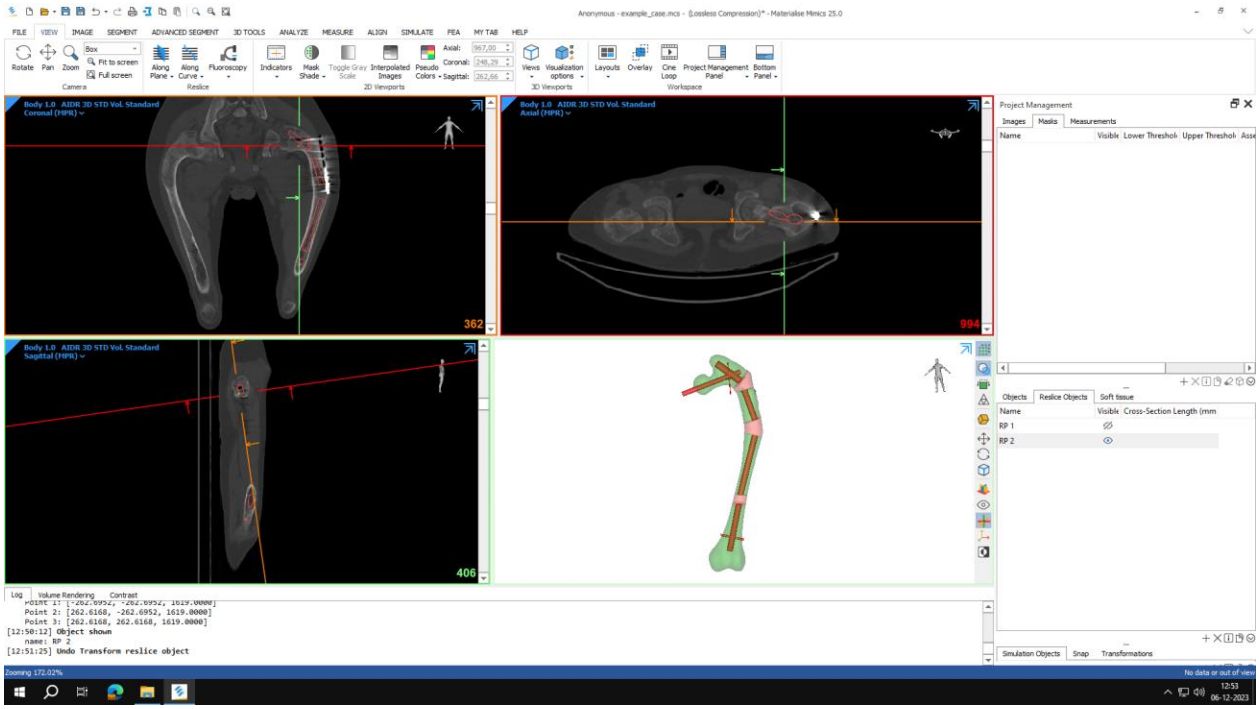

40, These nail parts are imported to Mimics to show the fit of the intra-operatively used femoral nail model in the preoperative situation. The nail fit can be evaluated in all axial slices.

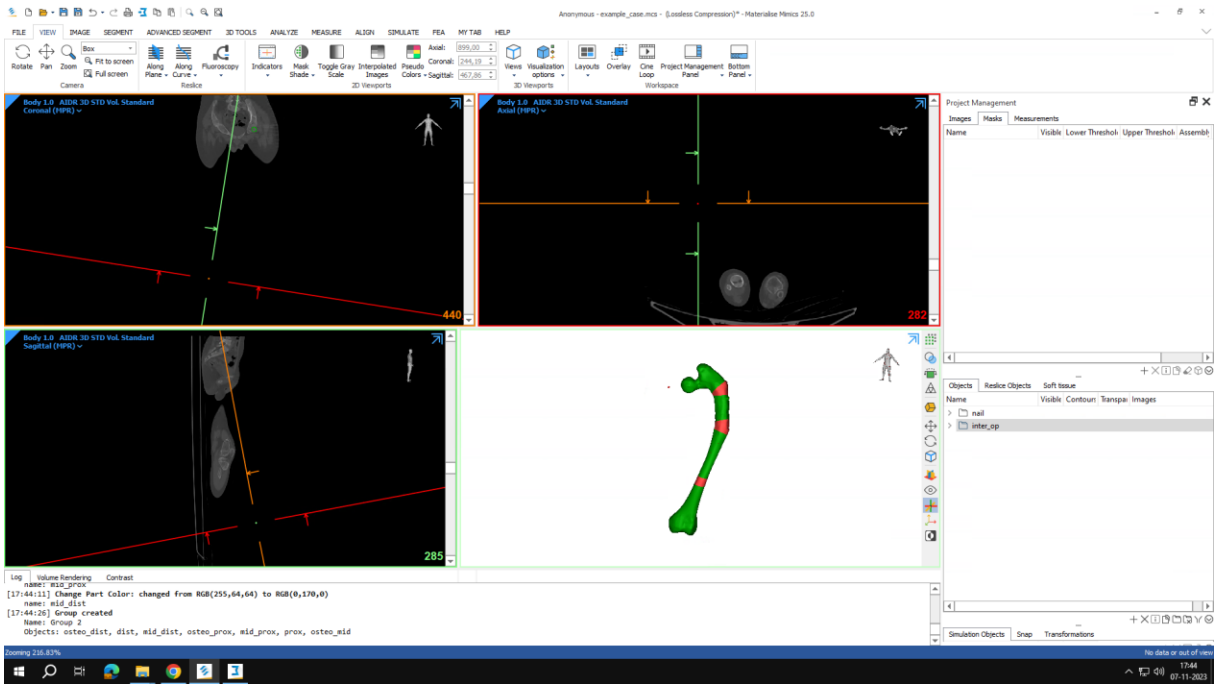

41, Importing the validated bony parts to Mimics, helps visualizing the bony parts that are osteotomized intra-operatively on the preoperative CT scan.

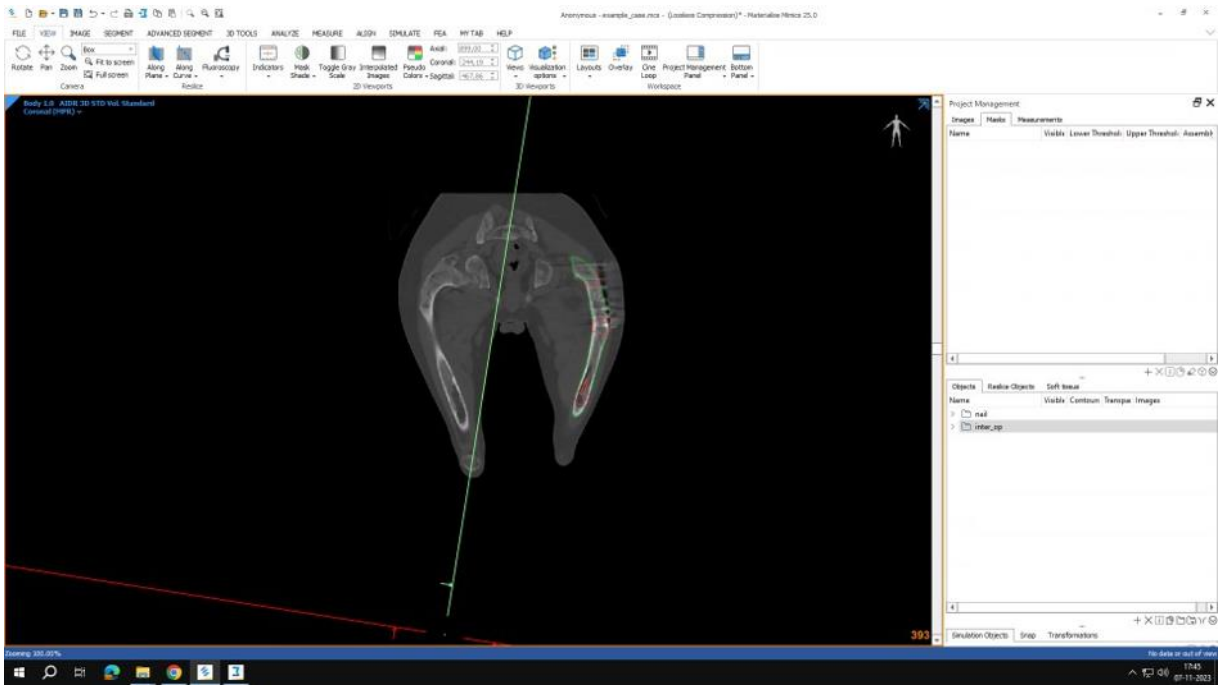

42, The CT-scan can be inspected closely and the resected parts are delineated with a red contour. The plan is fully validated and the cutting planes can be used to create cutting guides.